



THE HONG KONG
POLYTECHNIC UNIVERSITY

香港理工大學

Pao Yue-kong Library

包玉剛圖書館

Copyright Undertaking

This thesis is protected by copyright, with all rights reserved.

By reading and using the thesis, the reader understands and agrees to the following terms:

1. The reader will abide by the rules and legal ordinances governing copyright regarding the use of the thesis.
2. The reader will use the thesis for the purpose of research or private study only and not for distribution or further reproduction or any other purpose.
3. The reader agrees to indemnify and hold the University harmless from and against any loss, damage, cost, liability or expenses arising from copyright infringement or unauthorized usage.

IMPORTANT

If you have reasons to believe that any materials in this thesis are deemed not suitable to be distributed in this form, or a copyright owner having difficulty with the material being included in our database, please contact lbsys@polyu.edu.hk providing details. The Library will look into your claim and consider taking remedial action upon receipt of the written requests.

**CIRCUIT-SPECIFIC SONOGENETICS MODULATES
SPECIFIC BEHAVIOURS IN MICE**

XIAN QUANXIANG

PhD

The Hong Kong Polytechnic University

2021

The Hong Kong Polytechnic University

Department of Biomedical Engineering

**Circuit-specific sonogenetics modulates specific
behaviours in mice**

Xian Quanxiang

A thesis submitted in partial fulfillment of the requirements for
the degree of Doctor of Philosophy

July 2021

CERTIFICATE OF ORIGINALITY

I hereby declare that this thesis is my own work and that, to the best of my knowledge and belief, it reproduces no material previously published or written, nor material that has been accepted for the award of any other degree or diploma, except where due acknowledgment has been made in the text.

_____ (Signed)

____ Quanxiang Xian _____ (Name of student)

ABSTRACT

Controlling specific neural activities through physical intervention is an effective tool to gain great insight into brain functions and treatments for brain diseases. In the past few decades, many techniques have been developed, such as deep brain stimulation (DBS), transcranial direct current stimulation (tDCS), transcranial magnetic stimulation (TMS), focus ultrasound stimulation (FUS), chemogenetics and optogenetics. However, these methods are either invasive, lack of cell-type selectivity, or have low spatial resolution.

Low intensity ultrasound is an emerging and promising modality for brain stimulation. Although it has properties of non-invasiveness and enhanced spatial focus, the lack of cell-type selectivity is still a crucial concern. In recent years, studies showed that mechanosensitive ion channels were capable of sensitizing cells to ultrasound stimulation *in vitro*. Preliminary *in vivo* studies indicated that these channels could be activated by acoustic stimuli in mouse brain, which were mainly confirmed by c-Fos staining (a marker of neural activity). However, its rigorous characterization of the treatment and demonstration of robust behavioral effects remains to be elucidated. It is important to connect brain activity with behavioral effects with feasible intervention approaches that alter the dynamic of neural pathway, which might open a door to explore how brain neural activities control corresponding behavior.

Here, we demonstrate a sonogenetic approach which utilizes a mechanosensitive ion channel (MscL-G22S) to implement transcranial ultrasonic activation of well-defined neural circuits in forebrain and midbrain. Plane ultrasonic wave with approximately 5 mm diameter beam width was generated by our setup, which selectively activated MscL-expression regions of 1.5 mm diameter but not surrounding

areas.

Combining low intensity ultrasound stimulation and fiber photometry technique, we monitored the real time effects of sonogenetic stimulation on calcium dynamic of specific brain regions *in vivo*. MscL-expressing neurons of mice barrel cortex or dorsal striatum could be activated by low intensity ultrasound stimulation, generating robust and synchronized calcium responses, whereas EYFP-expressing (control group) mice showed no or smaller response to the same stimulation condition.

Furthermore, we found that transcranial MscL-mediated ultrasound stimulation enabled the evocation of whisker-barrel cortex pathway, resulting in stronger whisker deflection in head-restrained, awake mice. In addition, spatially and selectively activating neurons of the dorsal striatum enhanced motor function in freely behaving mice. Moreover, using this method, we successfully evoked endogenous dopamine release in nucleus accumbens (NAc) through modulating the mesolimbic pathway in mice. Finally, we specifically targeted dopaminergic neurons in the ventral tegmental area (VTA) with our strategy and modulated appetitive conditioning.

Together, we conclude that our sonogenetic method can manipulate neural activities of specific cell types and alter animals' behavior, which provides genetically and spatially targetable, and temporal precise activation of brain pathways without fiber implantation. Modulating animal's behavior with this approach may help to enrich our understanding of cell pathophysiology and almost certainly lead to development of novel treatment for neuropsychiatric and non-neural diseases.

Keywords Ultrasound stimulation, sonogenetics, mechanosensitive ion channel, neuromodulation, neural activity, neuronal circuit, behavior.

PUBLICATIONS ARISING FROM THE THESIS

Journal publications

1. **Xian, Q.***, Qiu, Z.*, Kala, S.*, Guo, J.*, Zhu, J., Wong, K.F., Guo, S.S.Y., Zhu, T., Hou, X. and Sun, L., 2021. Protocol for the sonogenetic stimulation of mouse brain by non-invasive ultrasound. *STAR protocols*, 2(2), p.100393.
2. **Xian, Q.***, Qiu, Z.*, Kala, S., Wong, K.F., Guo, J. and Sun, L., 2021. Behavioral and functional assessment of ultrasound neuromodulation on *Caenorhabditis elegans*. *IEEE Transactions on Ultrasonics, Ferroelectrics, and Frequency Control*, 68(6), pp.2150-2154.
3. Qiu, Z.*; Kala, S.*; Guo.; J.*; **Xian, Q.***; Zhu, J.; Zhu, T.; Hou, X.; Wong, K.; Yang, M.; Wang, H.; Sun, L., Targeted neurostimulation in mouse brains with non-invasive ultrasound. *Cell reports*, 2020. 32(7): p. 108033. (co-first author)
4. Hou, X.*; Qiu, Z.; **Xian, Q.***; Kala, S.*; Zhu, J.; Jing, J.; Guo.; J.; Wong, K.; Zhu, T.; Yang, M.; Sun, L., Precise Ultrasound Neuromodulation in a Deep Brain Region Using Nano Gas Vesicles as Actuators.. *Advanced Science*, 2021. (co-first author)
5. Qiu Z.*; Guo.; J.*; Kala, S.*; Zhu, J.*; **Xian, Q.**; Qiu, W.; Li, G.; Zhu, T.; Meng, L.; Zhang, R.; Chan, H.; Zhang, H.; et al.; Sun, L.,The mechanosensitive ion channel Piezo1 significantly mediates in vitro ultrasonic stimulation of neurons. *IScience*, 2019. 21: p. 448-457.
6. **Xian, Q.**, Kala, S., Qiu, Z., Kanna, S.; Guo, J., Wong, K.F., Hou, X. and Sun, L., 2021. Sonogenetic deep brain stimulation in freely moving mice. (to be submitted)

Conference presentations

1. **Xian, Q.**; Qiu, Z.; Kala, S.; Kanna, S.; Guo.; J.; Sun, L. Sonogenetic deep brain stimulation in freely moving mice. 2nd FUN Conference (Online), 2021/09/07-10.

(Oral)

2. **Xian, Q.**; Qiu, Z.; Kala, S.; Kanna, S.; Guo.; J.; Sun, L. Sonogenetic deep brain stimulation in freely moving mice. 20th annual international symposium for therapeutic ultrasound, Gyeongju, Korea (Online), 2021/06/06-09. (Invited talk)
3. Qiu, Z.*; Kala, S.; Guo.; J.*; **Xian, Q.***; Zhu, J.; Sun, L. Sonogenetic stimulation of mouse brain by non-invasive ultrasound. The World Molecular Imaging Society (WMIC) Virtual 2020, Online, 2020/10/07-09. (Oral)
4. Qiu, Z.*; Kala, S.*; Guo.; J.*; **Xian, Q.***; Zhu, J.; Sun, L., Targeted neurostimulation in mouse brains with non-invasive ultrasound. The 7th International Symposium on Focused Ultrasound 2020, Online, 2020/11/8-13. (Poster)
5. **Xian, Q.***; Qiu, Z.*; Kala, S.*; Guo.; J.*; Zhu, J.; Sun, L. Targeted deeper brain stimulation by non-invasive ultrasound. Francis Crick Symposium-Transforming Neurosciences: Questions & Experiments, Suzhou, China, 2019/04/16-20. (Oral)
6. **Xian, Q.***; Qiu, Z.*; Guo, J.; Sun, L.; Behavioral and functional assessment of low frequency low intensity ultrasound stimulation on *Caenorhabditis elegans*. Society of Neuroscience 2018, San Diego, United State, 2018/11. (Poster)

Awards

1. Best overall of iTRUSST presents the 2nd FUN Symposium, September 7-10, 2021, Online Conference.
2. Student Registration Award of 20th annual international symposium for therapeutic ultrasound, Gyeongju, Korea, June 6-9, 2021, online.

ACKNOWLEDGMENTS

I would like to show my sincere gratitude to my chief supervisor, Dr. Sun Lei for his patient guidance throughout my PhD study. The research study period was not easy, many obstacles needed to be faced and solved. Dr. Sun always encouraged me forward with his profound wisdom and knowledge. His curiosity in learning new knowledge and positive attitudes deeply inspired me. Thank Dr. Sun's patient teaching and guidance.

I would like to thank Dr. Qiu Zhihai and Dr. Guo Jinghui, for their great help and instructions. Both of them have taught me abundant useful thinking for my research project.

Also, I am grateful to my colleagues, Song Lin, Cao Fei, Shashwati Kala, Wong Kin Fung, Suresh Kanna, Zhu Jiejun, Hou Xuandi, Zhu Ting, Zhao Xinyi, Lei Ting, Zhang Yizhou, Huang Xiaohui, Wu Yong, and Jing Jianing. Thank you for their help and useful suggestion both in research projects and living aspects. I never forget the time we spent together.

Last but not least, big thanks to my parents their support and understanding.

TABLE OF CONTENTS

CERTIFICATE OF ORIGINALITY	III
ABSTRACT.....	IV
PUBLICATIONS ARISING FROM THE THESIS.....	VI
ACKNOWLEDGMENTS	VIII
LIST OF FIGURES	XIII
LIST OF TABLES.....	XXV
INDEX OF ABBREVIATIONS	XXVI
CHAPTER 1 Introduction	1
1.1 Brain stimulation	1
1.1.1 Deep brain stimulation (DBS)	5
1.1.2 Transcranial Direct electrical stimulation (tDCS)	7
1.1.3 Transcranial magnetic stimulation (TMS)	8
1.1.4 Optogenetic	9
1.2 Ultrasound stimulation	11
1.2.1 What is ultrasound?.....	11
1.2.2 Bioeffects of ultrasound.....	14
1.2.3 Research on ultrasound brain stimulation.....	17
1.3 Mechanisms and Sonogenetics.....	21
1.4 Challenges and research objectives	26
CHAPTER 2 MscL-mediated ultrasound activates corticospinal motor circuits in anesthetized mice	30
2.1 Materials and methods	30

2.1.1 Animal subjects.....	30
2.1.2 Stereotaxic injection	30
2.1.3 EMG recording in anesthetized mice.....	31
2.1.4 Experiment setup for the ultrasound brain stimulation.....	31
2.1.5 Immunohistochemical fluorescent staining	32
2.1.6 Statistical analysis.....	33
2.2 Results and discussion	33
2.2.1 Evoked stronger muscular responses to low intensity ultrasound stimulation in MscL-expressing anesthetized mice.	33
2.2.2 The latency responds to ultrasound stimulation is similar.....	36
CHAPTER 3 Functional stimulation of whisker-barrel cortex pathway using MscL-mediated ultrasound in awake mice.....	38
3.1 Materials and methods	38
3.1.1 Animal subjects.....	38
3.1.2 Stereotaxic injection	38
3.1.3 Fiber photometry recording in the barrel cortex of anesthetic mice.....	39
3.1.4 Measurement of whisker behavior.....	40
3.1.5 Immunohistochemical fluorescent staining	41
3.1.6 Statistical analysis.....	41
3.2 Results and discussion	42
3.2.1 Induced greater calcium activity in primary somatosensory cortex by MscL-mediated ultrasound stimulation	42
3.2.2 The MscL expression does not affect the physiological property of neuron and does not elicit an obvious immune, apoptosis response.....	46
3.2.3 Induced stronger whisker movement by MscL-mediated ultrasound	

stimulation of primary somatosensory cortex	50
3.2.4 Acoustics does not induce whisker movement in mice	54
CHAPTER 4 Spatially activation of dorsal striatum neurons and enhances motor function via MscL-mediated ultrasound	57
4.1 Materials and methods	57
4.1.1 Animal subjects	57
4.1.2 Virus injection	57
4.1.3 Fiber photometry recording of ultrasonic evoke neural activity in anesthesia mice	58
4.1.4. Measurement of locomotion by Open field recording	59
4.1.5 Ultrasound stimuli in dorsal striatum for c-fos staining	60
4.1.6 Immunohistochemical fluorescent staining	60
4.1.7 Statistical analysis	61
4.2 Results and discussion	61
4.2.1 MscL-mediated ultrasound stimulation selective and spatially activated the neurons of dorsal striatum	61
4.2.2 Induced larger and synchronized calcium activity by MscL-mediated ultrasound stimulation in dorsal striatum	66
4.2.3 Enhanced evocation of locomotor activity by MscL-mediated ultrasound stimulation of dorsal striatum	70
4.2.4 Benchmark with optogenetics	76
CHAPTER 5 Modulating mesolimbic circuit by MscL-mediated ultrasound stimulation	81
5.1 Materials and methods	81
5.1.1 Animal subjects	81

5.1.2 stereotactic injection	81
5.1.3 Fiber photometry recording of ultrasonic induced dopamine release in anesthesia mice	82
5.1.4 Real time place preference assay [84]	83
5.1.5 Immunohistochemical fluorescent staining	84
5.1.6 Statistical analysis.....	84
5.2 Results and discussion	84
5.2.1 Efficient sonogenetically-enabled dopamine release in the NAc by modulating the mesolimbic pathway	84
5.2.2 Inducing appetite preference by MscL-mediated ultrasound stimulation in excitatory neurons of VTA.....	91
5.2.3 Inducing appetite preference by MscL-mediated ultrasound stimulation in dopaminergic neurons of VTA.....	98
CHAPTER 6 Conclusions and future work	103
6.1 Optimization of ultrasound parameters	105
6.2 Potential applications of MscL-mediated ultrasound stimulation in neurological disorders.....	107
6.3 Optimizing the MS ion channel and exploring its mechanisms.....	108
6.4 Combining existing technologies to eliminate the need for surgical disruption.....	109
References	111

LIST OF FIGURES

Figure 1 Diagram schematic of the basal ganglia circuit in a normal state and in parkinsonism. (Adapted from [15]).	3
Figure 2 Summary of neuromodulatory methods based on spatial resolution and temporal resolution. (Adapted from [19])	5
Figure 3 Neuroimaging scan of DBS. (Adapted from [33]).	6
Figure 4 Diagram of the effect of tDCS electrical field on neurons. (Adapted from [43, 52]).	7
Figure 5 Schematic indication of the human cerebral cortex with TMS. (adapted from [57]).	9
Figure 6 Illustration of optogenetic technique. (A) The model of optogenetic (Adapted from [74]). (B) A simplified version of basic properties of this three optogenetic tool family (adapted from [77]). (C) An illustration of one behavior probing using optogenetics (adapted from [78]).	11
Figure 7 Detailed information about ultrasound parameters. (adapted from [91])	13
Figure 8 Diverse biological outcomes from ultrasound stimulation. (Adapted from [93]).	17
Figure 9 Examples of ultrasound stimulation applied to human. (A) Illustration of sites for transcranial ultrasound (TUS) (top). An example human module showed transcranial ultrasound application (below) (adapted form [118]). (B) Transcranial focus ultrasound stimulation can be targeted to the specific area (such as somatosensory cortex) in the human cortex (adapted form [119]). (C) fMRI data showed focus ultrasound stimulation evoked not only the targeted region (visual cortex) neural activity, but also affected other brain regions (adapted form [120]).	19

Figure 10 Mechanisms of ultrasound stimulation. (A) Diagram showed the potential mechanism of ultrasound in heating (Left panel), cavitation (Right panel). (Adapted from [91]) **(B)** Representative diagram of molecular circuits activated through mechanical force [112].....23

Figure 11 Illustration of *C. elegans* response to ultrasound stimulation in the microbubble environment which can enhance ultrasound signals. (Adapted from [131]).....24

Figure 12 Diagram of the process of sonogenetic technique. (A) The mainly experimental steps of sonogenetics method (Adapted from [137]). **(B)** An example of sonogenetics method. (Adapted from [134])25

Figure 13 Merits and demerits of common neuromodulatory methods. (Adapted from [89, 146]).....27

Figure 14 Technical information of the ultrasound system. (A) Schematic illustration of components of the US system. The function generator was responsible for generating waveforms. The amplifier provided voltages to the ultrasound transducer. **(B)** A diagram of the ultrasound temporal profile applied in the EMG experiment....32

Figure 15 An experimental flow of EMG recording in anesthetized mice. (A) A diagram of *in vivo* experimental plan. Briefly, mice were injected with CaMKII-promoted viruses in M1 region of the right brain. Four-week later, mice were stimulated with US stimulation and muscular contraction of the left forelimb triceps were detected by EMG electrodes simultaneously. **(B)** Images of mouse brains expression CamKII-EYFP (Left panel) or CamKII-MscL-EYFP (Left panel), indicating the regions of EYFP and MscL-EYFP expressed in M1 region. Primary motor cortex (M1). Caudoputamen (CP), cerebral cortex (CTX).34

Figure 16 Ultrasound stimulation induces larger muscular responses when applied to mouse primary motor cortex area expressing MscL. (A) Representative EMG

traces of the muscular contraction results from 0.05 MPa intensity sonication in mice expressing the EYFP or MscL viruses. **(B)** The relative amplitude of EMG response at ranges of 0.05 MPa to 0.5 MPa ultrasound stimulation. $n = 49$ times ultrasound stimulation. ‘N.R.’ indicates ‘no response’. Data are indicated as mean \pm S.D. Unpaired two-tailed t -test. **(C)** The success probability of individual sonication stimulation to cause the generation of EMG spikes at ranges of 0.05 MPa to 0.5 MPa ultrasound stimulation. $n = 7$ mice, except for CaMKII-EYFP $n = 3$ mice. ‘N.R.’ indicates ‘no response’. Data are shown as mean \pm S.D. Unpaired two-tailed t -test. .35

Figure 17 No significant difference of the latency responds to ultrasound stimulation. **(A)** EMG response latency measured from the left forelimb triceps in response to M1 stimulation by ultrasound. $n = 6$. Data are indicated as mean \pm S.D. Unpaired two-tailed t -test.37

Figure 18 An experimental setup and preparation for neural activity recording in the dorsal striatum in vivo. **(A)** A diagram of whisker stimulation and fiber photometry recording experiment. Anesthetized mice were treated with a range of sonication (0.1 – 0.4 MPa), respectively, and recording calcium signals from right side barrel cortices. **(B)** Images showed the low magnification of a mouse brain CamKII:EYFP or CamKII:MscL-EYFP co-expressing with CamKII: jRGECO1a in barrel cortex regions. **(C)** Confocal images dsplayed the high magnification of a mouse brain CamKII:EYFP or CamKII:MscL-EYFP co-expressing with CamKII: JTGECO1a in the barrel cortex.43

Figure 19 US stimulation elicits greater calcium activity in excitatory neurons of barrel cortex in MscL-expressing mice. **(A)** Averaged jRGECO1a fluorescence traces increase in the somatosensory cortex of the anesthetized EYFP- mice and MscL- mice in response to different ultrasound stimulations (0.15 MPa and 0.4 MPa). Light green rectangle shows the timing of ultrasound stimulation. $n = 6$ mice in EYFP group, $n = 5$

mice in MscL group. **(B)** Average peak Ca^{2+} activity in EYFP- mice and MscL- mice respond to NUS, 0.15 MPa, 0.4 MPa ultrasound stimulation. * $P < 0.05$, Unpaired two-tailed t -tests. Data are shown as mean \pm SEM. $n = 6$ mice in EYFP group, $n = 5$ mice in MscL group. **(C)** Representative traces showed calcium activity respond to 0.15 MPa ultrasound stimulation in EYFP- and MscL- mice. Light green rectangular shows the timing of ultrasound stimulation.....46

Figure 20 Calcium activity induced by air trigger in EYFP mice and MscL mice.

(A) Representative calcium traces showed calcium activity responded to air stream trigger in EYFP- and MscL- mice. Irregular patterns indicate each air stream trigger. **(B)** Average peak calcium transient responded to per air stream stimulation in EYFP- mice and MscL- mice. Unpaired two-tailed t -tests. $n = 3$ mice each group. Data are indicated as mean \pm SEM. NS, no significance.47

Figure 21 MscL expression is safe in cellular level. (A) Representative images showed50

Figure 22 An experimental setup for whisker movement recording in awake mice.

(A) Schematic of barrel cortex experimental scheme (Top). Briefly, mice were injected into their right barrel cortex with CamKII: EYFP or CamKII: MscL-EYFP. Four weeks later, mice were treated with ultrasound and recorded the left - side C2 whisker's movement. **(B)** Confocal images indicate expression of CamKII:EYFP (Left panel) or CamKII:MscL-EYFP (Right panel) in the barrel cortex (primary somatosensory cortex, S1). Hippocampus (CP), cerebral cortex (CTX).....51

Figure 23 MscL-mediated ultrasound stimulation of barrel cortex evokes stronger whisker movement.

(A) The images were taken over before and after ultrasound stimulation in EYFP (left) and MscL (right) mice. **(B)** Representative the angle changes of the C2 whisker from CamKII:EYFP and CamKII:MscL-EYFP awake mice following ultrasound stimulation on the surface of barrel cortex. Timing of ultrasound

stimulation is indicated as the red shadow. **(C)** Summary data for average angular velocity of whisker movement evoked by different parameters of ultrasound stimulation in EYFP and MscL- mice. In 0.1 MPa ultrasound stimulation, $n = 8$ mice in EYFP group, $n = 7$ mice in MscL group; In 0.15 MPa ultrasound stimulation, $n = 9$ mice in EYFP group, $n = 7$ mice in MscL group; In 0.4 MPa ultrasound stimulation, $n = 7$ mice in EYFP group, $n = 6$ mice in MscL group. Unpaired two-tailed t -test, * $P < 0.05$. Data are shown as mean \pm SEM.....54

Figure 24 Sound does not induce whisker movement in EYFP mice and MscL mice.

(A) Schematic illustration of US transducer delivers ultrasound wave to the mouse brain with or without US gel. Sham stimulation experiments were conducted with the similar conditions but maintaining enough gap by not applying US gel between the transducer and skull. **(B)** Summary data for average angular velocity of whisker movement evoked by ultrasound stimulation in the sham group. $n = 6$ mice in EYFP group, $n = 6$ mice in MscL group. Unpaired two-tailed t -test. Data are shown as mean \pm SEM.....55

Figure 25 Neural activity in the dorsal striatum under ultrasound stimulation in EYFP and MscL mice.

(A) Schematic illustration of our experimental scheme. Briefly, mice were injected in their the dorsal striatum on the injected side of the mouse's brain with hSyn:EYFP or hSyn:MscL-EYFP. Five weeks later, an ultrasound adapter was installed. Then a week later, mice were stimulated with 0.15 MPa ultrasound for 40 minutes. Mice were allowed to recover for 90 minutes, after which their brains were collected for immunofluorescent staining. Dorsal striatum (dSTR), Caudoputamen (CP), cerebral cortex (CTX). **(B)** Confocal images of the dorsal striatum after ultrasound stimulation. Images of dorsal striatum expressing hSyn:EYFP or hSyn:MscL-EYFP with c-Fos stained. Images showing the low magnification (Left panel) and high magnification (Right panel) of mouse brain hSyn-EYFP or hSyn-MscL-EYFP expressing in dorsal striatum. The green two-arrow indicated the range of ultrasonic

coverage. (C) The number of nuclear c-Fos⁺ positive cells / per slice imaged in the dorsal striatum (Left panel) and the cortex above targeted region (Right panel) of mice stimulated with ultrasound. *n* = 4 mice per group. Data are shown mean ± SEM of average c-Fos⁺ cells per stained slice. One-way ANOVA with post-hoc Tukey test. ..64

Figure 26 Auditory pathway does not mainly participate in the upregulation of the MscL-sonogenetic process. (A) Anatomical localization of auditory cortex in DAPI-labelled brain slice. (B) Images of c-fos in auditory cortex from MscL-expressing mice and EYFP mice that received US stimulation. (C) Quantification of the expression of c-fos in auditory cortex in EYFP-US mice and MscL-US mice. *n* = 3 mice per group. Data are shown mean ± SEM of average c-Fos⁺ cells per stained slice. One-way ANOVA with post-hoc Tukey test.65

Figure 27 An experimental setup and preparation for calcium activity recording of the dorsal striatum in vivo. (A) Schematic illustration of *in vivo* real-time calcium activity recording. The right dSTR of mice was co-transduced by AAVs for a calcium sensor (hSyn:jRGECO1a) and either MscL-EYFP or EYFP, at a 1:1 ratio. 5 weeks later, anesthetized mice were stimulated with US, and neuronal calcium responses were recorded simultaneously by an optical fiber implanted in the viral injected region. (B) Representative low-magnification pictures of dorsal striata (dSTR) expressing hSyn-EYFP (Left panel) or hSyn:MscL-EYFP and hSyn:jRGECO1a (Right panel). Caudoputamen (CP), cerebral cortex (CTX). (C) Representative high-magnification confocal images showing EYFP or MscL-EYFP and jRGECO1a fluorescence co-located in the same neurons in the dorsal striatum.68

Figure 28 US stimulation elicits greater calcium activity in dSTR neurons in MscL-expressing mice. (A) Averaged jRGECO1a fluorescence traces in the dorsal striatum of anesthetized EYFP- or MscL-mice prior to US stimulation. (B) Averaged jRGECO1a fluorescence traces increase in the dSTR of anesthetized EYFP- or MscL-mice in

response to one 0.15 MPa pressure ultrasound stimulation (0.5 MHz center frequency, 500 μ s pulse width, 300 ms stimulation duration, 1 kHz PRF, interval 3s). $n = 8$ trials, 5 mice in EYFP group, $n = 7$ trials, 5 mice in MscL group. Green rectangle shows the timing of ultrasound stimulation. **(C)** Average peak Ca^{2+} activity in EYFP- and MscL-mice in response to US pulses of varying intensities (0.05 – 0.2 MPa pressure, 500 μ s pulse width, 0.5 MHz center frequency, 300 ms stimulation duration, 1 kHz PRF, interval 3s). $n = 8$ trials, 5 mice in EYFP group, $n = 7$ trials, 5 mice in MscL group. * $P > 0.05$, unpaired 2-tailed t -tests. Data are shown as mean \pm SEM. **(D)** Latency between US stimulation (0.05 – 0.2 MPa pressure) and detection of an above-threshold. $n = 5$ mice in MscL group. One-way ANOVA with post-hoc Tukey test. Data are shown as mean \pm SEM. **(E)** Calcium traces of a EYFP mice and MscL mice undergo repeated ultrasound stimulation. Green rectangle shows the timing of ultrasound stimulation.

Figure 29 Ultrasound stimulation plan and preparation for locomotion test in awake, freely moving mice. **(A)** Schematic of our experimental scheme. Briefly, mice were injected in the dorsal striatum on the right side mouse’s brain with hSyn:EYFP or hSyn:MscL-EYFP. Three weeks later, an ultrasound adaptor was installed and one week after recovery that mice were stimulated with ultrasound. Mice were placed in a square box and their movement were recorded before, during and after ultrasound stimulation with a digital camera. The behavior documented in the video was then analyzed and quantified. **(B)** Schematic illustration of US adaptor and the wearable US transducer. This US transducer weighted ~ 1 g. **(C)** Confocal images indicate expression of hSyn:EYFP (top panel) or hSyn:MscL-EYFP (below panel) in the dorsal striatum (dSTR) of the right side of the mouse brain. Caudoputamen (CP), cerebral cortex (CTX).

..... 72

Figure 30 Expression of EYFP or MscL-EYFP in mice do not affect spontaneous locomotive movement. **(A)** Comparison of mobility average speed of the EYFP and

MscL mice before ultrasound stimulation. $n = 6$ mice per group. Unpaired two-tailed t -test. Data are shown as mean \pm SEM; NS, no significance. **(B)** Comparison of distance of the EYFP and MscL mice before ultrasound stimulation. $n = 6$ mice per group. Unpaired two-tailed t -test. Data are shown as mean \pm SEM; NS, no significance..... 73

Figure 31 Ultrasound stimulation evoked significant increase in locomotor behavior in mice with MscL expression in the dorsal striatum.

(A) Representative trajectories recorded from mice stimulated in the dorsal striatum pre-US, during US, and post-US with 0.3 MPa ultrasound application (each trace 1 min long). **(B)** Comparison of mobility average speed of the EYFP and MscL mice, with (0.3 MPa) and without ultrasound stimulation. $n = 6$ mice EYFP group and $n = 6$ mice MscL group. Data are shown as mean \pm SEM; Unpaired two-tailed t -test. **(C)** Summary of mobility average speed of EYFP and MscL-expression mice with ultrasound stimulation of different ultrasonic intensities from 0.1 – 0.35 MPa pressure. Green bars indicate the timing of ultrasonic stimuli. $n = 6$ mice EYFP group and $n = 6$ mice MscL group. Data are shown as mean \pm SEM; Two-tailed unpaired t -test. **(D)** Comparison of distance of the EYFP and MscL mice, with (0.3 MPa pressure) and without ultrasound stimulation. $n = 6$ mice EYFP group and $n = 6$ mice MscL group. Data are shown as mean \pm SEM; Unpaired two-tailed t -test. **(E)** Summary of distance of EYFP and MscL-expression mice with ultrasound stimulation of different ultrasonic intensities from 0.1 – 0.35 MPa pressure. Green bars indicate the timing of ultrasonic stimuli. $n = 6$ mice EYFP group and $n = 6$ mice MscL group. Data are shown as mean \pm SEM; Two-tailed unpaired t -test. 76

Figure 32 Light stimulation plan and preparation for locomotion test in awake and freely moving mice.

(A) Schematic of optogenetic experimental steps. Briefly, mice were injected in their dorsal striatum of the right side of the brain with hSyn:ChR2-mCherry, followed with optical fiber inserting at the same region. Four weeks later, a

light adaptor attached to the optical fiber and delivered appropriate light into the mouse brain. Mice were placed in a square box and their movement were recorded before, during and after light stimulation. **(B)** Confocal images indicating ChR2-mCherry in the dorsal striatum (dSTR)..... 77

Figure 33 Optogenetic stimulation evoked significant increase in locomotor behavior in mice with ChR2 expression in the dorsal striatum.

(A) Representative trajectories recorded from mice stimulated in the dorsal striatum pre-light, during light stimulation (50%, 10 ms, 15 Hz) periods, post-light (each trace 1 min long). **(B)** Summary of mobility average speed of hSyn:ChR2-mCherry mice, with (20% / 50% / 100% power, 10 ms, 15 Hz) and without light stimulation. $n = 3$ mice each group. Data are shown as mean \pm SEM; * $p < 0.05$, Unpaired two-tailed t -test. NS indicates light off. **(C)** Summary of distance of hSyn:ChR2-mCherry mice, with (20% / 50% / 100%, 10 ms, 15 Hz) and without light stimulation. $n = 3$ mice each group. Data are shown as mean \pm SEM; * $p < 0.05$, Unpaired two-tailed t -test..... 78

Figure 34 The increasing locomotor behavior evokes by optogenetic and sonogenetic is similar.

(A) Comparison of mobility average speed of hSyn:ChR2-mCherry mice, with (100%, 10 ms, 15 Hz) light stimulation and of hSyn:MscL-EYFP mice with 0.3 MPa ultrasound stimulation. $n = 3$ mice in optogenetic experiment, $n = 6$ mice in the sonogenetics experiment. Data are shown as mean \pm SEM; * $p < 0.05$, ** < 0.01 , Two-tailed unpaired t -test. **(B)** Summary of distance in hSyn:ChR2-mCherry mice, with (100%, 10 ms, 15 Hz) light stimulation and of hSyn:MscL-EYFP mice with 0.3 MPa ultrasound stimulation. $n = 3$ mice in optogenetic experiment, $n = 6$ mice in the sonogenetics experiment. Data are shown as mean \pm SEM; * $p < 0.05$, *** $P < 0.001$, Two-tailed unpaired t -test. 79

Figure 35 An experimental setup for dopamine signal recording in vivo.

(A) Schematic showing the hSyn-DA2m, hSyn-EYFP and hSyn-MscL-EYFP virus delivery,

fiber implantation and ultrasound stimulation in the mouse brain. Mice were injected AAV-hSyn-DA2m in the NAc of the right brain and hSyn-EYFP or hSyn-MscL-EYFP in the VTA at the same hemisphere. After virus injection, an optical fiber was inserted into NAc for detecting DA signals. 4-week later, mice were stimulated with ultrasound stimulation and detect DA signals simultaneously. **(B)** Confocal images of NAc region expressing DA2m (green) with DAPI (blue) in EYFP and MscL-expressing brain. **(C)** Confocal images of low magnificence of depicting DAPI (blue), TH (red), and EYFP neurons (green) in the VTA. **(D)** Confocal images of high magnificence of representing DAPI (blue), TH (red), EYFP (green) neurons in the VTA. White arrows indicated example EYFP+/TH+ neurons.....87

Figure 36 Sonogenetic stimulation of VTA neurons evokes DA release in NAc in vivo. **(A)** Averaged DA2m fluorescence signal without ultrasound stimulation in the NAc of the anesthetized EYFP- mice and MscL-expressing mice. $n = 6$ trials, 4 mice in EYFP group. $n = 6$ trials, 5 mice in the MscL group. **(B)** Average DA2m fluorescence signal response to ultrasound stimulation in the NAc of the anesthetized EYFP- mice and MscL-expressing mice. $n = 6$ trials, 4 mice in EYFP group. $n = 6$ trials, 5 mice in the MscL group. **(C)** Average peak DA2m activity responds to 0.3 MPa ultrasound stimulation in EYFP- mice and MscL-expressing mice. $n = 6$ trials, 4 mice in EYFP-group. $n = 6$ trials, 5 mice in the MscL-expressing group. * $P < 0.05$, ** $P < 0.01$, Unpaired two-tailed t -tests. Data are shown as mean \pm SEM. **(D)** DA2m fluorescence traces in the NAc of EYFP and MscL mice undergone repeated ultrasound stimulation (0.3 MPa). The blue and red examples represent the EYFP group and MscL group, respectively. Light green rectangular shows the timing of ultrasound stimulation.90

Figure 37 Ultrasound stimulation plan and setup for the place preference test in awake and freely moving mice. **(A)** Schematic of our experimental scheme. Briefly, mice were injected into their right ventral tegmental area with CamKII:EYFP or

CamKII:MscL-EYFP. Three weeks later, an ultrasound adaptor was installed and one week after recovery that mice were stimulated with ultrasound. Mice were put in a rectangle arena and were recorded their trajectories with a camera. The behavior documented in the video was then analyzed and quantified. **(B)** An illustration of the real time place preference apparatus. Our RPP apparatus consists of a chamber divides into two equal side, one side with vertical stripes walls and the other side with horizontal stripes walls. Mouse movement in the two sides during each preference test detected by a digital camera. An US indicated light indicates the start and end of ultrasound. **(C)** Confocal images indicating expression of CamKII:EYFP (Top) or CamKII:MscL-EYFP (Below) in the VTA. DAPI (blue), TH (red), EYFP (green) neurons, and in the VTA. White arrows showed representative EYFP+/TH+ neurons.93

Figure 38 Deep MscL-mediated ultrasound stimulation can induce appetitive conditioning. **(A)** Examples path-trajectories of a mouse with CamKII:EYFP or CamKII:MscL-EYFP expression during the appetition test. Red rectangle showed the US-stimulation side. **(B)** Percentage of time spent on the US stimulation side at 0.05 MPa pressure ultrasound in EYFP (control, gray) and MscL mice (orange) ($n = 4$ mice in EYFP- mice; $n = 4$ mice in MscL-expressing mice, Repeated two rounds. * $P < 0.05$, two-tailed unpair t -test. Data are shown as mean \pm SEM. **(C)** Average distance during 0.05 MPa sonication epoch on the US stimulation side was noticeable higher than the non-stimulation side in MscL group, and showed significantly different than the EYFP-US. ($n = 4$ mice in EYFP mice; $n = 4$ mice in MscL-expressing mice, * $P < 0.05$, two-tailed unpair t -test. Data are shown as mean \pm SEM. **(D)** Average mobility velocity during sonication epoch on the stimulation side was not obvious changes than the non-stimulation side in EYFP and MscL group. * $P < 0.05$, ** $P < 0.01$, one-way ANOVA with post-hoc Tukey test. Data are shown as mean \pm SEM.96

Figure 39 MscL-mediated ultrasound stimulation activates the excitatory neurons in VTA. (A) The workflow of appetite test with ultrasound stimulus. **(B)** Percentage of time spent on the US stimulation side at difference pressures of ultrasound stimulation in EYFP and MscL mice. $n = 4$ mice in EYFP- mice; $n = 4$ mice in MscL-expressing mice, Repeated two rounds. * $P < 0.05$, unpair two-tailed t -test. Data are shown as mean \pm SEM. **(C)** Average mobility velocity during different pressure sonication epoch on the stimulation side was not obviously different than the non-stimulation side in EYFP and MscL group. $n = 4$ mice in EYFP mice; $n = 4$ mice in MscL-expressing mice. * $P < 0.05$, ** $P < 0.01$, one-way ANOVA with post-hoc Tukey test. Data are shown as mean \pm SEM. 98

Figure 40 Ultrasound stimulation plan and setup for the real time place preference assay in TH-cre mice. (A) Schematic of our experimental scheme. Briefly, mice were injected into their right ventral tegmental area were co-injected with AAV-TH-cre mix with AAV- EF1 α ::DIO-EYFP or AAV-EF1 α ::DIO-mscl-EYFP. Three weeks later, an ultrasound adaptor was installed, and one week after recovery that mice were stimulated with ultrasound. Mice were put in a rectangle chamber and were monitored their trajectories. The behavior documented in the video was then analyzed and quantified. **(B)** Low magnification of confocal images indicating expression of TH:EYFP or TH:MscL-EYFP in the VTA. DAPI (blue), EYFP neurons (green), and TH (red) in the VTA. **(C)** High magnification of images showing TH:EYFP (Top) or TH:MscL-EYFP (Below) in the VTA. White arrows indicate example EYFP+/TH+ neurons. 100

Figure 41 Selective targeted dopaminergic neurons in VTA by MscL-mediated ultrasound stimulation enable change mice's appetitive conditioning. (A) Examples path-tracing of a mouse with TH-cre-EYFP or TH-cre-MscL-EYFP expression during the appetite test (0.1 MPa ultrasound stimulation). A Red bar indicates the stimulation side. A White bar indicates the non-stimulation side. **(B)**

Percentage of time spent on the stimulation side at NUS, 0.1 MPa, 0.15 MPa pressure of ultrasound in EYFP and MscL mice. $n = 5$ mice in EYFP mice; $n = 5$ mice in MscL-expressing mice. ** $P < 0.01$, unpair two-tailed t -test. Data are mean \pm SEM..... 101

LIST OF TABLES

Table 1 Descriptions of ultrasound parameters. (Adapted from [87])..... 14

INDEX OF ABBREVIATIONS

Deep brain stimulation	DBS
Transcranial direct currents stimulation	tDSC
Repetitive transcranial magnetic stimulation	rTMS
Transcranial focused ultrasound stimulation	tFUS
Transcranial alternating current stimulation	tACS
Transcranial random noise stimulation	tRNS
Focus ultrasound stimulation	FUS
High - intensity focus ultrasound	HIFU
Low - intensity focus ultrasound	LIFU
Ultrasound	US
No Ultrasound stimulation	NUS
Dorsal striatum	dSTR
Cerebral cortex	CTX
Hippocampus	HIP
Nucleus accumbens	NAc
Subthalamic nucleus	STN
Substantia Nigra	SNc
Dopamine	DA
Ventral tegmental area	VTA
Electromyograms	EMG
Real time place preference	RPP

CHAPTER 1 Introduction

Over the past few decades, the frequency of application of brain stimulation through various novel modalities in both research and therapeutic contexts has increased. Brain stimulation technology offers a significant merit over drug therapy because its effect on cells or neural pathways is more specific and focused. The technique is now being explored as a potential treatment for serious neurological diseases and conditions, including Parkinson's disease (PD) [1], essential tremor [2], chronic pain [3], and epilepsy [4, 5]. As research progresses, however, the shortcomings of existing technologies have become increasingly noticeable. Deep brain stimulation (DBS) has demonstrated immense promise in the therapy of psychiatric and movement disorders, but is limited by the need to insert electrodes inside the brain tissue and its low spatial selectivity [6]. TMS and tDCS are non-invasive approaches used widely in clinical research, but they also lack the ability to target only specific areas in the brain [7]. The invasiveness and relatively low spatial precision of these techniques poses a significant risk to the eventual clinical translation of such therapies, as they could introduce points of failure or serious side-effects. Therefore, there is a long-standing need to develop non-invasive brain stimulation modalities that can achieve neuromodulation with better spatiotemporal resolution.

1.1 Brain stimulation

The structure and function of the brain are complicated. A typical human brain consists of 100 billion neurons and 10–50-folds more neuroglia cells [8]. Understanding how brain cells and circuits develop and explore, especially at the rapid thinking speed, and revealing the complicated connections between brain function and behavior remain

significant challenges in the field of neuroscience [9]. These challenges are exacerbated by the potential of individual neurons to play crucial roles in brain function. Dan et al. indicated that a repetitive high-frequency burst spike could evoke a unique cortical neurons in animals, eventually modifying global brain states [10, 11]. Neuromodulatory cells can release their transmitters (dopamine, Glutamate, GABA) or hormones (insulin, neuropeptide, somatostatin) either locally or at a long distance from their targets and thereby regulate brain function [12]. Cells dysfunction can cause imbalances in neurotransmitter release and affect the excitation-inhibition balance [13], resulting in related diseases. For example, PD is mainly resulted from by the reduction of dopamine (DA)-generating neurons in substantia nigra (SNc) [14], which changes the firing rate of the basal ganglia-thalamo-cortical motor pathway (Fig. 1) [15]. It has been indicated that high-frequency stimulation might suppress the neural activity of the subthalamic nucleus (STN) [16]. In fact, DBS of the STN has demonstrated to be an effective treatment for PD sufferers. In recent years, it has been suggested that cortical pyramidal cell elicited hyperactivity in the parkinsonian model could be decreased by either activating somatostatin neurons [17] or reducing the glutamate levels [13, 18] in primary motor (M1) cortical region. Therefore, understanding the functions of neurons and roles of brain circuits in regulation emotion, awareness, and behavior could help researchers and scientists develop effective methods with which to modulate specific neurons and neural pathways. It could also promote the development of therapeutic for neurological and psychiatric disorders and improve the quality of patients' lives.

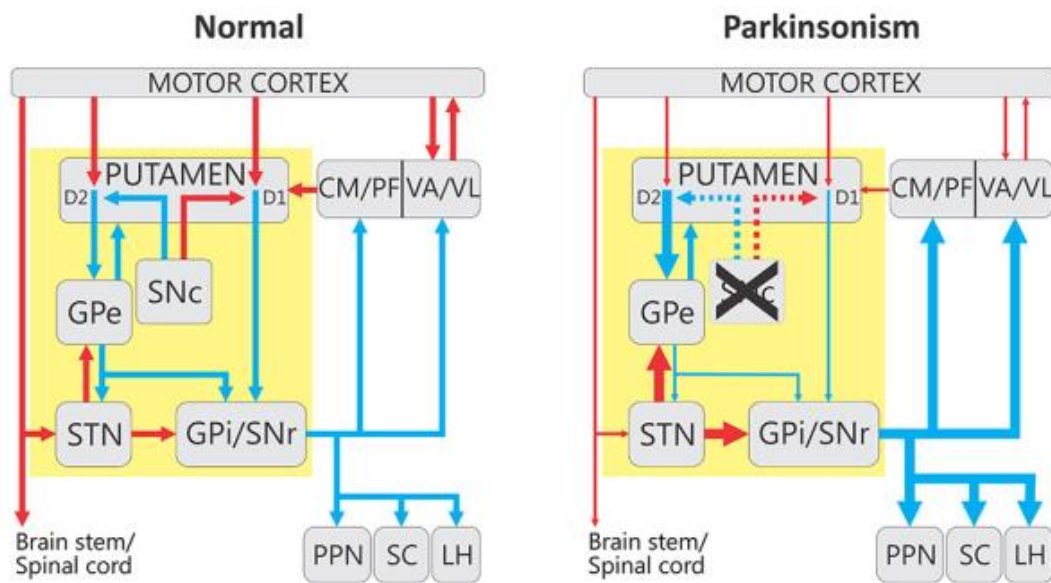


Figure 1 Diagram schematic of the basal ganglia circuit in a normal state and in parkinsonism. (Adapted from [15])

Neuromodulation has emerged as a promising way for investigating the neuronal function and neural pathways in the brain. It has been a long-standing goal to develop a technology that is non-invasive, selective, and has high spatial-temporal precision to achieve non-invasive and selective brain stimulation; this goal is closely tied to the aim of precise stimulation of specific neuronal types or sub-types involved in a given circuit to identify their roles in brain function. A variety of brain stimulation approaches, such as DBS, tDCS, repetitive TMS (rTMS), transcranial focused ultrasound stimulation (tFUS), tDSC, transcranial alternating current stimulation (tACS), optogenetic, and chemogenetics, have been developed and investigated over the past few decades (Fig. 2). However, all of the above methods either require surgical intervention, lack sufficient spatiotemporal resolution, or both [19]. The shortcomings of these techniques notwithstanding, the development of such novel neuromodulatory approaches has contributed to our understanding of brain function. An excellent example is

optogenetics, which uses light to control the activity of targeted cells that express light-sensitive ion channels or pumps and there by affect animal behavior [20]. Many neural circuits, such as those involved in learning, memory, fear, social behavior, and sleep, are now being examined using optogenetics [20-24]. However, the clinical applications of optogenetics are limited by the depth of light penetration into the brain and the requirement of the implantation of optical fibers in the brain.

Neuromodulation is also a novel technique in terms of medical treatment. Throughout the history, unconventional tools have facilitated scientific revolutions in multiple disciplines [25]. Several neuromodulation techniques have been applied to remedy neurological disorders and psychiatric diseases and, although these are not perfect, they have generally helped alleviate human suffering. For example, DBS is an outstanding method that is wildly used to alleviate the symptoms of PD and tremor but requires the implantation of an electrode in the brain [26, 27]. rTMS is another extraordinary technique that has been approved for the treatment of drug-resistant depression [28]. However, this method lacs sufficient selectivity. The development of non-invasive and selective neuromodulation modalities with high spatial-temporal precision is a critical requirement for the study of the structure and functions of neuronal circuits.

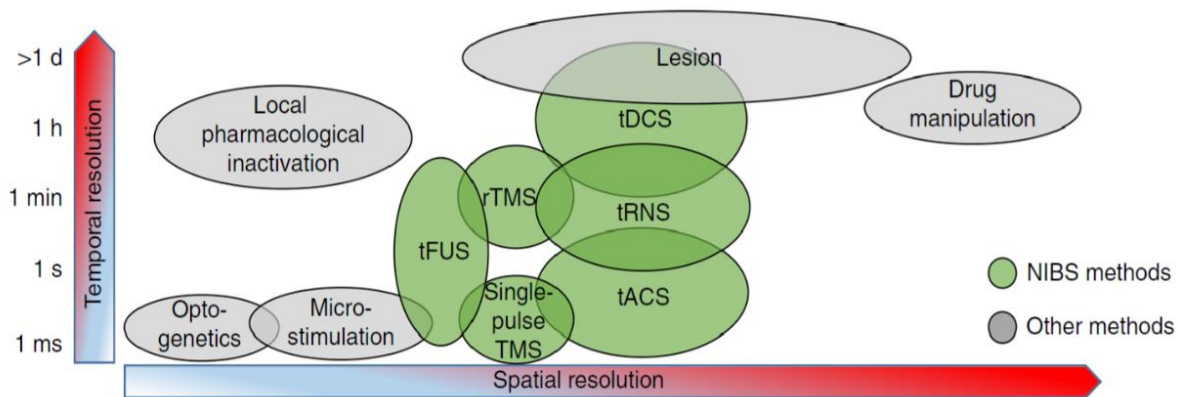


Figure 2 Summary of neuromodulatory methods based on spatial resolution and temporal resolution. (Adapted from [19])

1.1.1 Deep brain stimulation (DBS)

DBS is an effective neuromodulation approach that is prevalently utilized in the therapy of neurological and psychiatric disorders, such as PD [29], chronic pain [30], essential tremor [31], and obsessive-compulsive disorder [32]. This method requires opening the skull to access the brain and implant an electrode stereotaxically into STN or other targeted areas, depending on the characteristic of disease symptoms (Fig. 3) [33]. The electrical impulses stimulate the targeted brain area can adjust the chemical imbalances within the brain. This treatment can alleviate certain motor disorder symptoms despite the patients opposite action. DBS of the brain has been shown to be highly valid and to have much fewer adverse influences than drug therapy [34]. Many researchers are investigating the mechanisms by which DBS exerts its effects. For example, Deisseroth et al. utilized optical methods to target different brain regions involved in PD, indicating that afferents to the subthalamus might mediate the effects of DBS [35]. Additionally, some researches have proposed that the neuronal activity rates in globus pallidus internus (GPi) and STN are reduced during the DBS stimulation

[36, 37]. Recent studies have suggested that cortical regions are potential targets for the treatment of PD [13, 17].

However, DBS still poses significant challenges. First, clinical DBS stimulation protocols are invasive, as they require the implantation of electrodes deep inside the brain. This protocol is associated with several safety issues and potential side effects if implemented incorrectly. Second, the brain is highly heterogeneous and requires precise targeting to achieve the desired effects. DBS has some regional selectivity, but the range in which adjustments can be performed is limited after the electrode is inserted in the target region. Finally, the mechanism of DBS treatment is still unclear.

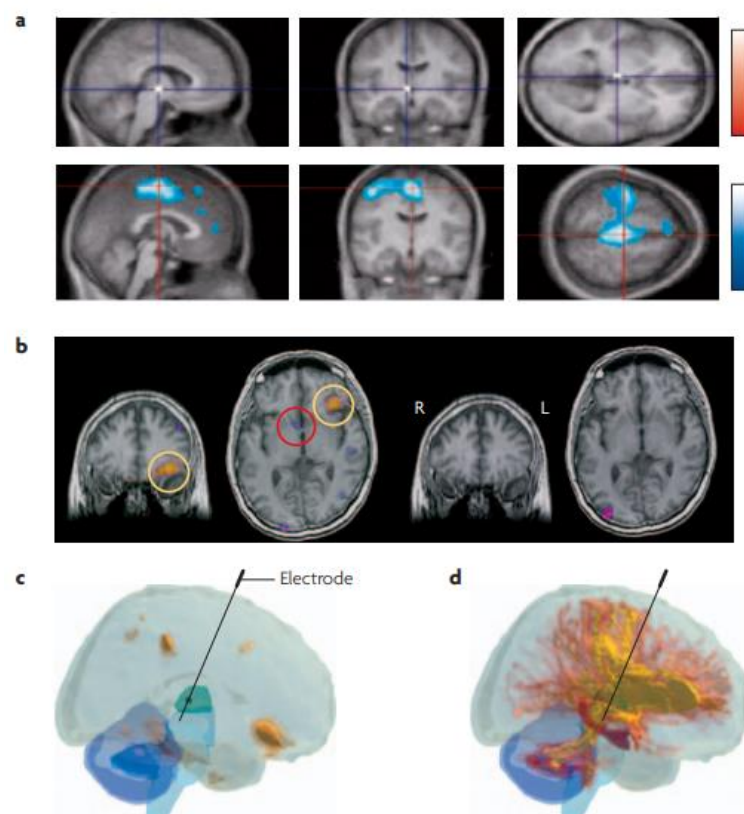


Figure 3 Neuroimaging scan of DBS. (Adapted from [33])

1.1.2 Transcranial Direct electrical stimulation (tDCS)

tDCS is a noninvasive neuromodulation method that passes a low electric current (≤ 1 mA) to an area above the target brain region through electrodes located on the scalp. In the past 20 years, two types of tDCS have been developed, conventional and high - definition tDCS [38]. tDCS manipulates the activity of neurons and neural pathways through the application of electrical currents. The neurons are treated with low DC, which modulated neural activity via a complicated series of long- or short-period effects on the target regions [39]. tDCS method can either excite [40] or inhibit [41, 42] neurons based on the DC delivered (Fig. 4) and is an important tool in the field of cognitive neuroscience [43]. Many studies have shown that tDCS can activate cells and increase neurotransmitters release, such as catecholamine [44], DA [45], gamma aminobutyric acid (GABA) [46]. tDCS therefore has the potential to treat Alzheimer's disease [47, 48] and schizophrenia [49, 50]. In addition, it has emerged as a potential modulator of psychiatric disorders, such as depression [51].

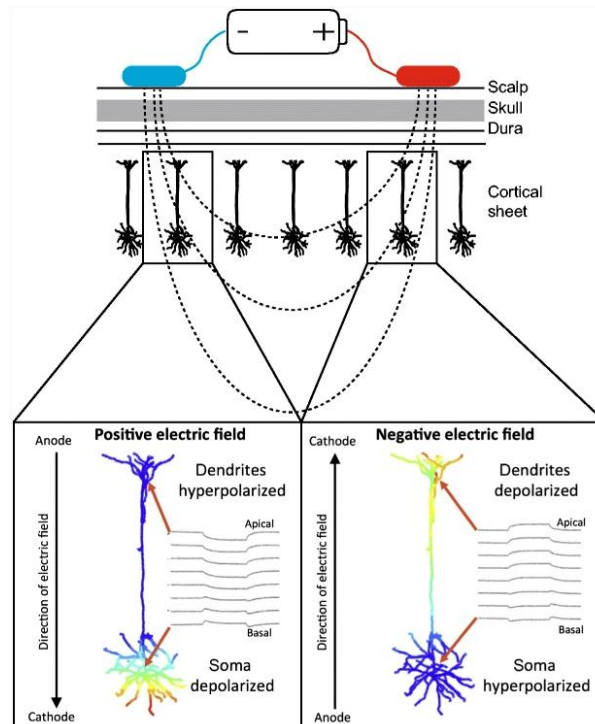


Figure 4 Diagram of the effect of tDCS electrical field on neurons. (Adapted from [43, 52])

To date, no clear side effects of tDCS have been reported. The most commonly reported effects of tDCS are tingling, itching, headache, and fatigue [53, 54]. Currently, tDCS is only used to target regions on the surface the brain, such as motor cortex, somatosensory cortex, and visual cortex [55]. The activation of deeper regions requires higher power, which might cause tissue damage. Therefore, tDCS should be studied in more detail before it is used in clinical practice.

1.1.3 Transcranial magnetic stimulation (TMS)

TMS is a promising experimental method that can non-invasively activate and thereby facilitate the study of surface brain regions, such as cortex, in both healthy and diseased individuals [56]. In this technique, a changing magnetic field is utilized to generate electric currents at a targeted brain region. A specialized coil is used to produce electrical currents that can pass all six layers of the cortex (Fig. 5) [57] and modulate neuronal activity. Some researchers have shown that the synaptic plasticity of the hippocampus can be either increased [58] or decreased [59] by controlling the frequency of stimulation. TMS can be used to both excite or inhibit the activity of cells [60-62], which implies that it has good diagnostic and therapeutic potential. A variety of studies have investigated the potential functions of low-intensity TMS and showed that TMS can be used to remedy an extensive range of neuropsychiatric diseases, such as depression [63, 64], chronic pain [65], and stroke [66]. TMS has already been approved for the therapy of drug resisted depression [67].

Recent research has focused on the development of novel materials such as nanoparticles, which can increase the sensitivity of cellular responses to low-intensity TMS. Xu et al. suggested that the intravenous injection of superparamagnetic iron oxide nanoparticles into rats might increase the responses of neurons to TMS [68]. In addition,

Zhang et al. combined TMS and the novel nanoparticles to selectively activate the prelimbic cortex, resulting in improvement of depressive-like symptoms in mice [69]. Earlier this year, Lee et al. used mechanosensitive ion channels (Piezo 1) to enhance the response of cortical neurons to magnetic m-Torquer stimuli and inducing locomotor movement [70]. However, major drawbacks of TMS include the low depth of penetration and spatial resolution (~ 1 cm) [71, 72]. Moreover, there is a possibility that long-term TMS excitatory stimulation may cause the seizure in humans [73].

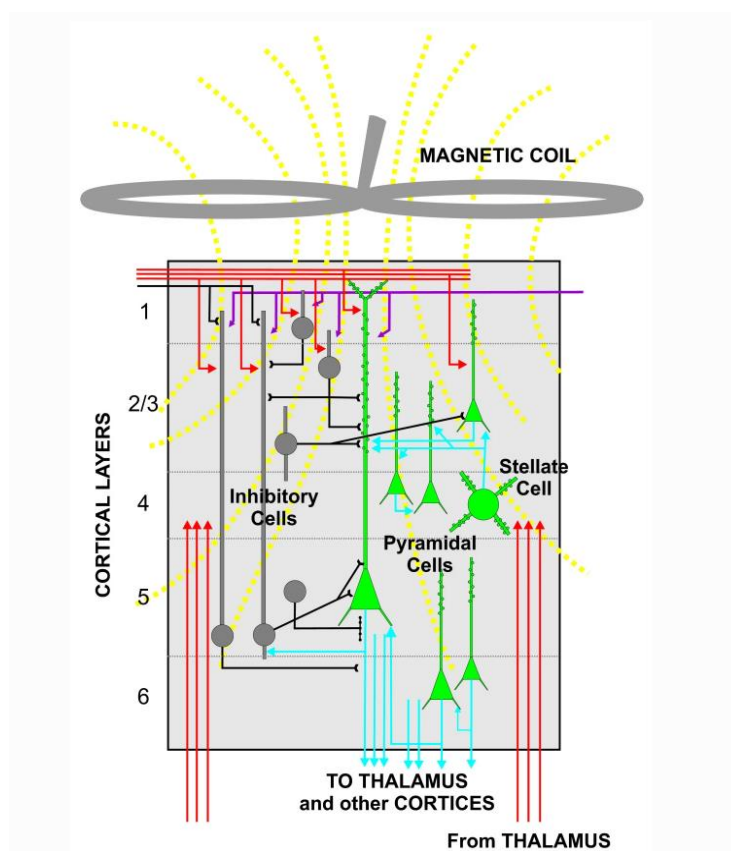


Figure 5 Schematic indication of the human cerebral cortex with TMS. (adapted from [57])

1.1.4 Optogenetic

Optogenetics technique is integration of genetic (light sensitive gene to target specific cells) and optical ways to excite or inhibit the clearly defined process in specific neurons of living tissue or in moving animals[74]. In mammals, after viral vectors'

injection, a light fiber implants to specific brain regions. 3-5 weeks later, this animal can be stimulated by light illumination fast and specifically and even as complex as freely moving mammals (Fig. 6A) [74, 75]. Using microbial opsin approaches, light can evoke inward currents and depolarize cell membranes, resulting in the activation of cells. While regulating the chloride ions can induce outward current and hyperpolarize the cell membrane, leading to inhibit the activity of cells [75-77] (Fig. 6B), and induce or suppress specific behavior in animal studies [78] (Fig. 6C). In recent years, optogenetics studies have expanded to the emotion, elucidating new insights about the pathways and mechanism that underlie reward [79], anxiety [80], some neurological and psychiatric disorders [81].

The technological advancements are expected to in the next coming years include upconversion nanoparticle-mediated optogenetics [82, 83], deep transcranial optogenetic [84] to enable deep brain stimulation and minimize the invasion levels. From previous research studies and preclinical trials, it is no doubt that optogenetics provides an effective approach of modulating cell activity and synaptic transmission and contributes to understand the neural circuits and poses the potential therapies for neurological diseases. Whereas the activation and inhibition by light stimulation require genetic alteration and fiber implantation. It has been reported that long-term expression of ChR2 in pyramidal cell in vivo caused generation of abnormal structure axon [85]. Essential safety and technical issues still limit the long term apply to be human.

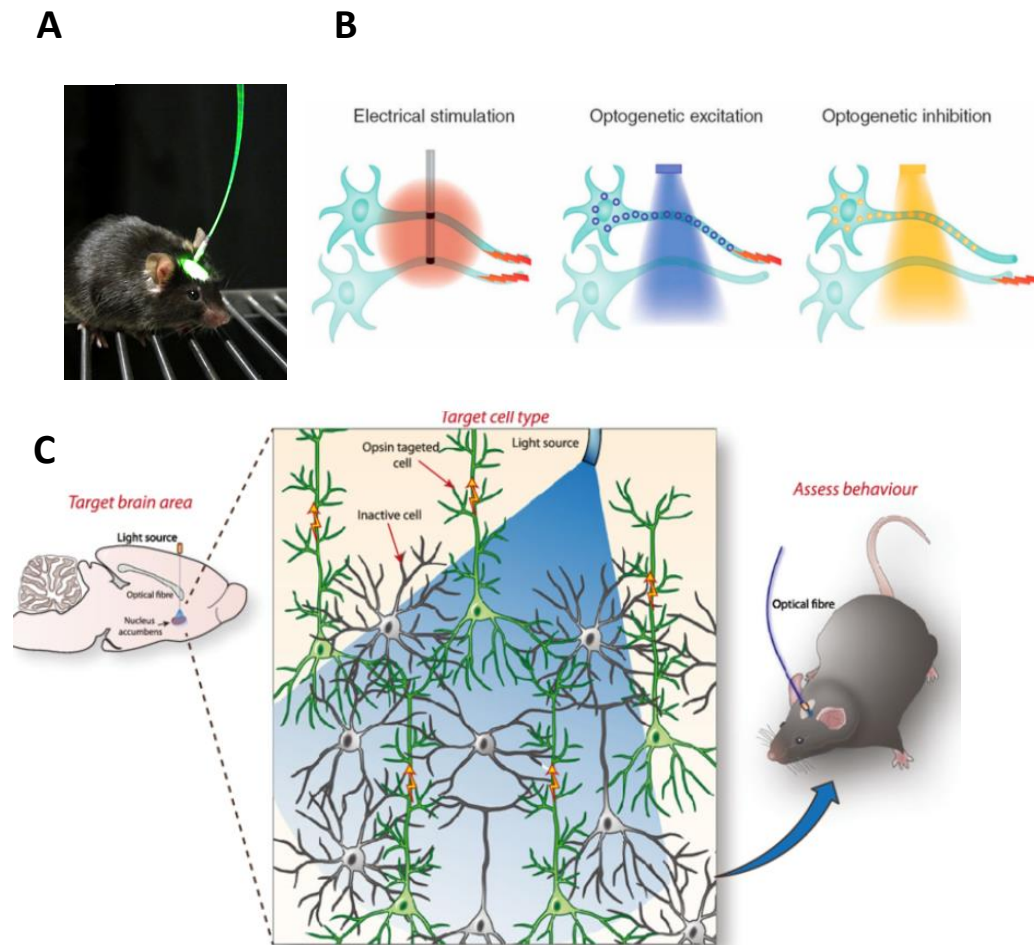


Figure 6 Illustration of optogenetic technique. (A) The model of optogenetic (Adapted from [74]). (B) A simplified version of basic properties of this three optogenetic tool family (adapted from [77]). (C) An illustration of one behavior probing using optogenetics (adapted from [78]).

1.2 Ultrasound stimulation

1.2.1 What is ultrasound?

Ultrasound is an interesting mechanical wave that carries a frequency beyond the range of human audition and passes the acoustic pressure from one location to another in a non-invasively manner and at a high depth penetration [86]. The ultrasound parameters depend on several elements such as fundamental frequency, intensity, pulse

repetition frequency, duty cycle, duration, (Fig. 7 and Table 1 [87]).

a. Fundamental frequency refers to the number of oscillation cycles/unit time. The 1–20 MHz range is defined as high-frequency ultrasound, which is used in medical applications, such as diagnostic techniques. The 0.7–3 MHz range is defined as medium-frequency ultrasound, which is used for therapeutic applications. Industrial or low frequencies fall in the 20–200 kHz range. The penetration efficiency depends on the fundamental frequency, which is related to the spatial resolution of the ultrasound. Higher frequencies can produce a deeper focus and achieve better spatial precision. However, high frequencies might attenuate the ultrasound energy and transform it to heat, which can spread to surrounding areas. The ultrasound efficiency can be optimized by regulating the fundamental frequency to fall within the required range.

b. Intensity is the sound energy produced by ultrasound. It is commonly represented as the spatial peak pulse average intensity. Intensity is one of the main elements of US bioeffects. Based on the intensity, focused ultrasound stimulation can be defined as either high-intensity focus ultrasound (HIFU) and low-intensity focus ultrasound (LIFU). The intensity of HIFU ranges from 100 W/cm² to 10000 W/cm² and is widely used in medical applications such as tumor ablation [88]. LIFU has intensities < 3 W/cm² and is used to reversibly manipulate neuronal activity as it only induces small changes in temperature [89].

c. Duration refers to the time period from the starting of the first pulse to the end of the last pulse. Previous research has suggested that a long duration

of ultrasound stimulation can induce inhibitory responses, whereas a short duration has excitatory effects on cortical neurons [90].

d. Duty cycle indicates the number of ultrasound cycles in one pulse. By modulating the duty cycle, sonication can be used to deliver either completely continuous patterns without any interruptions or pulsatile patterns with set intervals.

e. PRF is the number of pulses transmitted per unit time at a fundamental frequency [91] and determines the strength of acoustic pulse delivery.

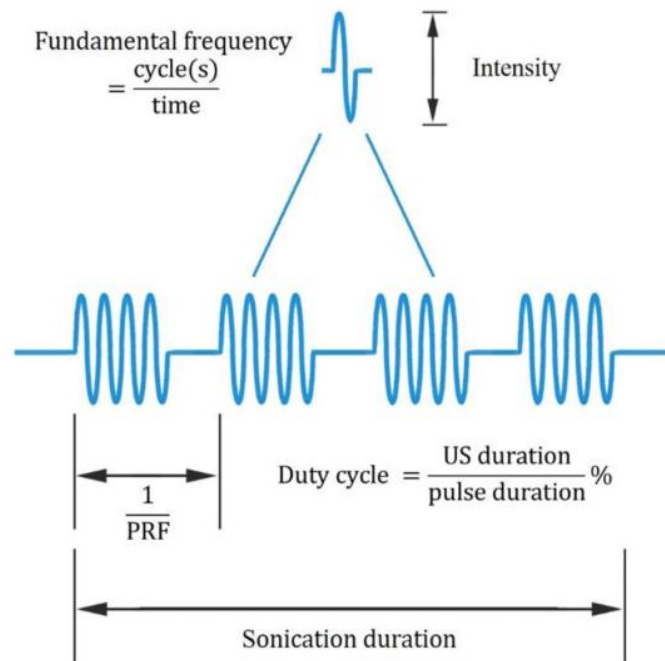


Figure 7 Detailed information about ultrasound parameters. (adapted from [91])

Table 1. Definitions of ultrasound parameters

Parameter	Abbreviation	Unit
Frequency	f	MHz
Pressure (peak instantaneous)	p	MPa
Intensity: spatial-peak, pulse-averaged	I_{SPPA}	W/cm^2
Intensity: spatial-peak, burst-averaged	I_{SPBA}	W/cm^2
Intensity: spatial-peak, temporal-averaged	I_{SPTA}	mW/cm^2
Pulse length	PL	ms
Pulse repetition frequency	PRF	Hz
Burst duration	BD	ms
Burst repetition frequency	BRF	Hz
Burst duty cycle	BDC	%
Burst interval	BI	s
Inter-stimulus interval	ISI	s
Total duty cycle	TDC	%
Number of pulses/bursts/trials	N	—
Total time	TT	s
Mechanical index	MI	—
Thermal index	TI	—

Table 1 Descriptions of ultrasound parameters. (Adapted from [87])

The effects of ultrasound stimulation primarily depend on the above factors. A clear understanding of these ultrasound parameters can help us better apply this technique in different contexts.

1.2.2 Bioeffects of ultrasound

Since World War II, ultrasound has been conventionally used in medicine and industry. The common applications of ultrasound in medicine includes diagnosis imaging, bone therapy, drug delivery, and tissue ablation [92, 93]. Recent advances in ultrasound have made it a promising technique for neuromodulation, which can be achieved by adjusting certain ultrasound parameters to produce diverse outcomes such as heat [94], cavitation [95], and mechanical force [96] (Fig. 8).

Heat is produced due to absorption and scattering as the ultrasound propagates in attenuation mode. The thermal effects of ultrasound are commonly used in medical

applications, as these are known to change tissue properties by reversibly reducing synaptic transmission or irreversibly inducing protein denaturation [97]. HIFU has been used to irreversibly and thermally ablate abnormal tissue in specific brain regions [98], the pancreas, liver, and breast. In addition, ultrasound is compatible with magnetic resonance (MRI), which can guide ultrasound waves to deep brain stimulation to treat movement disorder [99], obsessive-compulsive disorder (OCD) [100], major depressive disorder (MDD)[101], and chronic pain [102, 103]. This combination of techniques can balance abnormal neural activity in the brain by ablating specific target regions. Hyperthermia treatment requires cells to be maintained at 43–50 °C for 1 h [97]. In contrast, LIFU exerts little temperature change and can be used to reversibly inhibit and activate neuronal activity [89]. LIFU has received increased amounts of attention as a brain stimulation modality.

Cavitation is caused by the effects of high-frequency ultrasound on liquid media, which results in the formation of microbubbles. However, very few studies have shown the production of cavitation during LIFU. The type of cavitation achieved in such cases is generally non-inertial cavitation, in which microbubbles maintain steady, dynamic, and inertial cavitation. When the bubbles rupture, movement is initiated by the inertia of the liquid. The occurrence of such phenomena is multi-factorial and depends on the intensity, frequency, duty cycle, and gas used [104]. Acoustic cavitation has been used to transport both small and large molecules (including proteins and DNA) [105]. Controlling cavitation production has also been applied to target disable tissues such as the brain, eyes, and skin [106].

Acoustic radiation force is a primary non-thermal bioeffect of ultrasound. It occurs as a consequence of the transfer of momentum from propagating acoustic waves to the tissue through which it propagates, due to certain absorption and scattering mechanisms

[107]. The mechanical force on the BBB exerted by the surface blanking of microbubbles in the blood vessels as a result of focused ultrasound instantaneously increases the permeability of the barrier and allows drug delivery. Lipsman et al. demonstrated a method that used MR-guided FUS to open the blood brain barrier (BBB) in sufferers with Alzheimer's disease (AD), facilitating the development of novel therapeutics for patients with neurological diseases [108]. Other studies have shown that LIFU can activate Na^+ , Ca^{2+} , and K^+ channels without increasing the temperature [109, 110]. In addition, it has been shown that *Caenorhabditis elegans* in which lacked MS channels failed to respond to LIFU [111]. Shapiro et al. demonstrated that FUS can be used to activate cortical neurons through the action of MS ion channels and amplifiers [112]. In recent years, acoustic radiation forces have come to be recognized as promising candidates for use in neuroscience and therapeutics.

To conclude, the outcomes of ultrasound mainly depend on the fundamental frequency, intensity, duration, duty cycle, and PRF. Therefore, one must carefully consider and select ultrasound parameters based on the required application.

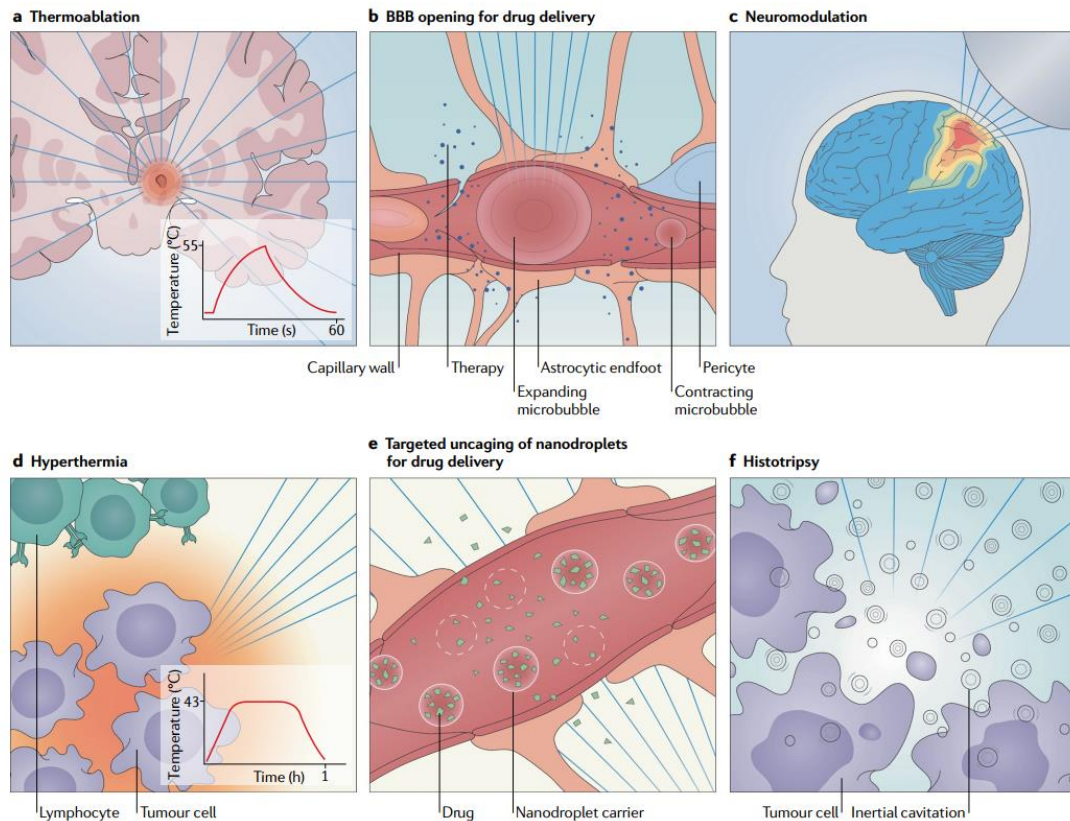


Figure 8 Diverse biological outcomes from ultrasound stimulation. (Adapted from [93])

1.2.3 Research on ultrasound brain stimulation

Over the past several decades, ultrasound has been used in clinics for diagnosis and imaging. The mechanical forces generated by ultrasound are now receiving attention as a promising method for non-invasively controlling neuronal activity in the central nervous system, manipulating behavior [113] and potentially treating cognition disorders [114]. Importantly, the safety of LIFU has been tested in human studies, and no obvious significant adverse reactions have been reported in the participants [115]. In addition, many animal studies (mice, macaques, and sheep) have used histological staining methods to examine the safety of transcranial FUS neuromodulation, all of which have found that FUS does not cause tissue damage [116, 117]. The safety of the

method therefore makes ultrasound an appealing neuromodulation technique.

An interesting human study (Fig. 9A) conducted in 2013 found that subjecting participants experiencing negative emotions to LIFU for appropriate durations could improve their emotions, indicating that FUS can safely exert neurophysiological influences on the function of brain and offering a hopeful noninvasive treatment for manipulating conscious and unconscious physical states and diseases [118]. In addition, it has been reported that ultrasound delivered to the somatosensory cortex of human can modulate brain activity (Fig. 9B) and enhance performance in sensory tasks without a response bias [119]. Importantly, unlike other methods, ultrasound stimulation is compatible with functional MRI (fMRI). By harnessing this property, the impacts of ultrasound stimulation on the brain of human have been examined using fMRI. The study found that ultrasound stimulation might not only excite the target region (such as the visual cortex in humans) but also affect optical and higher-order cognitive processes [120]. MR-guided FUS is extensively used in neurosurgery. However, before applying the technique to therapeutics, detailed experiments are required to elucidate the mechanisms and functions of ultrasound stimulation.

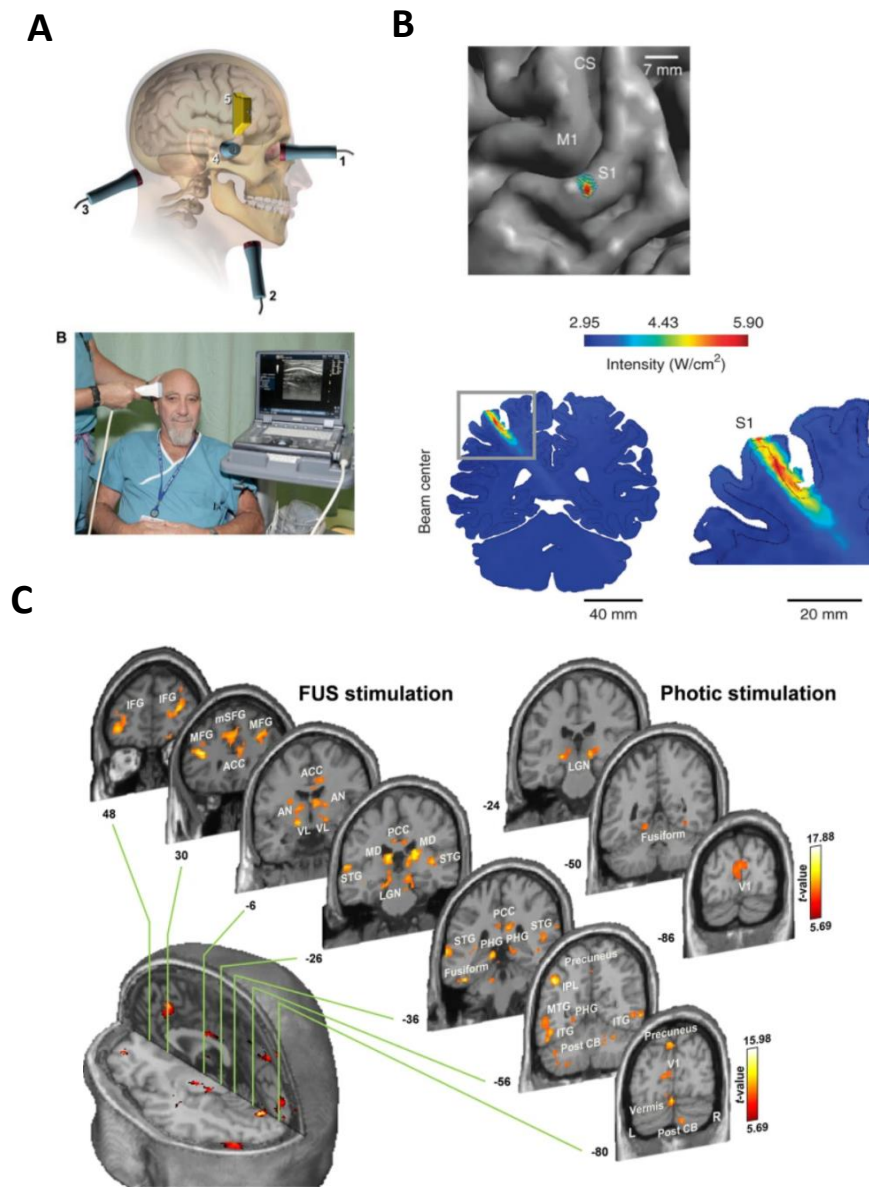


Figure 9 Examples of ultrasound stimulation applied to human. **(A)** Illustration of sites for transcranial ultrasound (TUS) (top). An example human module showed transcranial ultrasound application (below) (adapted form [118]). **(B)** Transcranial focus ultrasound stimulation can be targeted to the specific area (such as somatosensory cortex) in the human cortex (adapted form [119]). **(C)** fMRI data showed focus ultrasound stimulation evoked not only the targeted region (visual cortex) neural activity, but also affected other brain regions (adapted form [120]).

The effects of ultrasound stimulation have also been investigated in animals such as *C. elegans* and macaques. Ultrasound stimulation has been applied to cortical regions to elicit motor-related movements in the whiskers, tails, and limbs of rats [121, 122]. Min et al. controlled the levels of neurotransmitter through the thalamocortical pathway by stimulating the thalamus with US [123]. The effects of ultrasound stimulation on the corticospinal and thalamocortical circuits indicate that it can facilitate the treatment of clinically relevant diseases. LIUS has also been indicated to successfully control behavior in non-human primates [124]. A significant advantage of Ultrasound stimulation method is that it can be compatible with fMRI system, which helps guide ultrasound wave pass to targeted regions in the brain spatially and monitor the effects of sonication on the brain. Under fMRI guidance, ultrasound has been applied to specific brain regions in rabbits and used to alter the activity of the somatomotor and visual regions, as recorded using electrophysiological and functional brain mapping techniques [125]. In addition, fMRI can be used to monitor specific neural pathways, diagnosis the pathologic change and detect the effect of ultrasound stimulation. fMRI technology can therefore help us better understand the mechanisms that underlie ultrasound stimulation.

Despite these observations, several researchers have argued that the motor response caused by ultrasound stimulation might not arise due to the direct activation of motor cortical regions and might reflect indirect sensory effects (such as an auditory effect). Recently, two groups of researchers used different experimental designs to test opposing hypotheses. One group believed that low-intensity ultrasound affected the cortical neuron in mice [126] or guinea pigs [127] through indirect auditory mechanism and not through direct on motor cortical neurons. They also proposed that the frequencies of ultrasound stimulation applied to the animals were inaudible, but that

the ultrasound waves produced vibrations in the brain and skull that could pass to the ears. In contrast, the other group demonstrated that the cortical neurons responded to ultrasound stimulations even in deaf mice [128]. Another study used a fiber-optoacoustic converter to stimulate the somatosensory cortex and observed a robust local field potential in the ipsilateral somatosensory cortex, but they failed to induce any responses in the contralateral auditory cortex [129]. In addition, a primate study excluded the auditory involvement by showing that the impact of a 40-s ultrasound stimulation could last for as long as 1 h [130]. Collectively, the above data suggest that ultrasound stimulation directly affects the motor cortex and does not involve the auditory pathway.

A major challenge facing ultrasound stimulation is a lack of detailed information on the molecular, cellular, and neuronal mechanisms underlying the phenomenon. The brain has various types of cells, many of which endogenously express MS proteins. Therefore, an understanding of the physiological composition of each cell type might help accurately determine the ultrasound parameters required to achieve the desired activation or suppression effects. Understanding the mechanism of the ultrasound effect could also help selectively manipulate human brain function and accelerate the progress of ultrasonic neuromodulation and sonogenetic technique as useful toolkits in neuroscience.

1.3 Mechanisms and Sonogenetics

Compared with established brain stimulation methods such as DBS, optogenetics, and TMS, ultrasound stimulation has the unique advantage of non-invasiveness, which allows the delivery of sound waves to large depths and at high precision via a curved transducer placed inside the brain. However, ultrasound stimulation lacks sufficient cell-type selectivity and spatial resolution, and the fundamental mechanisms by which

it exerts its effects on the brain remain largely unknown.

As mentioned above, ultrasound can produce several physical effects, such as heat, cavitation, and mechanical forces, each of which can elicit different bioeffects [91]. Each bioeffect acts through distinct mechanisms, which amplifies the challenges of studying the general mechanisms of ultrasound stimulation (Fig. 10). Tyler et al. found that certain ultrasound parameters could open voltage-gated ion channels and generate action potentials in acute brain slices [110]. The mechanism of the heat effect has been suggested to happen through the propagation of ultrasound across the cell membrane, which would cause the ultrasound amplitude to decrease as its power is transformed into heat. Cavitation depends on the presence of microbubbles, which can change the cell membrane potential when subjected to ultrasound stimulation. Neuromodulation via mechanical forces generated by ultrasound is believed to involve MS ion channels. Shapiro et al. [112] recently provided a comprehensive explanation for the same, which states that FUS excites cortical neurons through the action of a Ca^{2+} MS ion channel. They tested this hypothesis by pharmacological and genetic inhibition and found that the TRPP2 and TRPC1 channels played more important roles in responding to ultrasound stimulation than other MS ion channels, such as Piezo1 and TRPP1 (Fig. 10B). These proteins are therefore potential candidates for sonogenetics. These proteins might be candidates of sonogenetic technique.

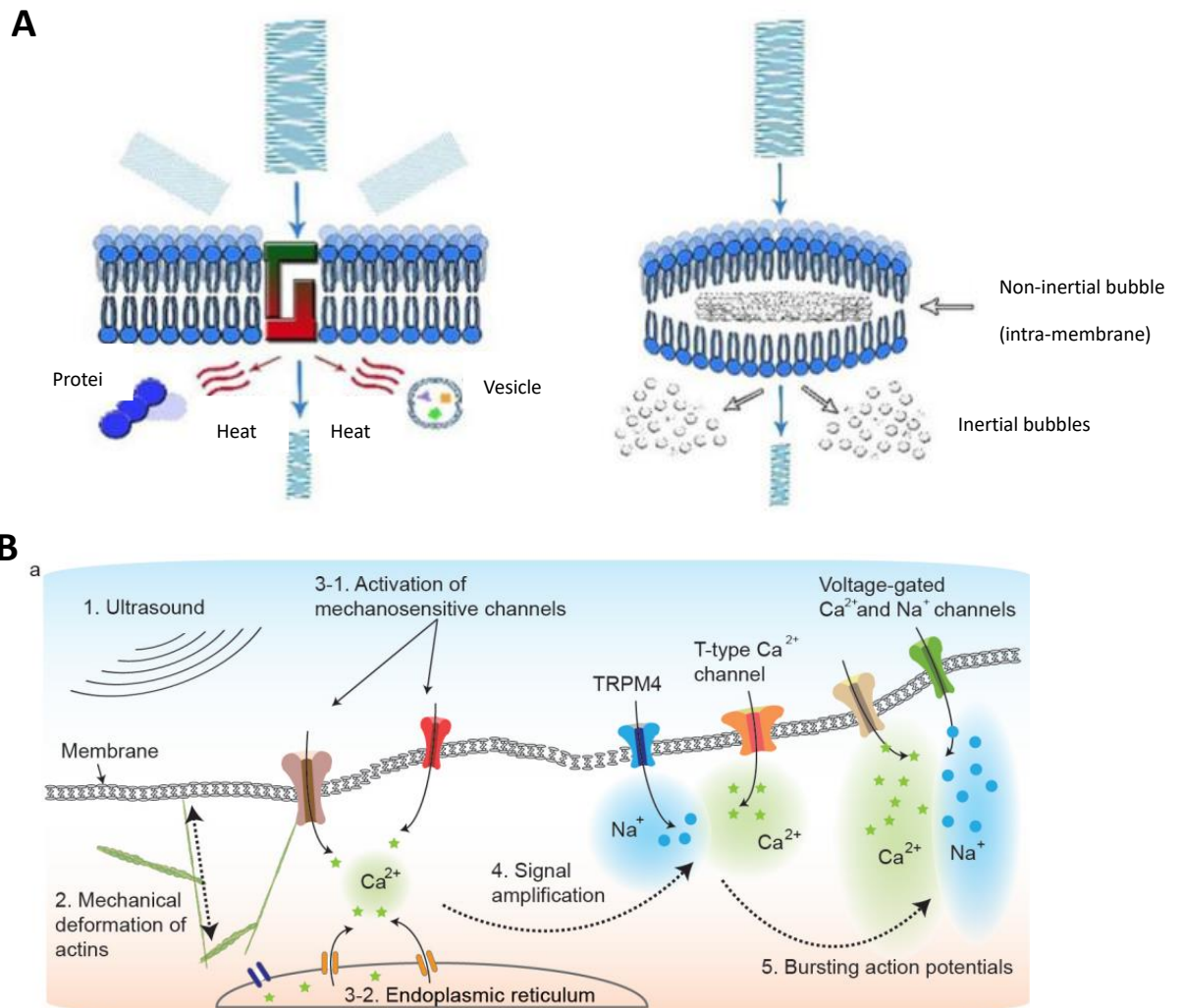


Figure 10 Mechanisms of ultrasound stimulation. (A) Diagram showed the potential mechanism of ultrasound in heating (Left panel), cavitation (Right panel). (Adapted from [91])

(B) Representative diagram of molecular circuits activated through mechanical force [112].

As MS ion channels have been found to mediate ultrasonic neuromodulation, sonogenetics has been proposed as a promising modality in this context. Sonogenetics, which is the manipulation of gene expression using ultrasound, was first proposed as a concept by Ibsen et al. in 2015 [131]. The misexpression of TRP-4, a MS ion channel, in *C. elegans* neurons sensitized the cells to ultrasound stimulation and resulted in behavioral changes in the worms [111, 131, 132] (Fig.11). The concept of sonogenetics is very similar to optogenetics, which is more well-established and uses light-sensitive proteins (opsins) to increase the sensitivity of neurons to optical stimulation. Sonogenetics uses ultrasound to modulate neurons that express MS ion channels. Compared with optogenetics, whose application is limited by the depth of light penetration, volume of light stimulation, and requirement of fiber implantation, sonogenetics is more advantageous in that it can provide deeper penetration without surgical intervention [91]. Sonogenetics is therefore an emerging non-invasive modality for cell-specific neuromodulation.

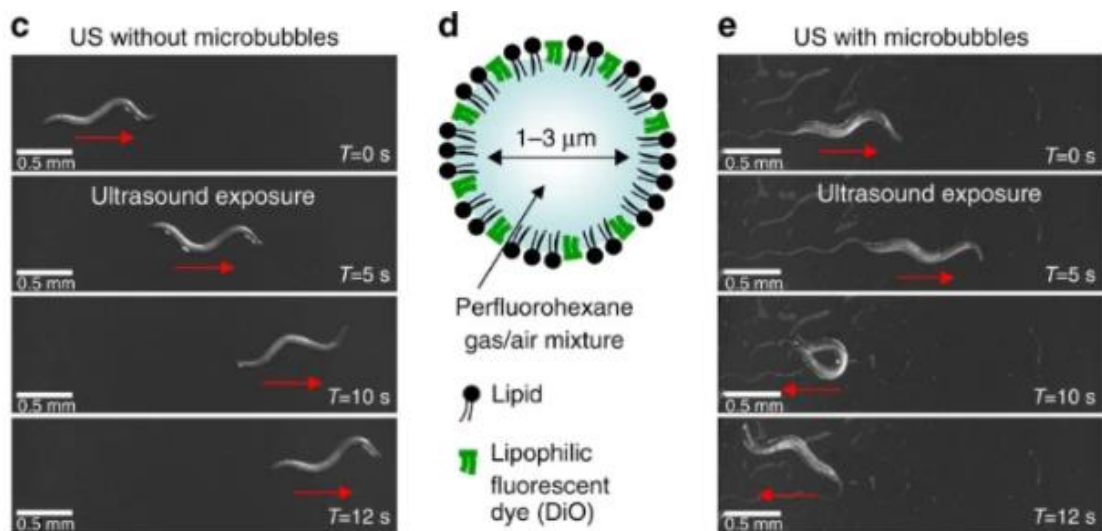


Figure 11 Illustration of *C. elegans* response to ultrasound stimulation in the microbubble environment which can enhance ultrasound signals. (Adapted from [131])

There are four major steps in sonogenetics [133-137]. 1) insertion of genes encoding MS ion channels into a viral vector (adeno-associated virus or lentivirus); 2) transfection of the cells with the integrated viral vector or injection of the viral vectors into specific brain regions; 3) expression of gene(s) from the viral vector for the required duration and application of low-intensity ultrasound stimulation; and 4) recording of neuronal activity and examination of behavior (Fig. 12A).

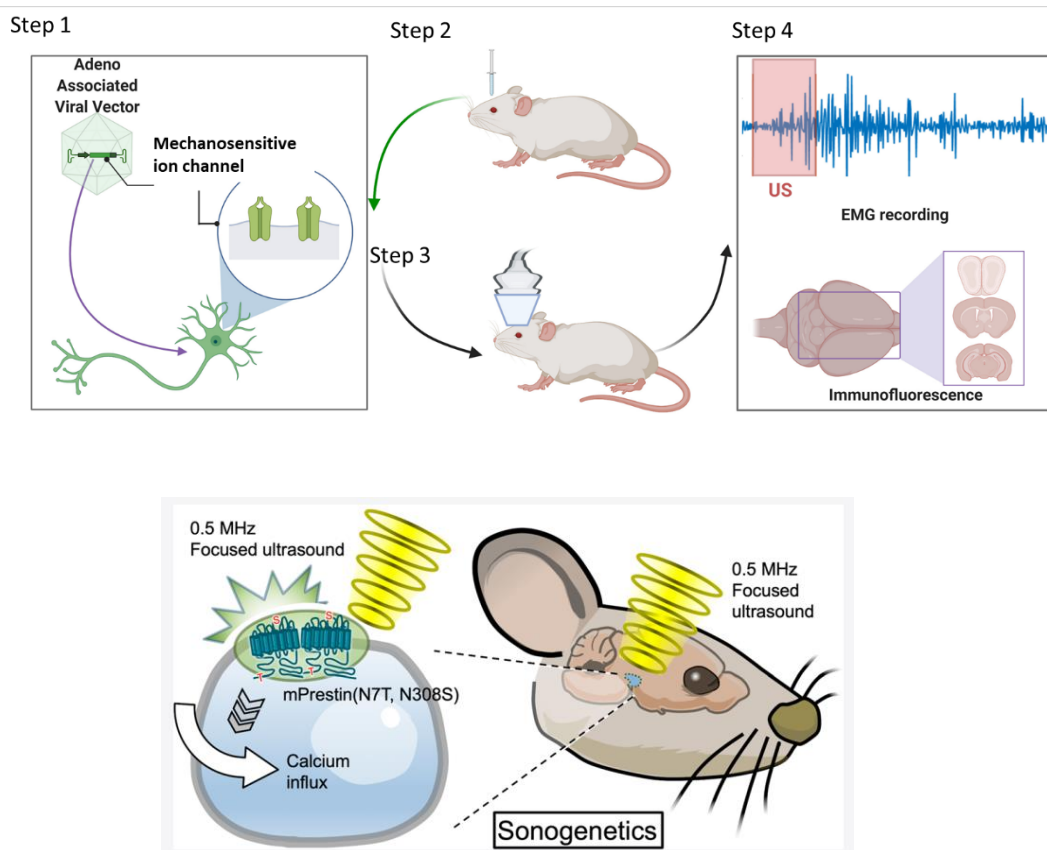


Figure 12 Diagram of the process of sonogenetic technique. **(A)** The mainly experimental steps of sonogenetics method (Adapted from [137]). **(B)** An example of sonogenetics method. (Adapted from [134])

Recent studies have investigated the applicability of several MS ion channels in sonogenetics. Potential MS proteins that can be used to sensitize cells include Piezo1 [138, 139], TRPC1 [112], mPrestin [134], MSCs: MscL [136, 140], TREK-1/2

[141, 142], TRAAK [143], TRPP1/2 [112], *hsTRPA1* [133] and so on. One example described the function of mechanosensitive ion channel was mPrestin (Fig.12B) [134], which was induced to express in ventral tegmental area neurons in mice. An ultrasound stimulation of 0.5 MHz could activate these neurons by inducing the influx of Ca^{2+} ions into the cells. In addition to mechanical sonogenetics, TRPV1, a temperature-sensitive ion channel, has also been used to enhance neuronal sensitivity to heat, which can be produced by ultrasound [135]. Many studies have shown the *in vitro* effectiveness of sonogenetics, and preliminary animal studies have suggested that these channels can be activated in the animal brain by sonication. However, these studies have neither clearly described the performance characteristics of such channels nor demonstrated significant behavioral effects. Before sonogenetics is widely adopted by researchers, more detailed *in vivo* experiments must be conducted to gather evidence of robust behavioral influences and understand the underlying mechanisms.

1.4 Challenges and research objectives

As mentioned above, a variety of neuromodulation techniques have the potential to be used as therapeutics. However, current neuromodulation methods do not satisfy the clinical requirements of non-invasiveness, effectiveness, and minimal surgical risk (Fig. 13). Ultrasound has been recognized as one of the safest and most versatile tools for this application, and it merges the fields of physics, imaging, engineering, biology, and neuroscience. Ultrasound is an alternative technology under current study, as it is significantly less invasive and offers the prospect of spatially - focused neuromodulation in deep brain regions without the need for implantation. Ultrasound has been shown to be capable of achieving neuromodulation in multiple model organisms, such as rats [121, 144], rabbits [125], sheep [145] and monkeys [124]. Further, it has been used to safely targeted human brain regions, such as the motor

cortex [114], somatosensory cortex [119] and primary visual cortex [120].

Parameter specify	Deep brain stimulation (DBS)	Transcranial current stimulation (tCS)	Transcranial magnetic stimulation (TMS)	Low intensity focused ultrasound stimulation (LIFU)
Invasiveness	Invasive	Noninvasive	Noninvasive	Noninvasive
Spatial resolution	~1 mm	Undetectable	~3-5 cm	Depending on the frequency 1-5mm
Depth of stimulation	Unlimited	Undetectable	~1-1.5 cm unless H-coil is used	10-15 cm or more
Duration of reversible effect	~5 s	24 h	~5 s	~10-40 min
fMRI brain mapping	Difficult	Difficult	Very difficult	Easily possible

Figure 13 Merits and demerits of common neuromodulatory methods. (Adapted from [89, 146])

However, the mechanism by which ultrasound exerts its effects on the brain is complex, as the technique has several bioeffects. The ultrasound parameters depend on several major elements [147] that can result in either thermal or non-thermal effects. It is therefore difficult to determine the detailed biophysical mechanisms of ultrasound stimulation. A major obstacle to studying the biophysical and cellular mechanisms of ultrasound is that when cells are grown *in vitro*, they are cultured on hard substrates such as plates that make it difficult to conduct electrophysiological experiments. The vibrations generated by ultrasound might vibrate the recording electrode and cause the cells to rupture. In recent ultrasound *in vitro* studies, researchers used soft or acoustically transparent substrates to record cellular responses to weak-intensity ultrasound stimuli, both in two-dimensional and three-dimensional culture conditions [112, 136]. However, to further ascertain the temporal resolution and profile of ultrasound effects, a recording method compatible with low-frequency ultrasound is required. Another essential question concerning ultrasound stimulation is its specificity and potential side effects. Ultrasound by itself lacks the selectivity required for targeted stimulation. It has been reported that cortical neurons contain many types of MS ion

channels, and astrocytes and microglia have also been shown to express Piezo1. It is therefore difficult to distinguish the cell types that respond to ultrasound.

Furthermore, the architecture of the brain encompasses the molecular interactions of trillions of synapses and billions of cell bodies, all of which are connected to compose local circuitries that are integrated into numerous brain areas. Moreover, brain circuits are not static but constantly change with neural activity and age and across developmental periods. Revealing how the brain functions therefore remains an extraordinary challenge. The outstanding modality of optogenetics has played an important function for advancing our knowledge of brain function and dysfunction. Unfortunately, many of these methods cannot be used in humans. Aside from methods that use ultrasound alone, researchers have developed sonogenetics, which is analogous to optogenetics and uses heterologously-expressed MS ion channels in target cells to mediate ultrasound stimulation [131]. The preferential expression of these channels in specific cells has been shown to enable efficient and region-specific neurostimulation, both *in vivo* and *in vitro* [112, 139], [134] [121, 136] [131, 141-143]. Notably, sonogenetics offers the prospect of a non-invasive treatment with deeper penetration capabilities than optogenetics. It might open a new door into how the brain records, processes, stores, recalls the large amounts of information.

Current studies on sonogenetics are still preliminary and have shown neurostimulatory effects through cellular investigations. Most *in vivo* studies of sonogenetics have been limited to testing neuronal activity by performing c-Fos staining and verifying motor responses under anesthesia. However, rigorous characterizations of these treatments and demonstrations of significant behavioral effects remain to be reported. The precise control of circuit operations to determine the dynamic circuits relevant to specific behaviors can help us better understand brain

function. Moreover, the modulation of animal behavior through sonogenetics could enhance our understanding of both fundamental and pathological neuronal processes and facilitate the development of novel therapies for neuropsychiatric diseases.

In this project, I aim to utilize an MS ion channel (MscL-G22S). Below we abbreviate MscL-G22S as MscL) to investigate MscL-mediated ultrasound stimulation and validate it in both anesthetized and freely - behaving mice using well-defined neural circuits and behaviors. To achieve this aim, I plan to:

1. Explore four well-defined brain regions (primary motor cortex, barrel cortex, dorsal striatum, VTA) using related behavioral paradigms.
2. Characterize the spatial distribution of MscL-mediated ultrasound-evoked activity in the intact brain.
3. Combine the ultrasound stimulation system with fiber photometry to examine the real-time effects of MscL-mediated ultrasound stimulation *in vivo*.
4. Test the influence of MscL-mediated ultrasound stimulation parameters on the above-mentioned four neural pathway responses.

CHAPTER 2 MscL-mediated ultrasound activates corticospinal motor circuits in anesthetized mice

In our previous study, we indicated that the capability of mechanosensitive ion channel (MscL) to sensitize cells and neurons to ultrasound stimuli *in vitro* [136]. In addition, evaluated by the important activation marker c-Fos, compared to the control group, MscL-expressing cells in cortical regions showed obviously larger neural activation when treated with low-intensity sonication [136]. In this project, we aimed at test the feasibility of our US protocol by stimulating mouse specific brain region expressing MscL. We first determined whether MscL-mediated neuronal activation in the motor cortex could induce behavior changes using the fine-wire electromyograms (EMG) method, measuring the EMG signals of the triceps in anesthetized mice upon ultrasonic stimuli.

2.1 Materials and methods

2.1.1 Animal subjects

Male, 6-8 weeks old, C57BL/6 mice, were used for this study. Animal were raised under standard housing condition with food and water available *ad libitum*. Mice usage and consideration were conducted based on the guidelines of the Department of Health - Animals (Control of Experiments) of the Hong Kong S.A.R. government.

2.1.2 Stereotaxic injection

Adult C57BL/6 mice were anesthetized by 10 mg/kg xylazine and 100 mg/kg ketamine. In EMG recording experiment, 1 μ l viral vectors (AAV-CamKII-EYFP or AAV-CamKII-MscL G22S-EYFP) were micro-injected into the primary motor cortex

region at the coordinate of DV -1.00 mm from the brain surface; AP 0.25 mm, ML - 1.50 mm, from Bregma, at the speed of 0.1 μ l per / min through an injection pump with a micro-syringe. The micro-syringe was paused in the injection region for additional 10 min before gently withdrawal. Mice were returned to their housing areas for recovery.

2.1.3 EMG recording in anesthetized mice

In vivo anesthetized recording of US-evoked EMG from mice: After four-week viral vectors expression, mice with either CamKII-EYFP or CamKII-MscL-EYFP viral vectors in their primary motor cortex were anesthetized appropriate isoflurane. Eye ointments were applied to eyes. A 0.5 MHz US transducer was located above the targeted region coupling with US gel. Ensured no bubble in the US gel. Exposed the left triceps with the surgical instrument. Two electrodes were implanted into the exposed triceps to monitor bioelectric potential change between the muscle tissues. A ground wire was contacted to the mouse's tail. Total five trials of ultrasound stimulation (0.05 – 0.5 MPa) were delivered upon each mouse. Each trial comprised of 7 – 10 times sonication. The interval of each ultrasound stimuli was 5 s. Mice were allowed to rest for 1 min between each trial's ultrasound treatment. EMG raw data was recorded by a multi-channel signal acquisition system (Medus, Bio-Signal Technologies). The data were processed with a customized MATLAB script (The MathWorks, Inc.).

2.1.4 Experiment setup for the ultrasound brain stimulation.

The acoustic components are consisted of a function generator (Tektronix), a power amplifier (Electronics & Innovation Ltd), and ultrasound transducers (Olympus). A 4 cm long plastic tube filled with degassed water was affixed with the transducer (Fig. 14A). The parameters of ultrasound used in this session were: 300 ms stimulation duration, a central frequency 0.5 MHz, 400 μ s pulse width, 1 kHz PRF, positive peak

pressure range from 0.05 to 0.50 MPa (Fig. 14B).

2.1.5 Immunohistochemical fluorescent staining

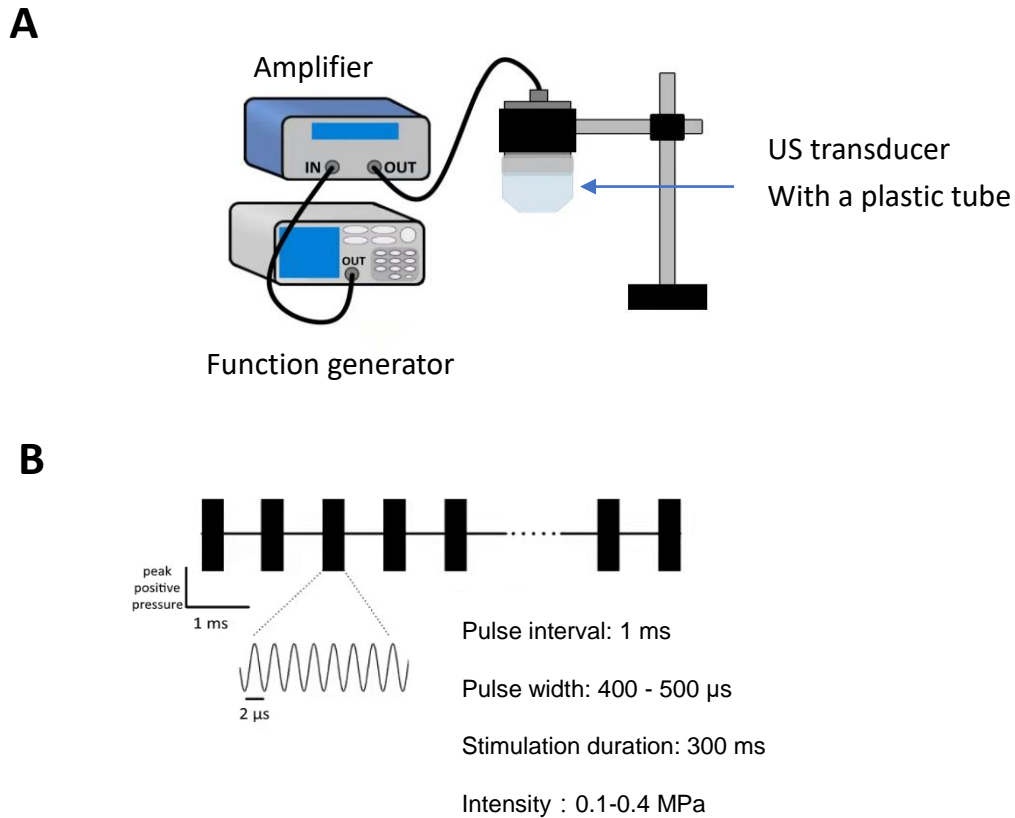


Figure 14 Technical information of the ultrasound system. (A) Schematic illustration of components of the US system. The function generator was responsible for generating waveforms. The amplifier provided voltages to the ultrasound transducer. **(B)** A diagram of the ultrasound temporal profile applied in the EMG experiment.

Mice perfusion was carried out with Phosphate-buffered saline (PBS) and then 4% paraformaldehyde (PFA, cat. no. P1110, Solarbio) in PBS for tissue fixation purpose. Mouse brain was anatomized and post-fixed overnight in 4% PFA. Then brain tissues were washed with PBS for 3 times. Coronal sections were collected from M1 brain area

based on coordinates +0.20 mm to 1.0 mm of Bregma. 40 μ m brain slices were collected by a vibratome machine. Slices were washed in PBS, placed the brain slices on the glass slide. Brain slices were captured a whole-brain frame by Nikon eclipse Ti2-E Live-cell fluorescence imaging system.

2.1.6 Statistical analysis.

All results were shown as the mean \pm SD. All statistical analyses were performed using the GraphPad Prism software. *P < 0.05, **P < 0.01, ***P < 0.001, and n.s. represents no significant.

2.2 Results and discussion

2.2.1 Evoked stronger muscular responses to low intensity ultrasound stimulation in MscL-expressing anesthetized mice.

We first investigated the effect of MscL-mediated ultrasound on primary motor cortex (M1). To introduce EYFP or MscL-EYFP into the excitatory neuron of the primary motor cortex (M1), AAV-CamKII-MscL-G22S-EYFP-pA or AAV-CaMKIIa-EYFP-pA was transfected into the primary motor cortex on the right brain of eight-week-old male mice. Four-week post-injection, mice were anesthetized with isoflurane, hair shaved; a mounted 0.5 MHz frequency transducer setup was placed above the transfected cortical area, and two electromyography (EMG) electrodes were inserted to left forelimb triceps muscle tissues (Fig. 15 A). Before performing the EMG recording experiment, we ensured that EYFP or MscL-EYFP (green signal) was expressed robustly in the M1 region of the brain slice (Fig. 15B).

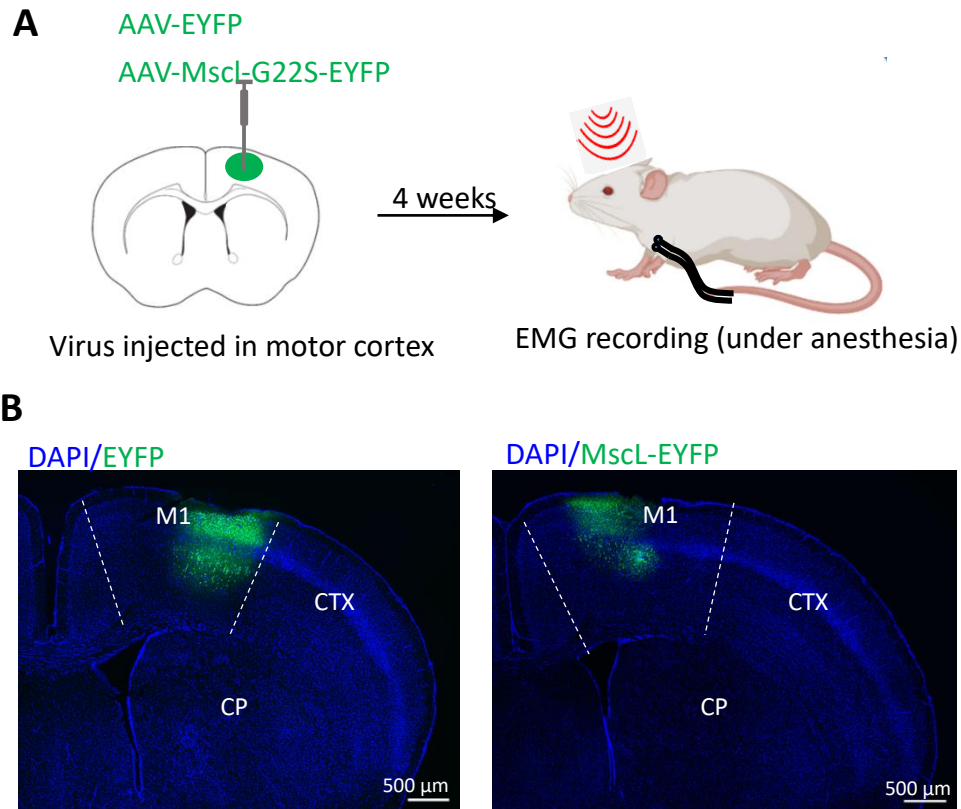


Figure 15 An experimental flow of EMG recording in anesthetized mice. (A) A diagram of *in vivo* experimental plan. Briefly, mice were injected with CaMKII-promoted viruses in M1 region of the right brain. Four-week later, mice were stimulated with US stimulation and muscular contraction of the left forelimb triceps were detected by EMG electrodes simultaneously. **(B)** Images of mouse brains expression CamKII-EYFP (Left panel) or CamKII-MscL-EYFP (Left panel), indicating the regions of EYFP and MscL-EYFP expressed in M1 region. Primary motor cortex (M1). Caudoputamen (CP), cerebral cortex (CTX).

Then, we treated the EYFP or MscL mice with a certain intensities range of ultrasound stimulation (0.05 MPa – 0.5 MPa) and recorded the EMG signal in response to US stimulation of the M1. We found that stimulation of MscL-expressing mice at low intensity could evoke a distinct muscular contraction, showed by the distinct EMG signals, while the EYFP mice produced no or smaller muscular responses in the same

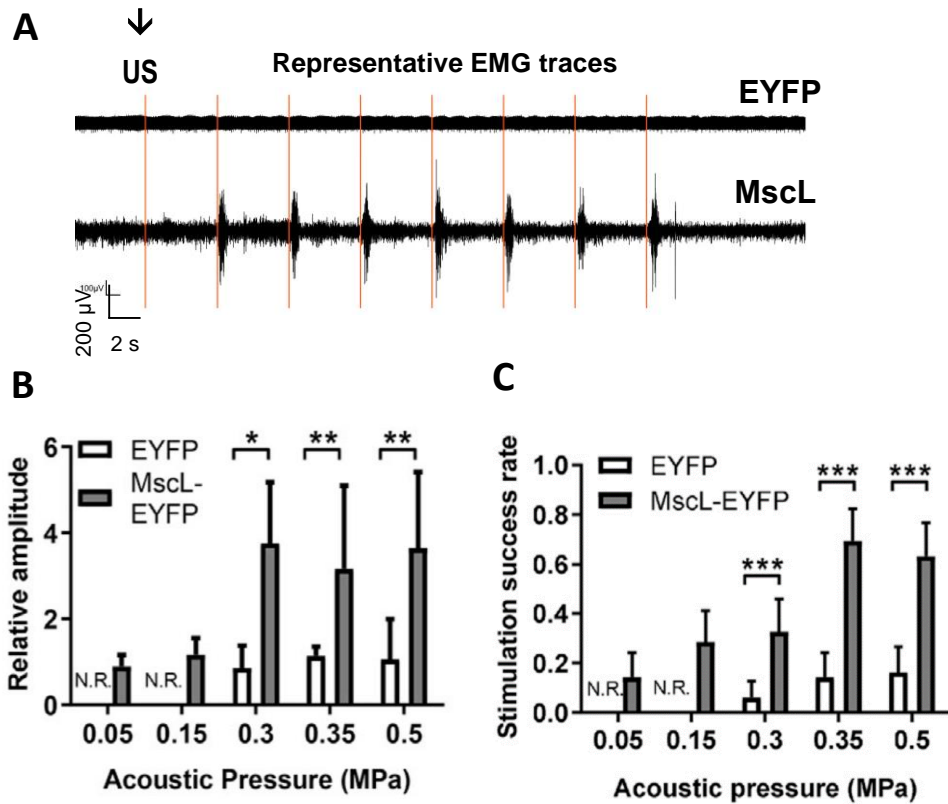


Figure 16 Ultrasound stimulation induces larger muscular responses when applied to mouse primary motor cortex area expressing MscL. **(A)** Representative EMG traces of the muscular contraction results from 0.05 MPa intensity sonication in mice expressing the EYFP or MscL viruses. **(B)** The relative amplitude of EMG response at ranges of 0.05 MPa to 0.5 MPa ultrasound stimulation. $n = 49$ times ultrasound stimulation. ‘N.R.’ indicates ‘no response’. Data are indicated as mean \pm S.D. Unpaired two-tailed t -test. **(C)** The success probability of individual sonication stimulation to cause the generation of EMG spikes at ranges of 0.05 MPa to 0.5 MPa ultrasound stimulation. $n = 7$ mice, except for CaMKII-EYFP $n = 3$ mice. ‘N.R.’ indicates ‘no response’. Data are shown as mean \pm S.D. Unpaired two-tailed t -test.

condition (Fig. 16A). We first analyzed the amplitude of EMG response to identify the outcome of MscL-mediated neural modulation between brain activity and behavior.

Compared to EYGP group, the relative amplitude of response was larger in MscL mice under the 0.3 MPa -0.5 MPa sonication. In addition, we observed a generalized mode of dose dependence (Fig. 16B). Then, we also measured the successful rate of EMG response per ultrasound stimulus. We found that in MscL mice, the successful rate of muscular contraction induced by ultrasound was significantly higher than EYFP mice (Fig. 16C). No obvious muscular response in the EYFP mice could be detected at the lower US pressures of 0.05 MPa to 0.15 MPa. And at larger acoustic intensities, EYFP mice with relatively small EMG muscular responses. However, MscL mice indicated notable responses at almost all tested acoustic intensities. Thus, this EMG result demonstrated that MscL can be significantly sensitized excitatory neurons of M1 to lower intensities of ultrasound stimulation.

2.2.2 The latency responds to ultrasound stimulation is similar

Furthermore, we examined whether the latency of muscular contraction responds to ultrasound stimulation was different between EYFP mice and MscL mice. The delay time is calculated as the time point between the delivery of the ultrasound stimulus and the time point when the EMG signal exceeds the threshold.

The latency of EMG response was about 150 ms in both groups, indicating no obvious diversity due to the viral vectors expressed (Fig. 17). This data resembled with previous results in mice [148]. Therefore, we suggested that ultrasound stimulation could efficiently induce significantly stronger EMG responses in the contralateral forelimb by mediating corticospinal pathway when applying primary motor cortex region expressing MscL.

A

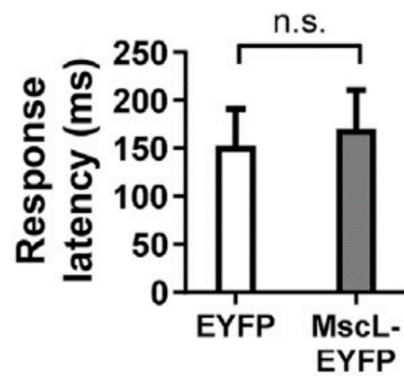


Figure 17 No significant difference of the latency responds to ultrasound stimulation. (A)

EMG response latency measured from the left forelimb triceps in response to M1 stimulation by ultrasound. $n = 6$. Data are indicated as mean \pm S.D. Unpaired two-tailed t -test.

CHAPTER 3 Functional stimulation of whisker-barrel cortex pathway using MscL-mediated ultrasound in awake mice

Next, to examine whether our ultrasound protocol can modulate specific neural activity and result in related behavior changes in awake mice, we selected primary whisker somatosensory cortex (wS1) as our targeted area, which offers a considerably easy and well-defined model for studying motor activity. Neural activities of rodent barrel cortex (whisker somatosensory cortex) are related with the whisker deflection in the contralateral side of the mouse's body [149-151]. It has been shown that optogenetic stimulation of primary whisker somatosensory cortex drove the contralateral whisker deflection [152]. In this session, we tested whether the expression of MscL in the excitatory neurons of primary somatosensory cortex could efficiently mediate whisker movement responses upon US stimulation.

3.1 Materials and methods

3.1.1 Animal subjects

The animal subjects used in this part are the same as described section 2.2.1.

3.1.2 Stereotaxic injection

Adult C57BL/6 mice were anesthetized with Ketamine and Xylazine (as mentioned above). Viral vectors were micro-injected into the targeted areas in the right side of mouse brain by standard stereotaxic procedures. AAV vectors were instilled at the rate of 0.05 μ l per minute through an injection pump with a 45-gauge micro-syringe. The micro-syringe was held in the injection area for extra 10 min before withdrawal.

a) For whisker behavior recording experiments, 200-500 nl either AAV-CamKII-EYFP or AAV-CamKII-Mscl G22S-EYFP was injected into the barrel cortex separately using these coordinates: AP -1.70 mm, ML -2.10 mm; and DV -0.60 mm.

b) For the fiber photometry recording experiment in the barrel cortex, the volume proportion of vectors in the mixes for injections were 1:1 for AAV-CamKII-jRGECO1a and AAV-CamKII-EYFP or AAV-CamKII-Mscl G22S-EYFP. 500 nl mixed viruses were injected into the barrel cortex using these coordinates: AP -1.70 mm, ML -2.10 mm; and DV -0.60 mm. After needle withdrawal, a 1.25 mm optic fiber which was attached to the inserted ceramic ferrule via a ceramic sleeve, which was located in the virus injection area. The fiber photometry experiment was performed after at least 4-5 weeks virus expression.

Mice were placed to their housing areas for housing.

3.1.3 Fiber photometry recording in the barrel cortex of anesthetic mice

Five weeks after virus expression, the transfected mice were anesthetized isoflurane. The hair of the mice was shaved with a scissor. A 70% cotton was used to disinfect and moisten the shaved area. Appropriate US gel was applied on the surface of the shaved region. An 0.5 MHz frequency ultrasound transducer with a plastic waveguide was deposited on it, make sure the central of the transducer was located adherent the optical fibers in the brain. The fiber photometry recording in the barrel cortex was conducted by a 40 uW 570-nm LED. The emission light passed by the same optic fiber, was bandpass filtered, monitored by a brand photoreceiver and recorded by a real -time processing program. After finishing the preparation work, mice were

allowed to rest for 2 min. The mice were stimulated with a trigger air stream for 5-10 times. We recorded both the trigger signal and the calcium signal. Next, mice were treated with two different pressures of ultrasound stimulation trials separately. Each trial included 6-8 times US stimulation. After each round stimulation, the mice were allowed to rest for around 1 min. The calcium fluorescence in the barrel cortex was capture with a fiber photometry equipment. The influences of sonication on calcium dynamic were monitored in real time. Data were processed using custom MATLAB scripts.

3.1.4 Measurement of whisker behavior

Before the recording session, both side of whiskers were trimmed, only leaving C2 whiskers. Whisker movement of the head-restrained mouse with a narrow chamber to settle the mouse and only expose the nose and whisker area of the mice. The movement of the four limbs of mice was limited. Shaved the mice's hair with a scissor. A 70% alcohol cotton was used to sterilize the shaved area. Appropriate US gel was placed on the shaved region (above the barrel cortex) coupling with an US transducer. An ultrasound indicated light was placed next to the mice and separated then with an opaque piece of paper to prevent them interfering with the mice's behavior. A camera was placed 10 cm away from the whisker for recording the movement of whisker. After finishing setup, the mouse was allowed to habituate the surrounding area at least 5 min. The left C2 whisker was filmed at 25 Hz to show C2 whisker. Recorded the behavior of the mouse's C2 whisker for 1 – 2 min without stimulating the ultrasound. Next, mice were stimulated by three different intensities of ultrasound (0.1, 0.15, 0.4 MPa). Each trial included 6 - 8 times US stimulation. After each trial stimulation, the mice were allowed to rest for 1-2 min. Whisker movement analyses were performed during 10 s period of ultrasound stimulus and compared to 10 s pre-stimulus period. We used

automated, freely available software to track the whisker angle and curvature [153, 154]. All whisker trackings were done on mice with only left side of C2 whisker. The angle of whisker was estimated as the angle between the whisker and a line perpendicular to the mouse's midline. Whisker angular velocity (deg/s) was computed as the change in the whisker angle for the period analyzed.

3.1.5 Immunohistochemical fluorescent staining

The process of staining as mentioned above. Coronal brain slices were performed from mouse brain from -1.3 mm to -2.1 mm of the bregma for barrel cortex sections. In this session, slices were staining with Iba1 (ab178847, abcam, dilution 1:500) or caspase 3 (ab13847, abcam, 1:200) antibody for 16-18 h at 4 °C. Then, slices were cleaned with PBS 5 min/3 times. Slice were incubated with anti-rabbit IgG (H+L) secondary antibody for 2 h at room temperature. Slices were washed with PBS 5 min/3 times. Brain slices were placed on the glass slides and mounted with Mounting medium . The number of cells indicating Iba1 (red) and caspase 3 signals (red) and DAPI (blue) per 733 x 733 μm slices was counted using ImageJ software. The counting processes were dingle-blinded, conducted by a team member who did not participate this experimental process. All brain slices were captured using confocal microscope. Also using Nikon eclipse Ti2-E Live-cell fluorescence imaging system to get the whole-brain pictures.

3.1.6 Statistical analysis

Results were presented as the mean \pm s.e.m. Statistical analyses were carried out by the software of GraphPad Prism.

3.2 Results and discussion

3.2.1 Induced greater calcium activity in primary somatosensory cortex by MscL-mediated ultrasound stimulation

To investigate the sensitivity and function of MscL *in vivo*, we performed ultrasonic stimulation on anaesthetized mouse while recording Ca^{2+} activity in the primary somatosensory cortex with the fiber photometry method synchronously. Traditional electrophysiology has high temporal precision, but the number of cells recorded is small, and it lacks cell-type specificity. An alternative technique is fiber photometry, which provides a sensitive and simple approach to measure specific cell-type population neural activities in real time. First, CamKII:MscL-G22S-EYFP or CamKII:EYFP mixed with CamKII:jRGECO1a (a red fluorescent genetically encoded Ca^{2+} indicator) were co-injected into the primary somatosensory cortex of right side of mice's brain, and an optical fiber was inserted into the similar coordinates. Four to five weeks post-virus injection, mice were anesthetized with isoflurane, then recorded the neural activity *in vivo* in real time while treated with different intensities of ultrasound stimulation (0.15 MPa and 0.4 MPa) (Fig.18A). Both low and high magnification of mouse brain images showed robust jRGECO1a (red) and EYFP or MscL-EYFP co-expressed in the cortex barrel field of the right side mouse's brain (Fig. 18B, C).

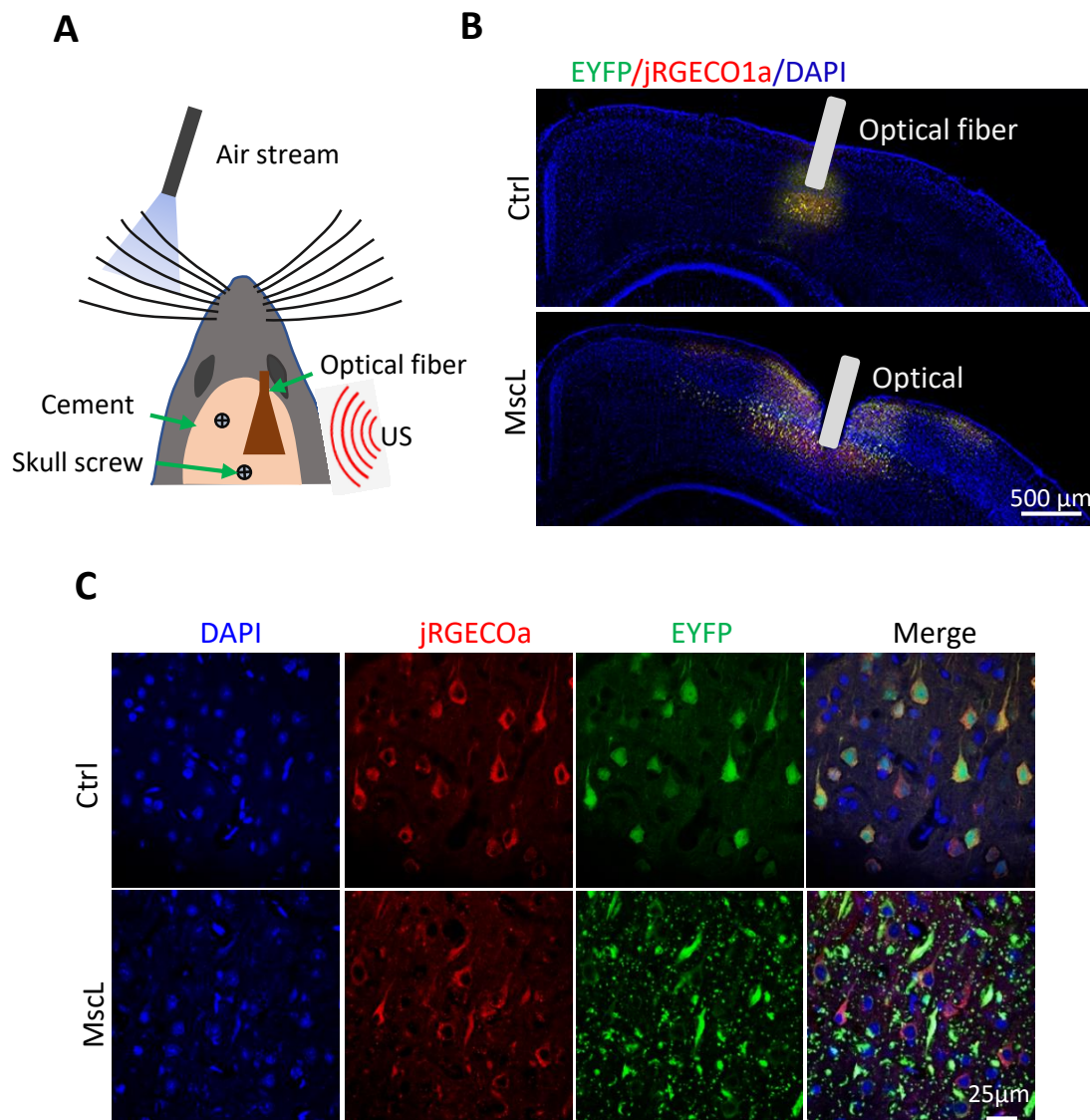


Figure 18 An experimental setup and preparation for neural activity recording in the dorsal striatum *in vivo*. **(A)** A diagram of whisker stimulation and fiber photometry recording experiment. Anesthetized mice were treated with a range of sonication (0.1 – 0.4 MPa), respectively, and recording calcium signals from right side barrel cortices. **(B)** Images showed the low magnification of a mouse brain CamKII:EYFP or CamKII:MscL-EYFP co-expressing with CamKII: jRGECO1a in barrel cortex regions. **(C)** Confocal images displayed the high magnification of a mouse brain CamKII:EYFP or CamKII:MscL-EYFP co-expressing with CamKII: jRGECO1a in the barrel cortex.

Next, EYFP mice and MscL mice were anesthetized with isoflurane. An 0.5 MHz ultrasound transducer with a waveguide was placed on mice's head gluing with ultrasound gel. Before the ultrasound was stimulated, there were no noticeable changes in calcium fluorescent signals in EYFP group (EYFP-NUS = $0.11 \pm 0.05\%$) and MscL group (MscL-NUS = $0.07 \pm 0.03\%$) were observed (Fig. 19A). At 0.15 MPa, we found distinct calcium fluorescent changes in both groups. In addition, the peak $\Delta F/F_0$ in the MscL mice was notably larger than the EYFP group (MscL-Peak $\Delta F/F_0 = 0.61 \pm 0.08\%$; EYFP-Peak $\Delta F/F_0 = 0.37 \pm 0.06\%$, *P=0.0417) under this stimulation condition (Fig. 19A, B). Then, we applied higher pressure ultrasound stimulation (0.4 MPa) to mice, as expected, the neural activities of both groups were activated. MscL mice showed significantly greater calcium concentration compared to EYFP group (EYFP - 0.4 MPa US Peak $\Delta F/F_0 = 0.28 \pm 0.04\%$, MscL - 0.4 MPa Peak $\Delta F/F_0 = 0.65 \pm 0.10\%$) (Fig. 19B). It might relate to the endogenous mechanosensitive ion channel in the brain, such as TRPP2, TRPC1, TRPP1, Piezo1 [112].

In addition, we tested whether the ultrasound stimulation could generate neural activation stably and repeatedly in the excitatory neurons which expressed MscL in vivo. Five burst of ultrasound pulses, each with 0.15 MPa pressure and 3 s interval, were delivered to the US transducer. From the results of the data, we observed synchronous and stabilize calcium activity in response to these five US stimulation trials in both EYFP and MscL expressing mice, but also significantly larger peak $\Delta F/F_0$ the calcium transients of in MscL group showed than the EYFP group (Fig. 19C).

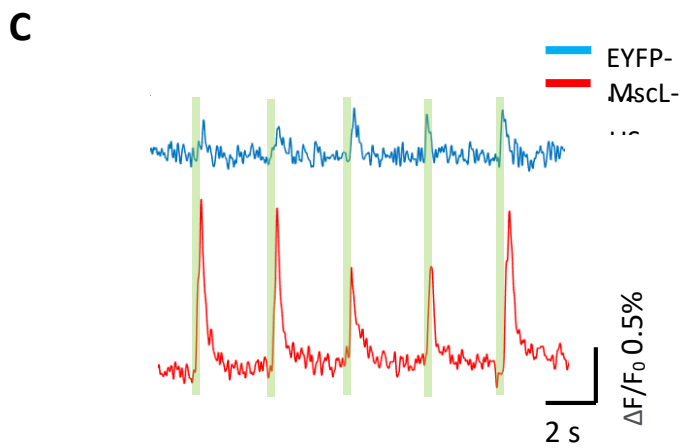
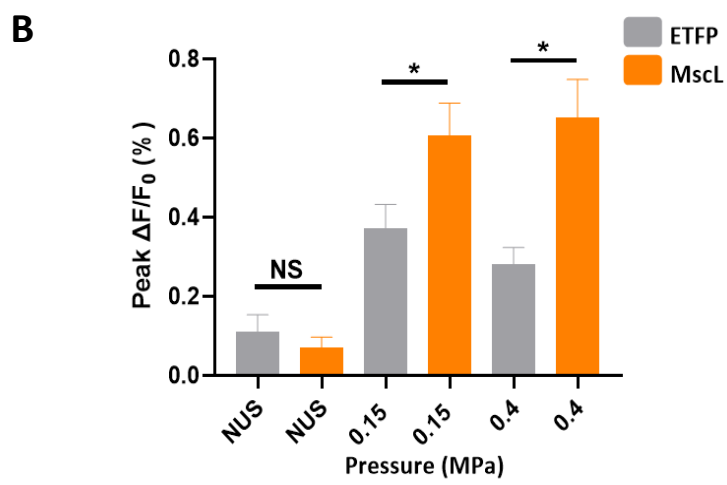
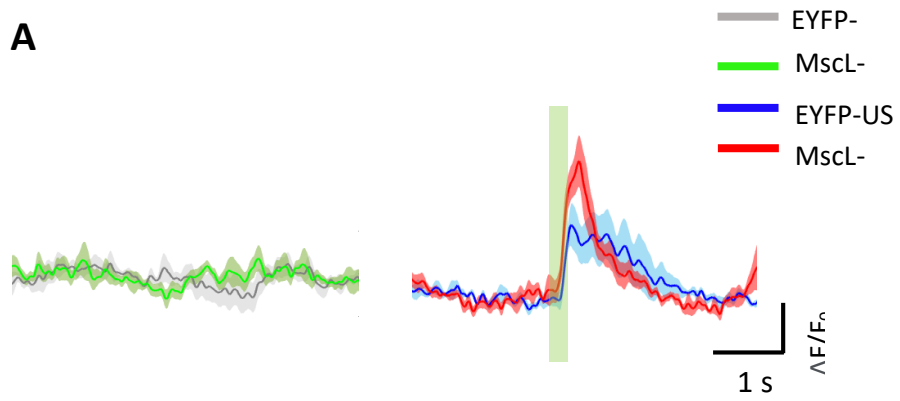


Figure 19 US stimulation elicits greater calcium activity in excitatory neurons of barrel cortex in MscL-expressing mice. (A) Averaged jRGECO1a fluorescence traces increase in the somatosensory cortex of the anesthetized EYFP- mice and MscL- mice in response to different ultrasound stimulations (0.15 MPa and 0.4 MPa). Light green rectangle shows the timing of ultrasound stimulation. $n = 6$ mice in EYFP group, $n = 5$ mice in MscL group. **(B)** Average peak Ca^{2+} activity in EYFP- mice and MscL- mice respond to NUS, 0.15 MPa, 0.4 MPa ultrasound stimulation. * $P < 0.05$, Unpaired two-tailed t -tests. Data are shown as mean \pm SEM. $n = 6$ mice in EYFP group, $n = 5$ mice in MscL group. **(C)** Representative traces showed calcium activity respond to 0.15 MPa ultrasound stimulation in EYFP- and MscL- mice. Light green rectangular shows the timing of ultrasound stimulation.

3.2.2 The MscL expression does not affect the physiological property of neuron and does not elicit an obvious immune, apoptosis response

To confirm the safety of MscL expression, we tested whether the expression MscL would alter physiological properties of neurons. It has been reported that once applying airstream stimulation to a side of whiskers, robust calcium transients in the contralateral barrel cortex can be evoked [155]. As mentioned above, excitatory neurons in the right barrel cortex were simultaneously transduced by AAVs for CamKII:EYFP or CamKII:MscL-EYFP, and by AAV-CamKII-jRGECO1a, coding for genetically-encoded calcium sensor with red fluorescence, at a 1:1 ratio in mice. Five-week post-transduction, the left side of the mice's whisker were applied to air stream trigger, and an optical fiber was used to monitor jRGECO1a fluorescence intensity simultaneously. We observed both groups responded to air pump application, showing by robust and

synchronous calcium signals. No obvious difference of air stream trigger-evoked Ca^{2+} dynamic in EYFP- mice (Peak $\Delta F/F_0$, EYFP = $0.83 \pm 0.18\%$) and MscL- mice (Peak $\Delta F/F_0$, MscL = $0.87 \pm 0.16\%$) (Fig. 20A, B), suggesting that the expression of MscL did not change whisker-induced responses in neurons in the mouse brain.

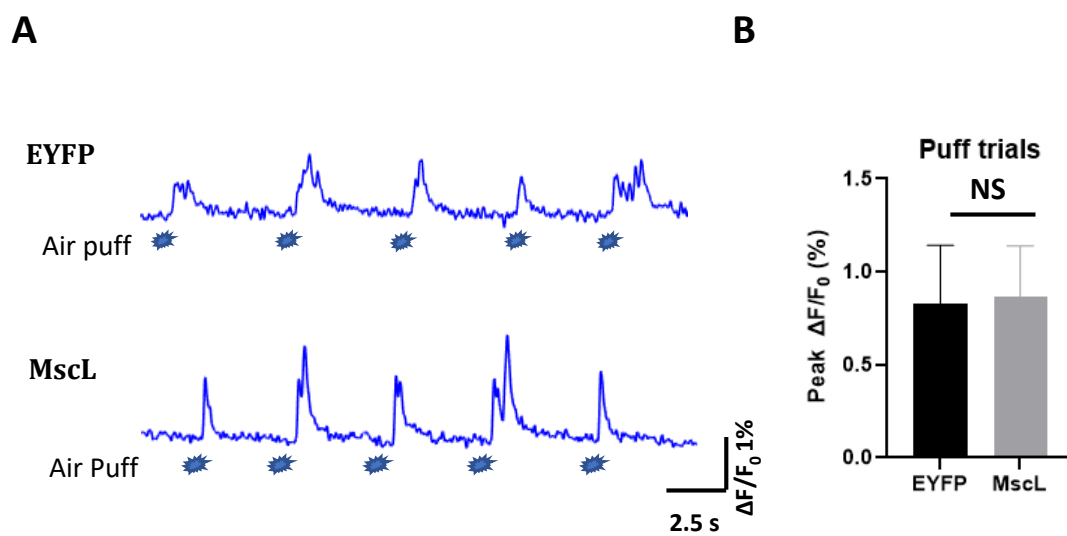


Figure 20 Calcium activity induced by air trigger in EYFP mice and MscL mice. (A) Representative calcium traces showed calcium activity responded to air stream trigger in EYFP- and MscL- mice. Irregular patterns indicate each air stream trigger. **(B)** Average peak calcium transient responded to per air stream stimulation in EYFP- mice and MscL- mice. Unpaired two-tailed *t*-tests. *n* = 3 mice each group. Data are indicated as mean \pm SEM. NS, no significance.

To further confirm the effect of MscL expression, we investigated the cellular-level effects of virus expression in brain tissues by utilizing antibodies against Iba1, an immune response monitor, and cleaved caspase-3, a cell death indicator in

CamKII:EYFP and CamKII:MscL-EYFP mice. Images showed that the cell nuclei were intact in both groups. Data suggested that MscL expressed in the barrel cortex region did not cause a clear alteration in the numbers of glial cell compared to EYFP group (Fig. 21A, B. EYFP- Iba1 positive cells = 137.3 ± 4.67 ; MscL- Iba1 positive cells = 134.0 ± 4.36). Besides, we did not detect noticeable diverse in the number of apoptotic cells in neither EYFP nor MscL brain slice (Fig. 21C, D. EYFP-Caspase 3 positive cells = 5.28 ± 2.24 , MscL-caspase 3 positive cells = 3.89 ± 1.06). In summary, these data indicated the overexpressing MscL in the primary somatosensory cortex does not produce obvious immune response and apoptosis response.

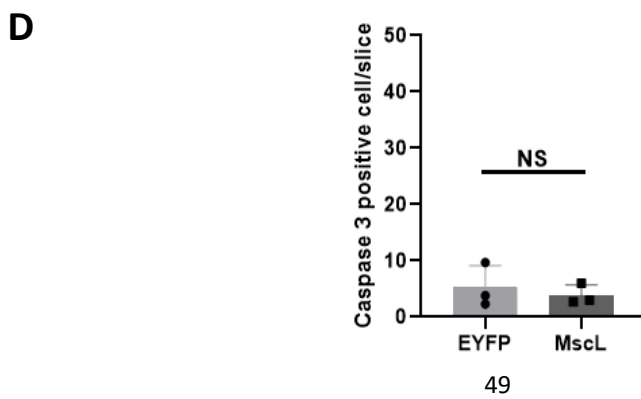
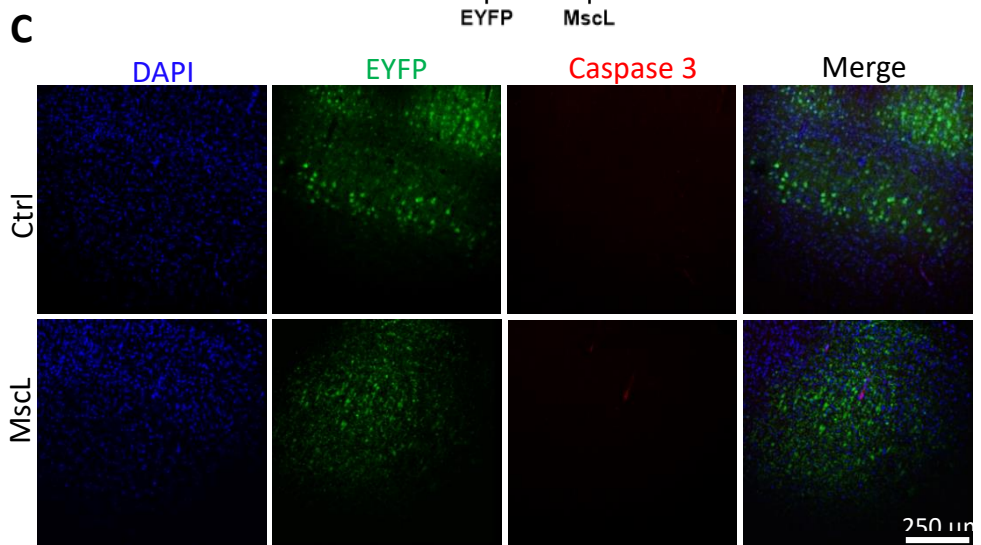
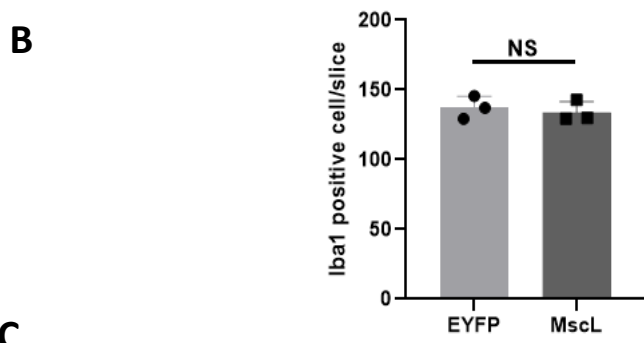
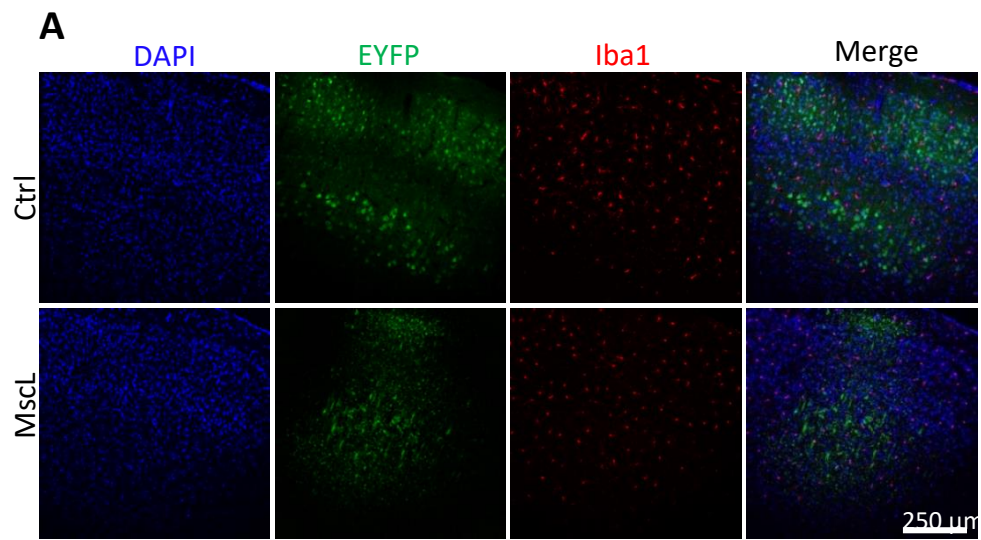
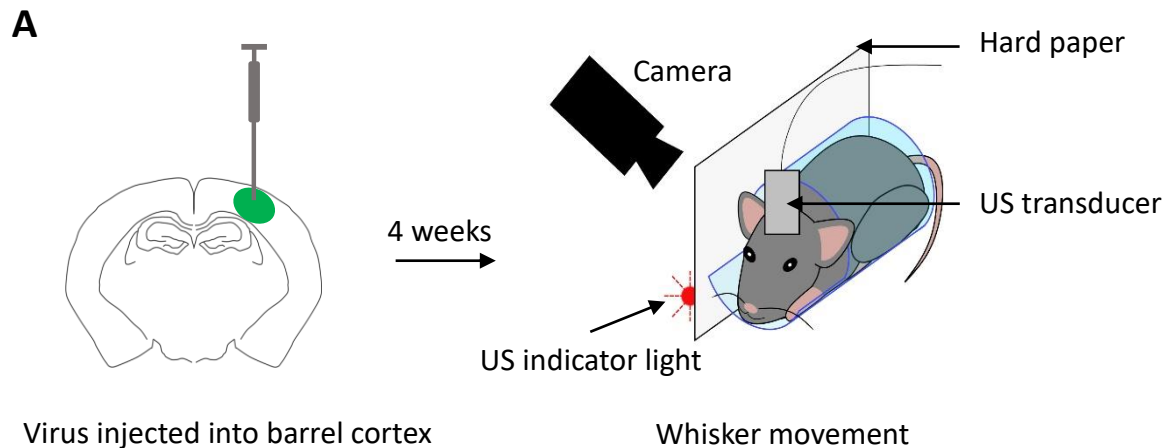


Figure 21 MscL expression is safe in cellular level. (A) Representative images showed CamKII:EYFP- and CaMKII:MscL- mouse brain slice stained with Iba1, which is marker of inflammation. DAPI (blue), EYFP / MscL – EYFP (green), Iba 1 (Red). **(B)** Numbers of positively Iba 1 cells in barrel cortex. Unpaired two-tailed *t*-tests. *n* = 3 mice each group. Data are indicated as mean ± SEM. NS, no significance. **(C)** Representative images showed CamKII:EYFP- and CaMKII:MscL- mouse brain stained with caspase 3, which is marker of apoptosis. DAPI (blue), EYFP / MscL – EYFP (green), Caspase 3 (Red). **(D)** Numbers of positively Caspase 3 stained cells in barrel cortex where the expression EYFP or MscL-EYFP expression located. Unpaired two-tailed *t*-tests. *n* = 3 mice each group. Data are indicated as mean ± SEM. NS, no significance.

3.2.3 Induced stronger whisker movement by MscL-mediated ultrasound stimulation of primary somatosensory cortex

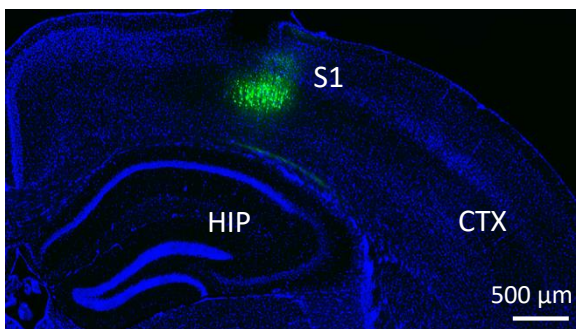
AAVs coding for MscL-EYFP or EYFP-alone under a CaMKII promoter were utilized to induce expression in excitatory neurons of barrel cortex in the right-side brain. Viral vectors were allowed to express for four weeks. The mouse was treated with isoflurane and restrained in a plastic tube. The whiskers were cut off before the experiment, leaving only the C2 whisker. Mice were allowed to habituate for 5-10 min before ultrasound stimulation and whisker recording. In awake mice with CaMKII-MscL expression in the barrel cortex of right hemisphere, ultrasound wave passed through the surface of right primary somatosensory cortex by low intensity ultrasound. The movement of the left side (contralateral side) of C2 whisker was captured with a camera (Fig. 22A).

After 4-week virus expression, mouse brain was sliced for verifying the effect of virus expression and determine the scope of virus expression. Confocal images



B

DAPI/EYFP



DAPI/MscL-EYFP

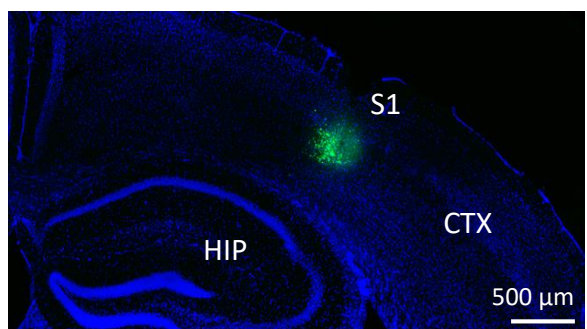


Figure 22 An experimental setup for whisker movement recording in awake mice. (A) Schematic of barrel cortex experimental scheme (Top). Briefly, mice were injected into their right barrel cortex with CamKII: EYFP or CamKII: MscL-EYFP. Four weeks later, mice were treated with ultrasound and recorded the left - side C2 whisker's movement. **(B)** Confocal images indicate expression of CamKII:EYFP (Left panel) or CamKII:MscL-EYFP (Right panel) in the barrel cortex (primary somatosensory cortex, S1). Hippocampus (CP), cerebral cortex (CTX).

confirmed that robust EYFP or MscL-EYFP fluorescent signal located in the S1 of right-side mouse brain (Fig. 22B).

Next, we applied a range of ultrasound parameters (0.1 MPa – 0.4 MPa) on mice and recorded the whisker movement concurrently. The movement of the contralateral C2 whisker in awake mice was monitored for 10 seconds pre- and during- ultrasound stimulation (0.5 MHz central fundamental frequency, 500 μ s pulse width, 300 ms stimulation duration, 1 ms pulse interval, 3s stimulation interval). The average increases in angular velocity following US stimuli in each mouse were calculated and compared. Mice were allowed to wake up and habituate for 5 min. Both groups adapted to the environment, showing by C2 whisker was in a relatively quiet state. In general, after ultrasound stimulation MscL mice showed much greater C2 whisker deflection compared to EYFP group (Fig. 23A - C). At 0.1 MPa, the average angular velocity upon ultrasound stimulation was -3.36 deg for EYFP mice, and 19.69 deg for MscL mice, but no significant difference was shown. The result showed that the whisker movement responses showed some degree of dose-dependence, with increasing pressure US stimulation evoking larger average angular velocity in EYFP and MscL groups (Fig. 23C). We observed that MscL group and EYFP group both showed changes in whisker angle during US "ON" period (both 0.15 MPa and 0.4 MPa), but a more intense and long-lasting in the MscL mice, with more frequent changes of angle observed as well. The intensities of 0.15 MPa (EYFP = 14.24 deg, MscL = 91.79 deg) and 0.4 MPa (EYFP = 38.43 deg, MscL = 88.62 deg) US stimuli elicited increased whisker angular velocity in all mice, but velocities were significantly greater in MscL mice (Fig. 23C). The threshold US pressure required to stimulate C2 whisker movement was substantially lower in MscL mice compared to EYFP mice.

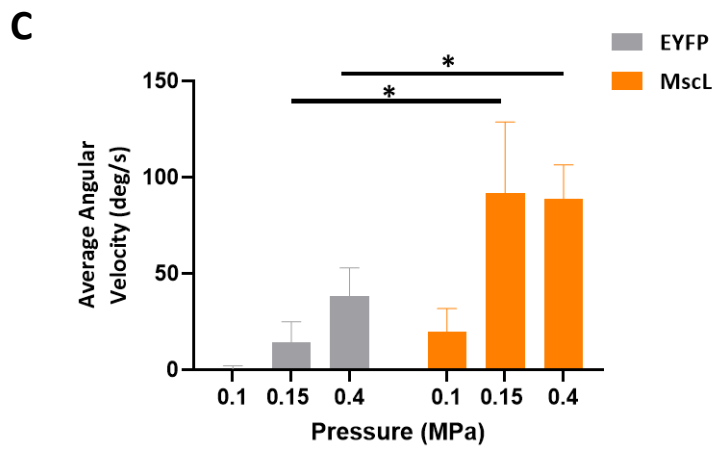
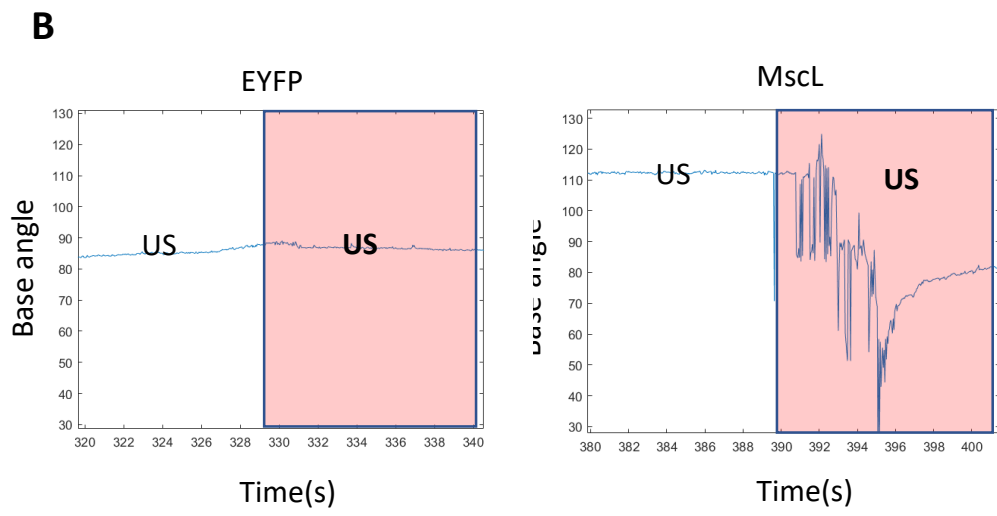
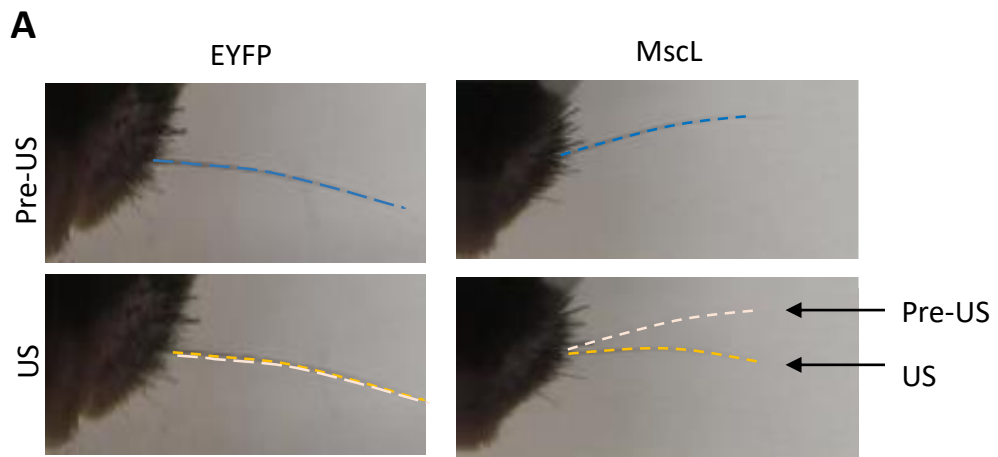


Figure 23 MscL-mediated ultrasound stimulation of barrel cortex evokes stronger whisker movement. **(A)** The images were taken over before and after ultrasound stimulation in EYFP (left) and MscL (right) mice. **(B)** Representative the angle changes of the C2 whisker from CamKII:EYFP and CamKII:MscL-EYFP awake mice following ultrasound stimulation on the surface of barrel cortex. Timing of ultrasound stimulation is indicated as the red shadow. **(C)** Summary data for average angular velocity of whisker movement evoked by different parameters of ultrasound stimulation in EYFP and MscL- mice. In 0.1 MPa ultrasound stimulation, $n = 8$ mice in EYFP group, $n = 7$ mice in MscL group; In 0.15 MPa ultrasound stimulation, $n = 9$ mice in EYFP group, $n = 7$ mice in MscL group; In 0.4 MPa ultrasound stimulation, $n = 7$ mice in EYFP group, $n = 6$ mice in MscL group. Unpaired two-tailed t -test, * $P < 0.05$. Data are shown as mean \pm SEM.

3.2.4 Acoustics does not induce whisker movement in mice

Some studies argued that ultrasonic stimuli through the auditory circuit [126, 127]. On the other hand, early studies have used brain slice [110], deaf mice model [128] to confirm that ultrasound directly produced neural activation. In order to demonstrate the role of MscL-mediated ultrasound, we set up EYFP mice as a control group. If the auditory circuit is involved, we would detect the similar whisker deflection between EYFP group and MscL group. However, data obtained indicated that the whisker movement of MscL expression mice response to the same ultrasound stimulation was much larger than EYFP group (Fig. 23). It can somehow imply that ultrasound stimulation induced stronger whisker movement in MscL mice was not resulted from the audible effect. The mice hearing range is around 1,000-100,000Hz. Our US protocol

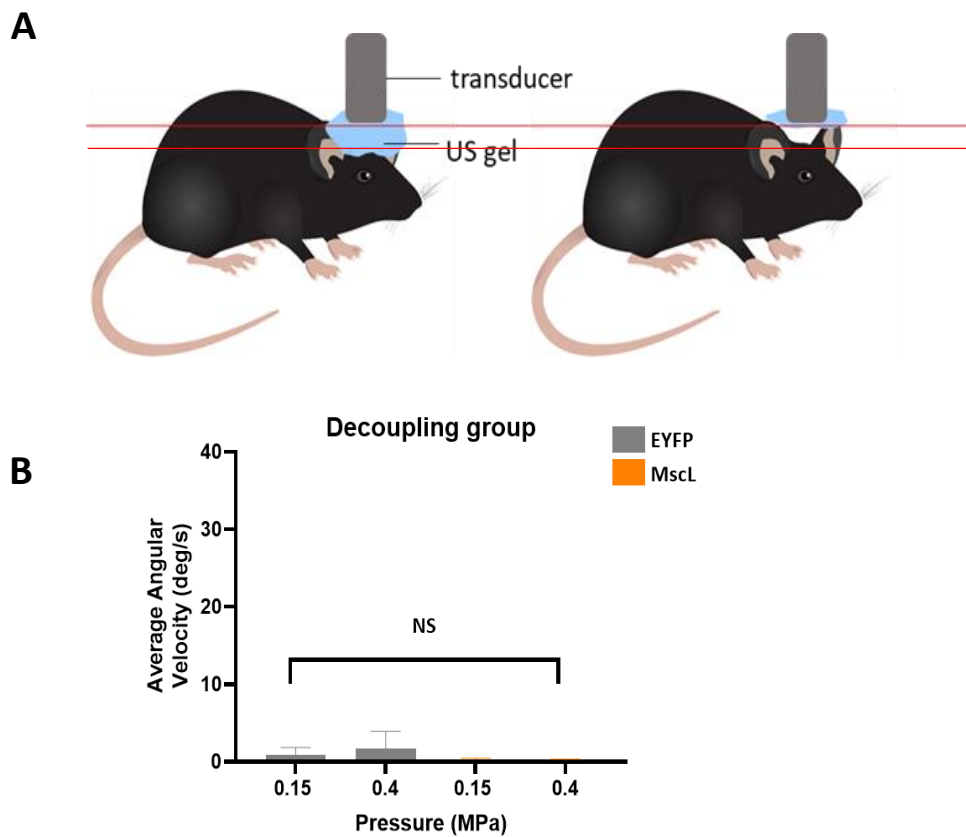


Figure 24 Sound does not induce whisker movement in EYFP mice and MscL mice. (A) Schematic illustration of US transducer delivers ultrasound wave to the mouse brain with or without US gel. Sham stimulation experiments were conducted with the similar conditions but maintaining enough gap by not applying US gel between the transducer and skull. **(B)** Summary data for average angular velocity of whisker movement evoked by ultrasound stimulation in the sham group. $n = 6$ mice in EYFP group, $n = 6$ mice in MscL group. Unpaired two-tailed t -test. Data are shown as mean \pm SEM.

used 1KHz pulse repetition frequency (PRF), which is a frequency the mouse could be heard. To further exclude the effect of sound, we designed a simple sham experiment to examine whether the sound generated by ultrasound could evoke whisker movement. In the experimental group, ultrasound wave passed into the brain via US gels. Acoustic wave cannot pass without a medium, but the sound generated by the ultrasound

transducer still existed. In the sham group, there was a gap between the transducer and the mouse brain, but the distance between the transducer and mouse brain was the same as the distance of the experimental group, previously described (Fig. 24A). We observed that no distinct whisker changes were detected in any mice treated as a sham condition (no coupling gel between transducer and the scalp), with the average velocity change for all mice below 2 deg/s (Fig. 24B). Collectively, these data proposed that ultrasound stimulation evoked stronger whisker movement through direct neural stimulation in MscL expressing mice, without participation of the auditory circuit.

Therefore, these results indicated that MscL-mediated ultrasound stimulation could be effectively applied for the primary somatosensory cortex and induced stronger whisker movement in awake mice.

CHAPTER 4 Spatially activation of dorsal striatum neurons and enhances motor function via MscL-mediated ultrasound stimulation

Furthermore, we tested whether our US stimulation method could spatially and selectively activate deeper regions of the brain. We selected dorsal striatum, a deep region (a region located ~2.75 mm below the skull) with a well-function and behavior pattern, which is relative to initiate, control movement of the body [156, 157], as our targeted region. Two aims of this session of the study are, to test the spatial selectivity of our MscL-mediated US stimulation method; and to determine its effectiveness enough to trigger motor function in awake and freely - behaving animals.

4.1 Materials and methods

4.1.1 Animal subjects

The animal subjects used in this part are the same as described section 2.2.1.

4.1.2 Virus injection

Adult C57BL/6 mice were anesthetized with mixtures of the appropriate ketamine and xylazine. Viral vectors were transferred into the targeted areas on the right mouse brain by standard stereotaxic micro injection procedures. AAV vectors were injected at the rate of 0.05 ul per minute through a microinjection pump with a 45-gauge syringe. The micro-syringe was hold in the place for extra 10 min before gently withdrawal.

- a.) For the staining and behavioral experiment on the dorsal striatum in mice, 500 nl either AAV-hSyn-EYFP or AAV-hSyn-MscL G22S-EYFP was

unilaterally infused into the dSTR using these coordinates: AP +0.50 mm, ML -1.8 mm; and DV -2.75 mm [158]. Ultrasound adaptors installments were performed after virus expressed for three weeks.

b.) For the fiber photometry experiment of the dorsal striatum, 500 nl mixed vectors were transfected into the dSTR unilaterally. The volume proportion of vectors in the mixes for infusions were 1:1 for AAV-hSyn-jRGECO1a and AAV-hSyn-EYFP or AAV-hSyn-Mscl G22S-EYFP. The coordinates were the same as above. After needle withdrawal, a 1.25 mm fiber was inserted into the location of virus injection area. Fiber photometry was performed after at least 4-5-week virus expression.

c.) For the optogenetic stimulation experiment, 500 nl AAV-hSyn-ChR2-mCherry was unilaterally infused into the dSTR at the coordination of AP +0.50 mm, ML -1.8 mm; and DV -2.75 mm. An optical cannula was then implanted into the same location.

Mice were returned to their housing areas for recovery.

4.1.3 Fiber photometry recording of ultrasonic evoke neural activity in anesthesia mice

4-5-week of virus expression, the mice were anesthetized with isoflurane. Disinfected and moistened the shaved skin with 70% alcohol cotton. Applied appropriate US gel on the it. An 0.5 MHz fundamental frequency ultrasound transducer with a plastic waveguide was put on the injected side of the brain, make sure the central of transducer was located near the optical fibers in the brain. The calcium dynamic recording in the dSTR was conducted by a 40 uW 570-nm LED. The emission light

traveled cross the same optic fiber, was bandpass filtered, monitored through a brand photoreceiver and recorded with a processor. Mice were allowed to rest for 2 min before performing the experiment. Using the fiber photometry method, the influences of ultrasound stimulation on calcium dynamic in the dSTR of mice were recorded. Recorded 2 min of spontaneous calcium activity before applying ultrasound stimulation. The transfected mice were treated with certain parameter ranges of ultrasound stimulation (0.05 MPa – 0.0.2 MPa). Each trial included 6-8 times US stimulation. After each trial stimulation, the mice were allowed to rest for 1-2 min. Calcium fluorescence was captured with fiber photometry system (Thinker Tech Nanjing BioScience Inc). Data were processed by custom MATLAB scripts.

4.1.4. Measurement of locomotion by Open field recording

a) In ultrasound stimulation experiment

Mice were habituated to the procedure area for about 30 min before the experiments. After that, anesthetized with 2% isoflurane, using an 70% alcohol cotton to disinfect the hole of the adaptor where explored the brain skull and placed some US gel in it. Then, the transducer was connected to the US adaptor (the mice were under anesthesia in this whole process). After the installment of ultrasound transducer, placing the mice into the central of open field box (40 cm length × 40 cm width × 30 cm height). A digital camera was located at ~45 cm over the behavioral test chamber for recording the animal trajectories and movement. Before ultrasound stimulation, mice were allowed to freely move for 2-3 min. Then mice were treated with 4 trials of different intensities of ultrasound stimulation separately (0.1 MPa – 0.35 MPa). Each trial lasted to 1-2 min. After each stimulation, mice were allowed to rest for 2 min. The movement distance and the mobility speed were extracted from the trajectory using

software.

b) In optogenetic stimulation experiment

Mice were habituated to the procedure area for about 30 min before the experiments. Then a light source was connected to mice through a fiber-optic cable. The mouse was placed into the central of the same open field box and allowed to recover for 20 min. A digital camera was placed about ~45 cm above the behavioral test chamber for recording the animal trajectories and movement. Mice were allowed to freely move for 2-3 min before light stimulation. Then mice were treated with 3 trials of optical stimulation separately. The parameters of light are 20% / 50% / 100% power respectively, 10 ms pulse width, 15 Hz frequency. Each trial continuous to 1-2 min. The distance of mice's movement and the mobility speed were extracted from the trajectory using custom software.

4.1.5 Ultrasound stimuli in dorsal striatum for c-fos staining

4-5 weeks post-injection, mice were anesthetized with ketamine and xylazine. The hair of the mouse's head was shaved. Then appropriate US gel was placed above the targeted region to facilitate acoustic coupling. A 0.5 MHz transducer was put roughly upon the right side of dorsal striatum region. Mice were stimulated with ultrasound for 40 minutes with an interval of 10 seconds. Mice were allowed to stay their cage after US stimulation.

4.1.6 Immunohistochemical fluorescent staining

Coronal brain slices of dorsal striatum and auditory cortex were collected from mouse brain. To minimize nonspecific antibody binding, brain slices were incubated in the blocking buffer for 2 h. Then, slices were incubated overnight in primary anti-c-Fos

antibody solution diluted in blocking buffer. Then slices were washed and incubated with secondary antibodies diluted in the blocking buffer for two hours at room temperature. After washing for 3 time with PBS, the slices were placed on the glass slides. Mounted on glass slides by small drops mounting medium. The number of c-Fos⁺, counted by a team member who did not know the grouping (dingle-blinded). Images were captured by the confocal microscope. Nikon eclipse Ti2-E Live-cell imaging system was used to get the half brain pictures.

4.1.7 Statistical analysis.

Results were showed as the mean \pm s.e.m. Statistical analyses were processed with the software of the GraphPad Prism. *P < 0.05, **P < 0.01, ***P < 0.001, NS represents no significant.

4.2 Results and discussion

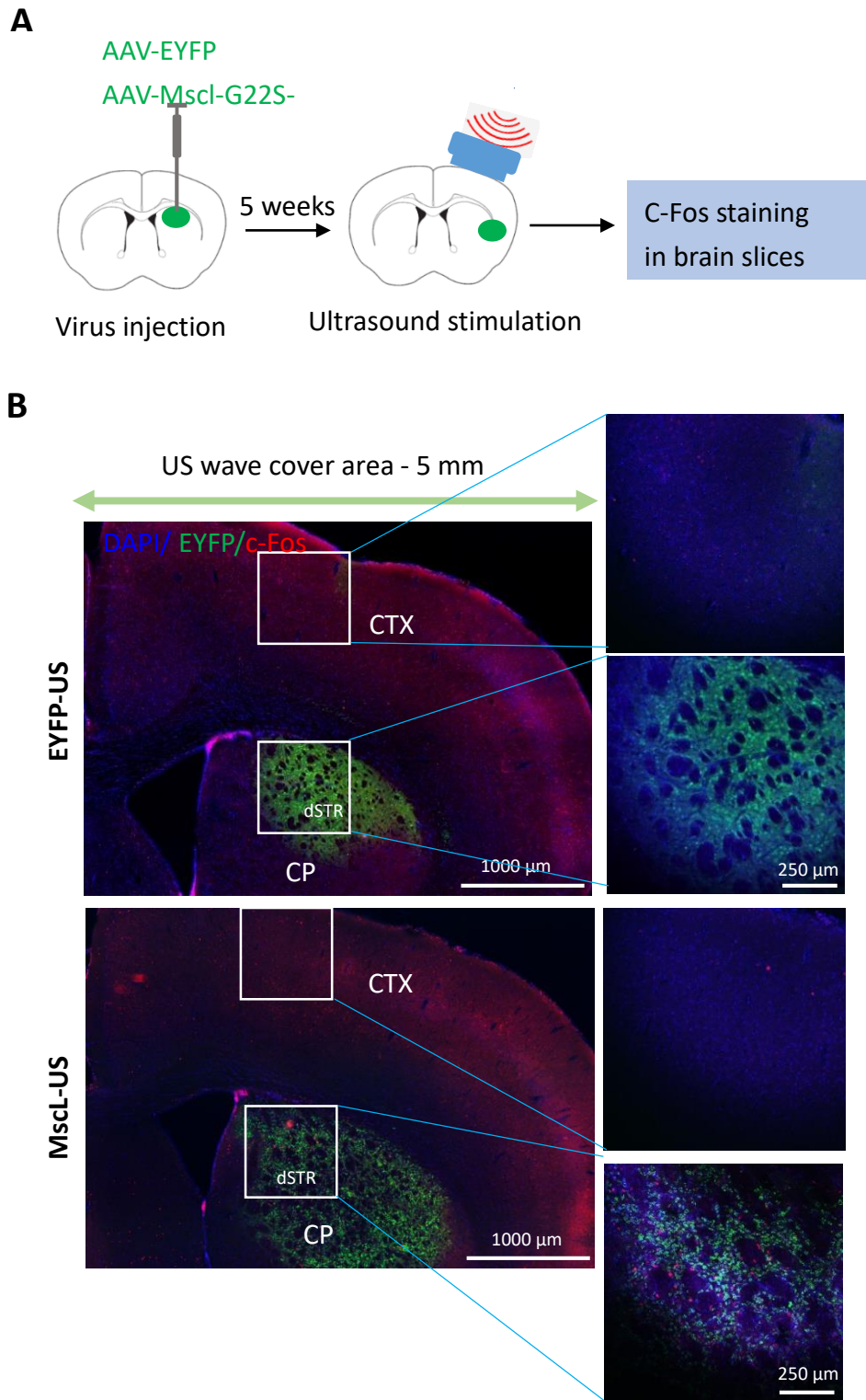
4.2.1 MscL-mediated ultrasound stimulation selective and spatially activated the neurons of dorsal striatum

To test whether MscL-mediated ultrasound stimulation enable to selective and spatial activate neurons in deeper regions, we induced expression of EYFP or MscL in dorsal striatum neurons by injecting AAV-hSyn-EYFP or AAV-hSyn-MscL into the right hemisphere 6-8 weeks mice, positioned by stereotaxis. Five-week after viral injection, the mice were under anesthetized status and treated with US for 40 min (0.5 MHz central frequency, 0.15 MPa, resting interval 10 s) (Fig. 25A). These mouse brains were then examined for the nuclear c-Fos (a neural activation marker) expression in both sides of dSTR region and both sides of the cortical regions directly above the

targeted dSTR.

Robust EYFP expression in the dorsal striatum of both EYFP and MscL mice can be observed (Fig. 25B, left panel). The number of c-Fos expression was found to be significantly higher in the treatment side of the MscL mice (87.00 c-Fos⁺ positive cells/slice) than the contralateral side of the same mice (11.13 c-Fos⁺ cells/slice) or any of the same regions in mice expressing only EYFP (treatment side = 13.54 c-Fos⁺ cells/slice; contralateral = 7.685 c-Fos⁺ cells/slice) immunofluorescence staining of brain slices (Fig. 25C). Crucially, we found that the cortical regions located directly above the dorsal striatum on the stimulation side did not show a significantly higher level of c-Fos, indicating that the treatment was able to concentrate the effects of US in the region expressing MscL and not surrounding areas. This is especially important that the transducer generated ~5 mm diameter (The ultrasound adaptor reduced the surface area of coupled between the ultrasonic transducer and the mouse head) of omnidirectional acoustic wave into the mouse brain, the half mouse brain was unavoidably insonated (Fig. 25). The MscL expressing region in dorsal striatum is around 1.5 mm beneath the skull bone, where can be modulated by ultrasound stimulation. Thus, we could confirm that our MscL + US stimulation scheme could

target neurons in the dorsal striatum for spatially - specific neuronal activation in the



dorsal striatum using our Mscl + US targeting scheme.

C

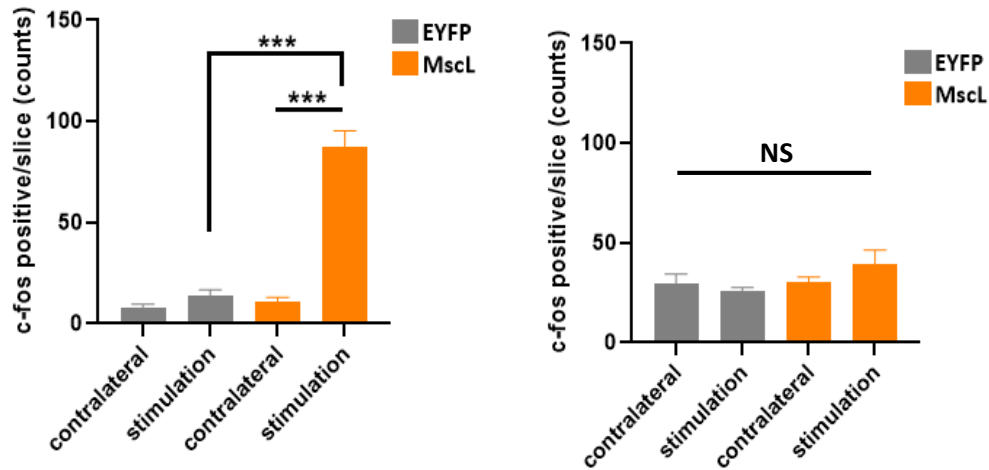


Figure 25 Neural activity in the dorsal striatum under ultrasound stimulation in EYFP and MscL mice. (A) Schematic illustration of our experimental scheme. Briefly, mice were injected in their the dorsal striatum on the injected side of the mouse' s brain with hSyn:EYFP or hSyn:MscL-EYFP. Five weeks later, an ultrasound adapter was installed. Then a week later, mice were stimulated with 0.15 MPa ultrasound for 40 minutes. Mice were allowed to recover for 90 minutes, after which their brains were collected for immunofluorescent staining. Dorsal striatum (dSTR), Caudoputamen (CP), cerebral cortex (CTX). **(B)** Confocal images of the dorsal striatum after ultrasound stimulation. Images of dorsal striatum expressing hSyn:EYFP or hSyn:MscL-EYFP with c-Fos stained. Images showing the low magnification (Left panel) and high magnification (Right panel) of mouse brain hSyn-EYFP or hSyn-MscL-EYFP expressing in dorsal striatum. The green two-arrow indicated the range of ultrasonic coverage. **(C)** The number of nuclear c-Fos+ positive cells / per slice imaged in the dorsal striatum (Left panel) and the cortex above targeted region (Right panel) of mice stimulated with ultrasound. $n = 4$ mice per group. Data are shown mean \pm SEM of average c-Fos+ cells per stained slice. One-way ANOVA with post-hoc Tukey test.

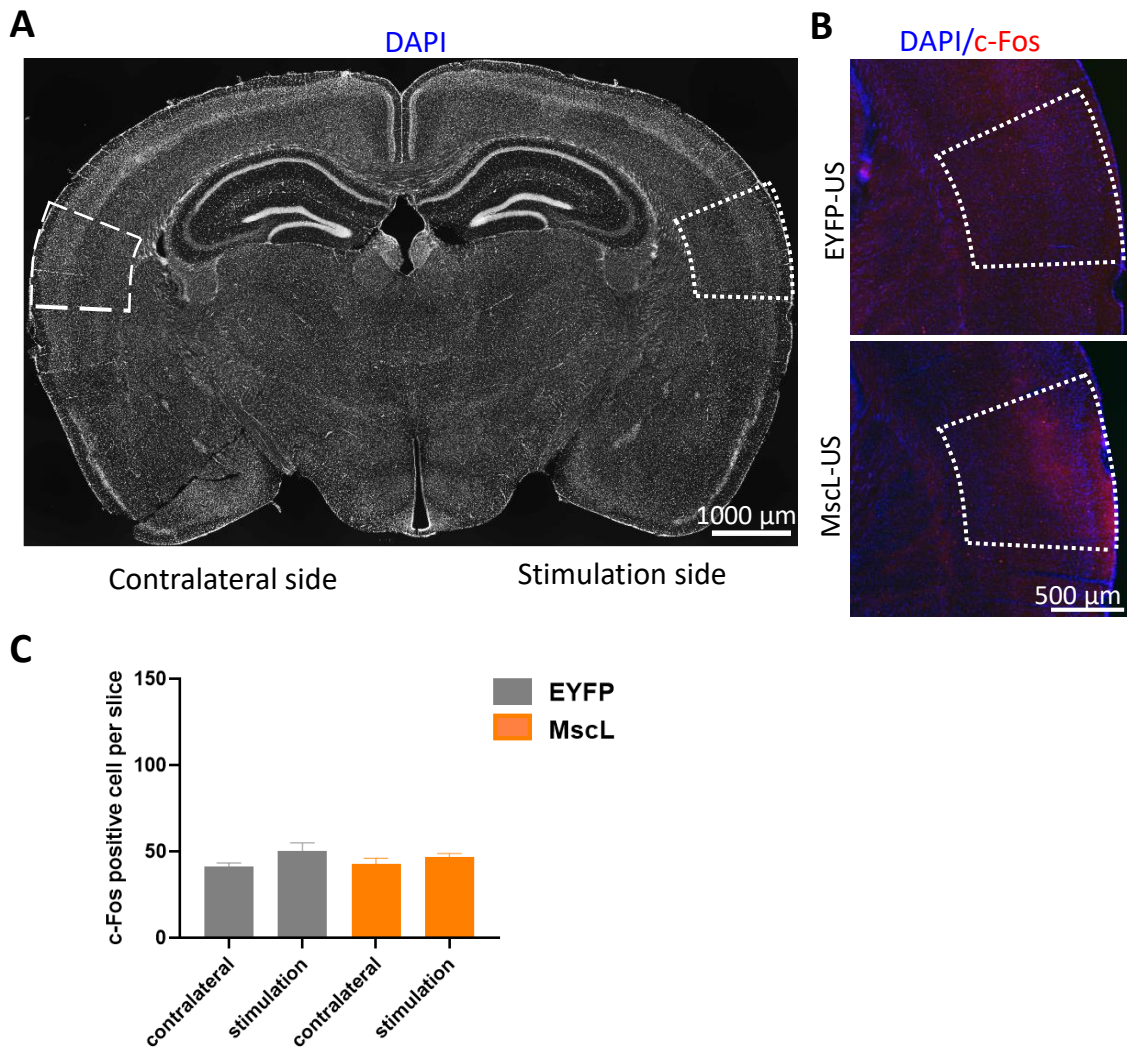


Figure 26 Auditory pathway does not mainly participate in the upregulation of the MscL-sonogenetic process. (A) Anatomical localization of auditory cortex in DAPI-labelled brain slice. **(B)** Images of c-fos in auditory cortex from MscL-expressing mice and EYFP mice that received US stimulation. **(C)** Quantification of the expression of c-fos in auditory cortex in EYFP-US mice and MscL-US mice. $n = 3$ mice per group. Data are shown mean \pm SEM of average c-Fos+ cells per stained slice. One-way ANOVA with post-hoc Tukey test.

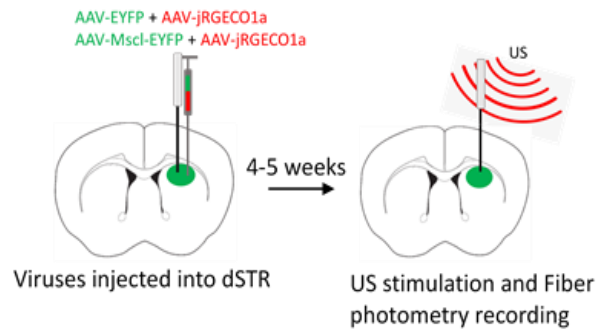
Next, to examine whether auditory pathway is directly involved in this upregulation, we performed c-Fos immunofluorescence experiment in the auditory cortex in the same mice. Mice's brain slices contained auditory cortex region was staining with c-Fos antibody. Both sides of auditory cortex were analyzed. No obviously different c-Fos expression in the auditory cortex region of EYFP mice and MscL mice. Above upregulation was specific to the dorsal striatum no noticeable increased the number of c-Fos positive cell in both side of auditory cortex in these animals can be observe, suggesting that MscL-mediated ultrasound stimulation did not play major role in MscL-sonogenetics process.

4.2.2 Induced larger and synchronized calcium activity by MscL-mediated ultrasound stimulation in dorsal striatum

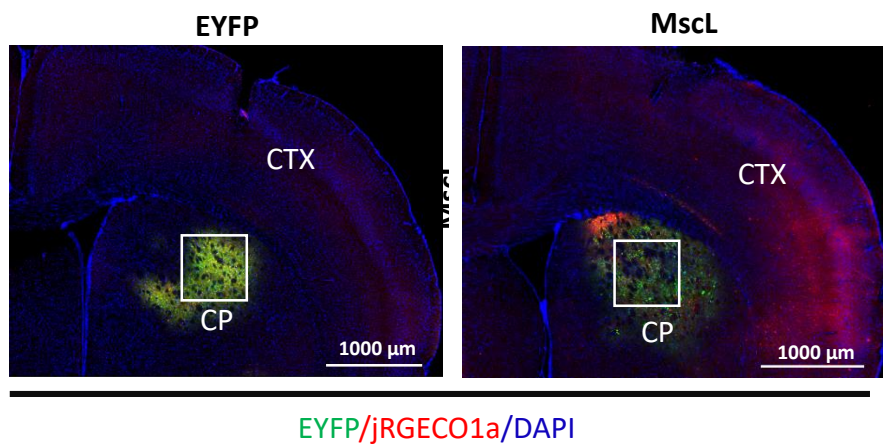
To characterize the calcium dynamics in vivo of the neurostimulation evoked by MscL + US, we explored in real-time through fiber photometry in anesthetized mice. Neurons in the right dorsal striatum were simulataneously transduced by AAVs for hSyn:EYFP or hSyn-MscL-EYFP, and by AAV-hSyn-jRGECO1a, coding for genetically-encoded calcium sensor with red fluorescence, at a 1:1 ratio. Then a fiber optical fiber was implanted into the same region. Five - week post-transduction, the mice were transcranial stimulated with a range of US intensities (0.1 MPa – 0.4 MPa), and an optical fiber was used to monitor jRGECO1a fluorescence intensity (Fig. 27A). Low-magnification and high magnification confocal images showed robust EYFP / MscL-EYFP and jRGECO1a co-expressing fluorescence in the dorsal striatum, and some of them colocalized (Fig. 27B-C).

Next, mice were anesthetized with isoflurane and treated certain pressures range

A



B



C

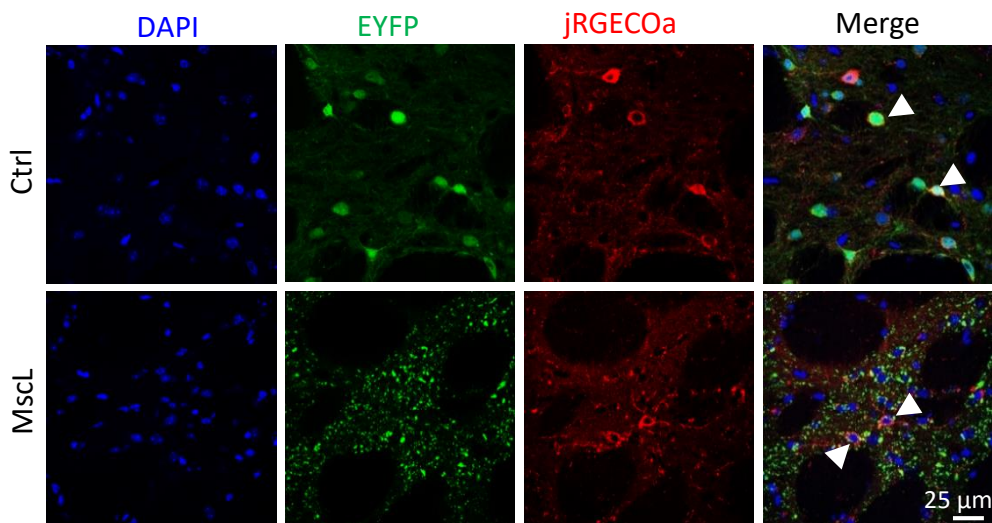


Figure 27 An experimental setup and preparation for calcium activity recording of the dorsal striatum in vivo. (A) Schematic illustration of *in vivo* real-time calcium activity recording. The right dSTR of mice was co-transduced by AAVs for a calcium sensor (hSyn:jRGECO1a) and either MscL-EYFP or EYFP, at a 1:1 ratio. 5 weeks later, anesthetized mice were stimulated with US, and neuronal calcium responses were recorded simultaneously by an optical fiber implanted in the viral injected region. **(B)** Representative low-magnification pictures of dorsal striata (dSTR) expressing hSyn-EYFP (Left panel) or hSyn:MscL-EYFP and hSyn:jRGECO1a (Right panel). Caudoputamen (CP), cerebral cortex (CTX). **(C)** Representative high-magnification confocal images showing EYFP or MscL-EYFP and jRGECO1a fluorescence co-located in the same neurons in the dorsal striatum.

of ultrasound stimulation. Prior to US stimulation, both groups showed comparable levels of baseline fluorescence (Peak $\Delta F/F_0$ for EYFP = 1.25%, and MscL = 1.77%, Fig. 28A, C). However, upon delivery of one 0.15 MPa pressure US pulse, MscL-expressing neurons showed a rapid and obvious increase in jRGECO1a fluorescence intensity while EYFP-only neurons did not (Peak $\Delta F/F_0$ for EYFP = 2.26%, and MscL = 5.62%, Fig. 28B-C). Fluorescence responses to 0.15 MPa US in the MscL dSTR regions were 2.28-fold that of the EYFP dSTR. 0.05 MPa – 0.2 MPa US reliably evoked dSTR neural activity in MscL group, and a generalized pattern of dose-dependence was observed (Fig. 28C). In contrast, the EYFP mice showed a small, but not obvious increase in fluorescence after US stimulation, their responses did not show obvious dose dependence. The latency of MscL-expressing neurons respond to ultrasound stimulation is 250.6-297.3 ms (Fig. 28D).

We next examined whether the ultrasound stimulation can activate neurons stably

and repetitive in this deeper region (striatal neurons) which expressed MscL in mice. The mice received five consecutive ultrasound stimulations at intervals of 3 s. The results showed that stable calcium transients in response to each US stimulation trial in MscL expressing mice, while EYFP mice did not (Fig. 28E).

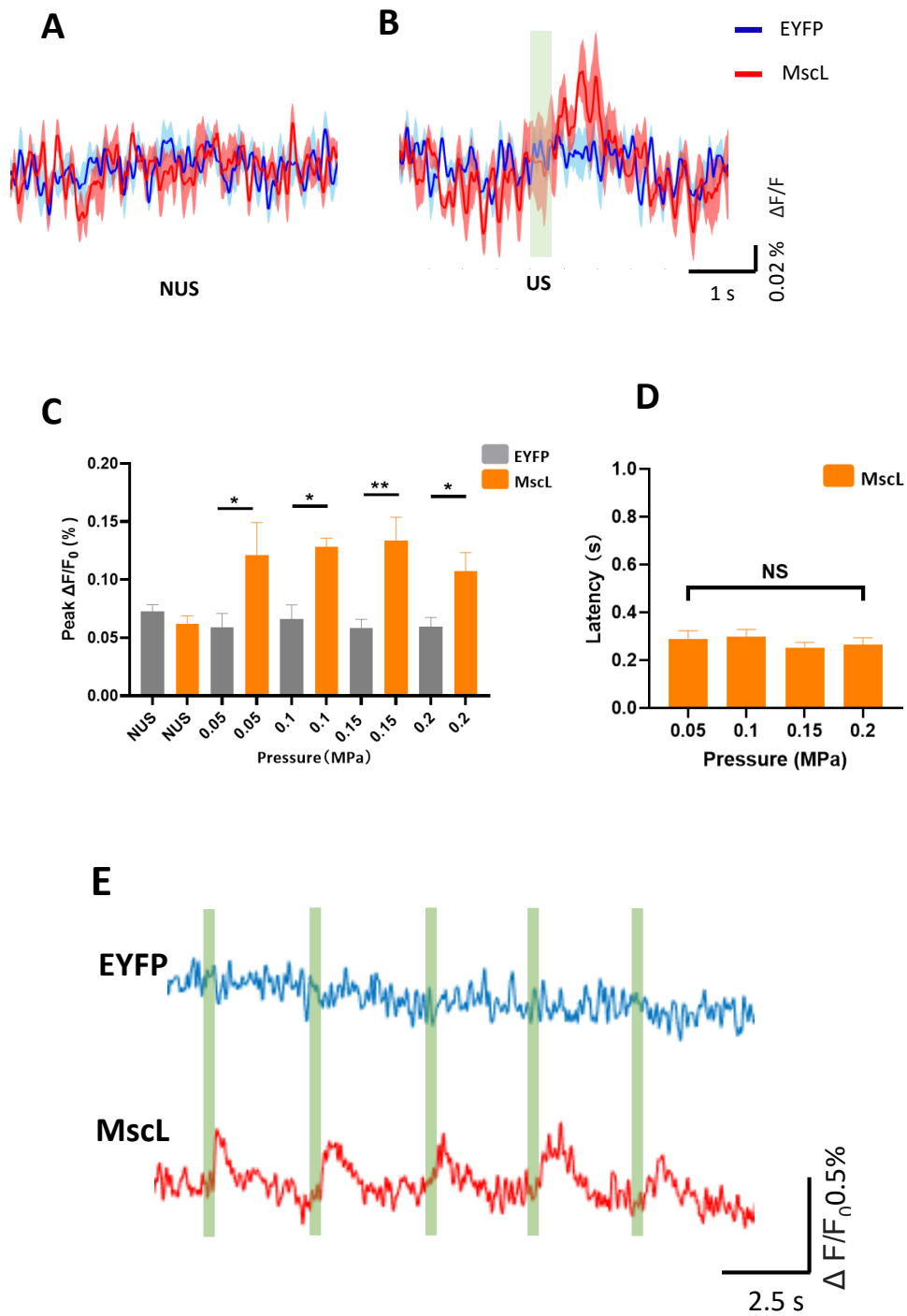


Figure 28 US stimulation elicits greater calcium activity in dSTR neurons in MscL-expressing mice. **(A)** Averaged jRGECO1a fluorescence traces in the dorsal striatum of anesthetized EYFP- or MscL-mice prior to US stimulation. **(B)** Averaged jRGECO1a fluorescence traces increase in the dSTR of anesthetized EYFP- or MscL-mice in response to one 0.15 MPa pressure ultrasound stimulation (0.5 MHz center frequency, 500 μ s pulse width, 300 ms stimulation duration, 1 kHz PRF, interval 3s). $n = 8$ trials, 5 mice in EYFP group, $n = 7$ trials, 5 mice in MscL group. Green rectangle shows the timing of ultrasound stimulation. **(C)** Average peak Ca^{2+} activity in EYFP- and MscL-mice in response to US pulses of varying intensities (0.05 – 0.2 MPa pressure, 500 μ s pulse width, 0.5 MHz center frequency, 300 ms stimulation duration, 1 kHz PRF, interval 3s). $n = 8$ trials, 5 mice in EYFP group, $n = 7$ trials, 5 mice in MscL group. * $P > 0.05$, unpaired 2-tailed t -tests. Data are shown as mean \pm SEM. **(D)** Latency between US stimulation (0.05 – 0.2 MPa pressure) and detection of an above-threshold. $n = 5$ mice in MscL group. One-way ANOVA with post-hoc Tukey test. Data are shown as mean \pm SEM. **(E)** Calcium traces of a EYFP mice and MscL mice undergo repeated ultrasound stimulation. Green rectangle shows the timing of ultrasound stimulation.

4.2.3 Enhanced evocation of locomotor activity by MscL-mediated ultrasound stimulation of dorsal striatum

Next, to evaluate whether our MscL-mediated sonication method was effective and specific enough to trigger motor responses in awake and freely mice. AAVs under a human synapsin (hSyn) promoter were utilized to express EYFP alone or MscL-EYFP in the right dorsal striata of mice (Fig. 29A), which is related to motor behavior [31-

33], as mentioned above. Three weeks later, an ultrasound adaptor was assembled on the mouse's head, and the mouse was allowed to recover for one week. Before performing behavioral recording, brain slices were used to confirm the effect of viral expression and examine whether the virus expressed in the correct area. Confocal images confirmed that robust EYFP or MscL-EYFP fluorescent signal located in the dorsal striatum of right side of the mouse brain (Fig.29B).

To prevent the mice from being frightened during the process of transducer installation, the mice were anaesthetized with isoflurane throughout the transducer installment process. Placed US gel into the hole of the adaptor, no bubble generated in the process, and connected the wearable transducer to the adaptor carefully. After the mouse woke up, placed it in the middle of the square open-field box (Fig. 29A) for habituation. Then mice were treated with or without ultrasound, and their behaviors were recorded and analyzed. The result of ultrasound stimulation testing consisted of three 1 min epochs (pre-stimulation ("Pre"), ultrasound stimulation ("US"), post-stimulation ("Post")). We did not observe obvious difference locomotion evidence between EYFP mice and MscL-EYFP mice in the "Pre" period (Mob. Speed EYFP = 58.91 mm/s, MscL = 64.34 mm/s; Distance EYFP = 1871 mm, MscL = 1638 mm) (Fig. 30), indicating the expression of MscL in the dorsal striatum did not affect the mice's normal spontaneous movement compared to EYFP mice.

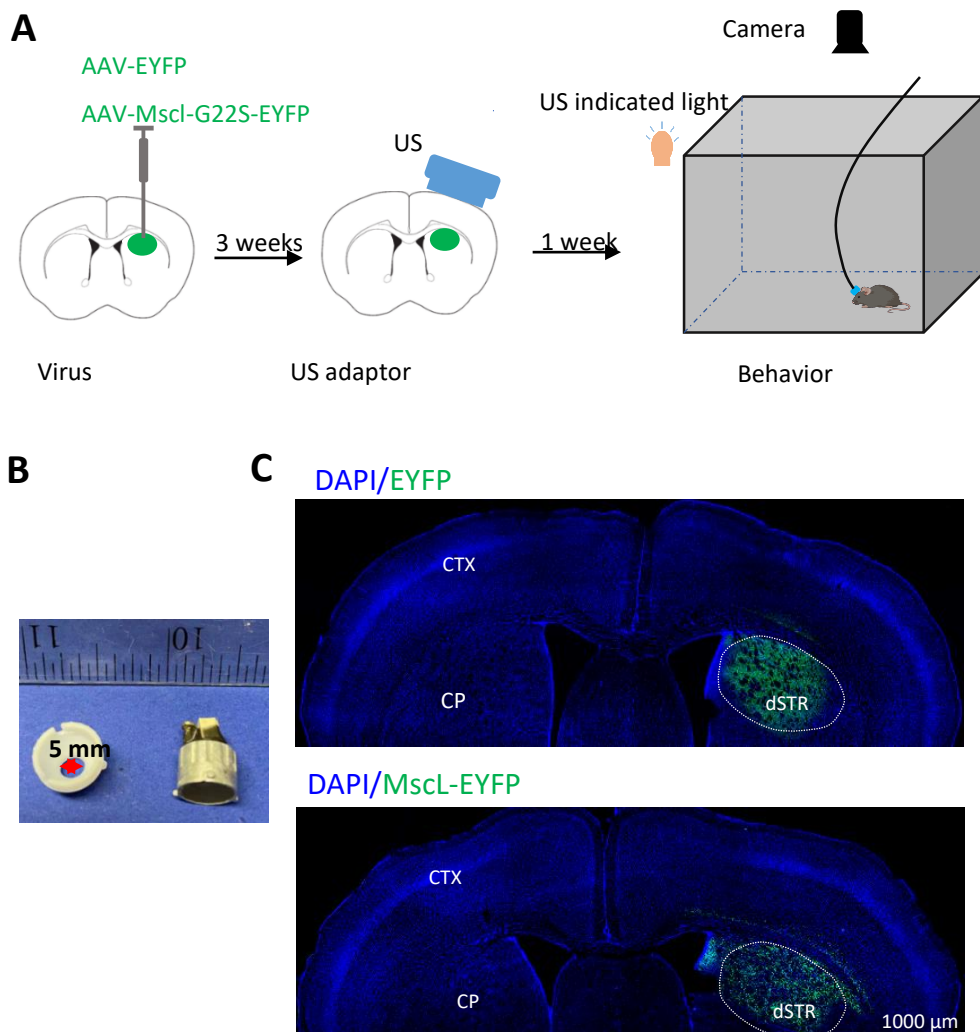


Figure 29 Ultrasound stimulation plan and preparation for locomotion test in awake, freely moving mice. **(A)** Schematic of our experimental scheme. Briefly, mice were injected in the dorsal striatum on the right side mouse's brain with hSyn:EYFP or hSyn:MscL-EYFP. Three weeks later, an ultrasound adaptor was installed and one week after recovery that mice were stimulated with ultrasound. Mice were placed in a square box and their movement were recorded before, during and after ultrasound stimulation with a digital camera. The behavior documented in the video was then analyzed and quantified. **(B)** Schematic illustration of US adaptor and the wearable US transducer. This US transducer weighted ~1g. **(C)** Confocal images indicate expression of hSyn:EYFP (top panel) or hSyn:MscL-EYFP (below panel) in the dorsal striatum (dSTR) of the right side of the mouse brain. Caudoputamen (CP), cerebral cortex (CTX).

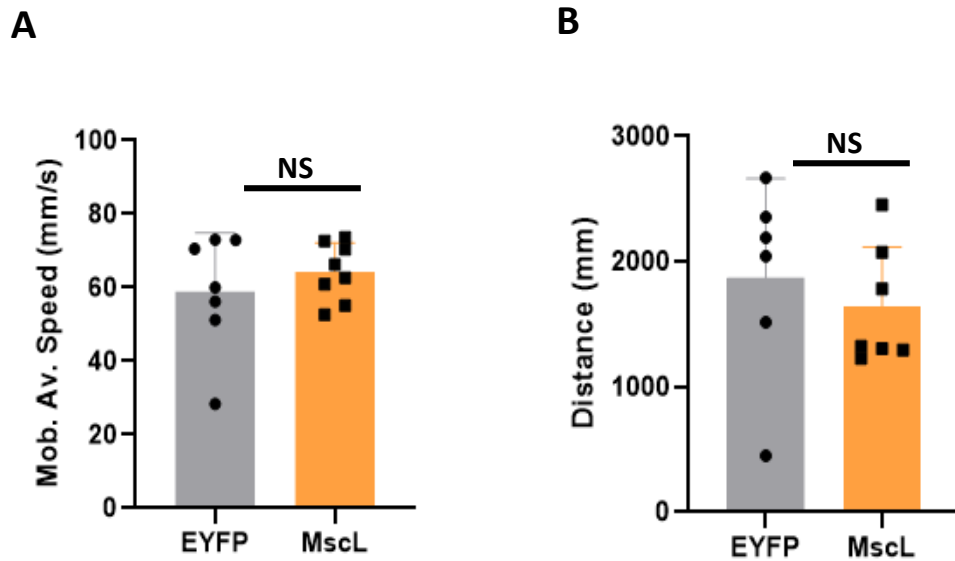


Figure 30 Expression of EYFP or MscL-EYFP in mice do not affect spontaneous locomotive movement. (A) Comparison of mobility average speed of the EYFP and MscL mice before ultrasound stimulation. $n = 6$ mice per group. Unpaired two-tailed t -test. Data are shown as mean \pm SEM; NS, no significance. **(B)** Comparison of distance of the EYFP and MscL mice before ultrasound stimulation. $n = 6$ mice per group. Unpaired two-tailed t -test. Data are shown as mean \pm SEM; NS, no significance.

Then, to test the parameters of low intensity ultrasound on EYFP mice and MscL mice, we performed ranges of ultrasound pressure stimulation (0.1 MPa – 0.35 MPa). We quantified average mobility speed and distance in each epoch (“Pre”, “US”, “Post”). If the mouse is activated by ultrasound stimulation, the mice will increase its motor function, indicating by increasing average mobility speed and increasing distance. At 0.1 MPa, the average mobility speed and distance of both groups did not show any changes in both groups. At 0.15 MPa, there were no obvious movement changes in EYFP group response to US stimulation, while MscL group showed a certain degree increased both in average mobility speed and distance at the same condition (Speed during US: MscL = 70.61 mm/s, EYFP = 61.43 mm/s; Distance during US: MscL =

2989 mm, EYFP = 2210 mm). However, mice with MscL expression in the dorsal striatum were detected a notable increase their locomotor activity during 0.3 MPa pressure of ultrasound treatment, and returning to their baselines post-US, compared to only a minor change for EYFP mice (mobility speed during US: MscL = 81.69 mm/s, EYFP = 65.87 mm/s; distance during US: MscL = 3871 mm, EYFP = 1864 mm) (Fig. 31A, B, D). MscL mice increased their average mobility speeds and distances movement significantly higher during the periods of 0.3 MPa and 0.35 MPa intensities of US stimulation than EYFP mice (Fig. 31C, D), and all mice reduced their activity in the periods between rounds of stimulation (Fig. 31B-E). EYFP mice also shown small increases in their motor activity during US stimulation, but the magnitude of these changes was smaller, and not significant compared to the pre-US and post-US measurements. We suggested that expressing MscL in the dorsal striatum could significantly enhance the motor function of awake and freely moving mice when stimulated by low intensity of ultrasound.

Taken together with the data shown earlier, our findings suggest that dSTR neurons expressing MscL can much better mediate effects of low-intensity US, responding to the pulses by greatly increased Ca^{2+} influx and neuronal activation and increased locomotor behavior.

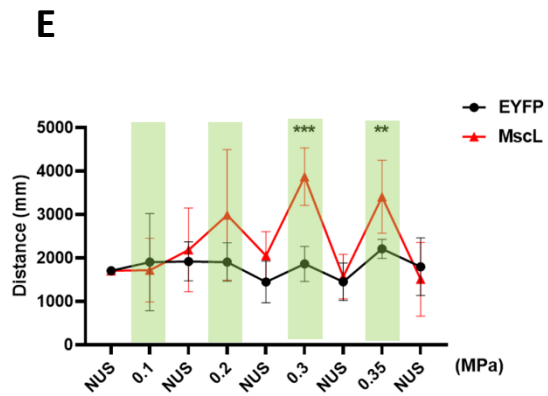
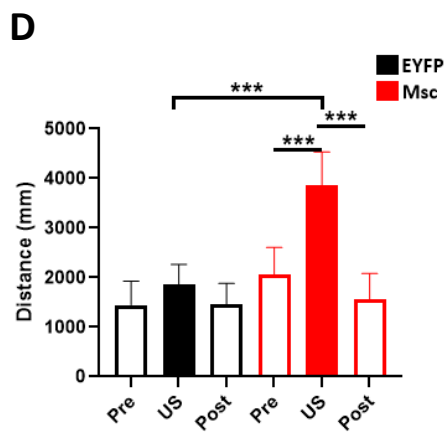
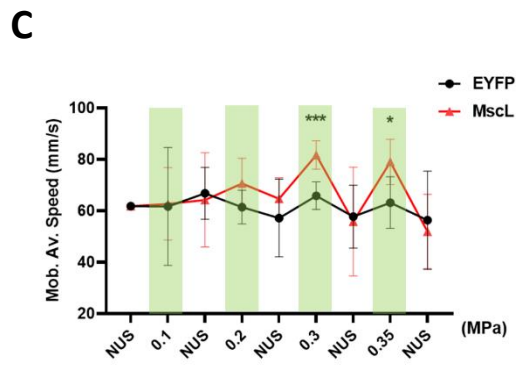
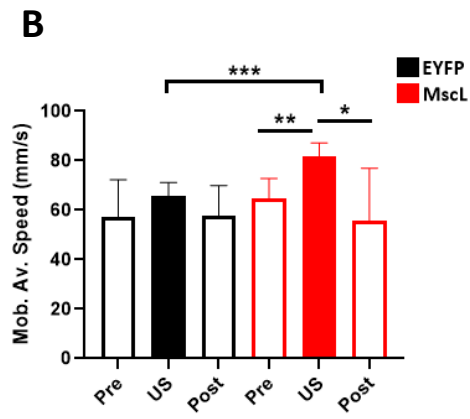
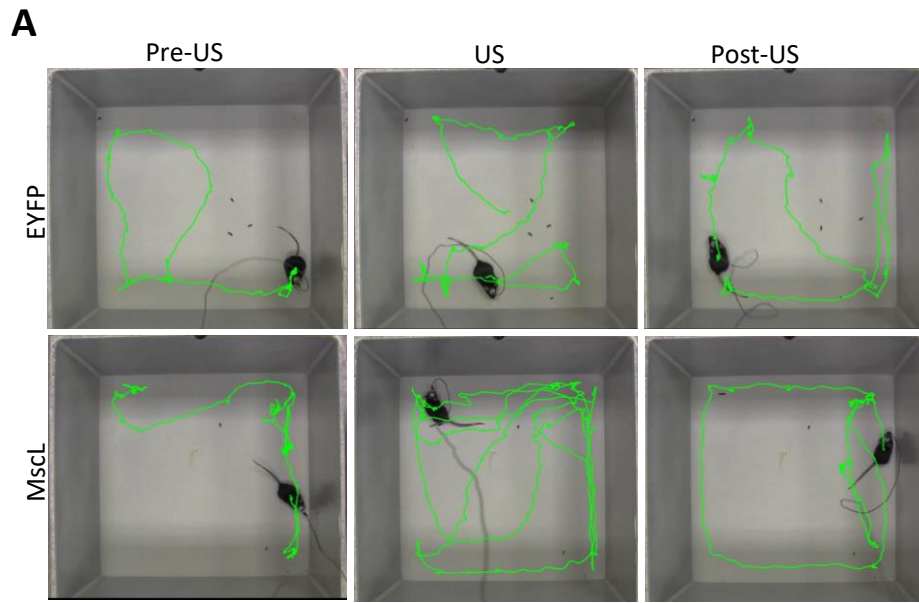


Figure 31 Ultrasound stimulation evoked significant increase in locomotor behavior in mice with Mscl expression in the dorsal striatum. (A) Representative trajectories recorded from mice stimulated in the dorsal striatum pre-US, during US, and post-US with 0.3 MPa ultrasound application (each trace 1 min long). **(B)** Comparison of mobility average speed of the EYFP and Mscl mice, with (0.3 MPa) and without ultrasound stimulation. $n = 6$ mice EYFP group and $n = 6$ mice Mscl group. Data are shown as mean \pm SEM; Unpaired two-tailed t-test. **(C)** Summary of mobility average speed of EYFP and Mscl-expression mice with ultrasound stimulation of different ultrasonic intensities from 0.1 – 0.35 MPa pressure. Green bars indicate the timing of ultrasonic stimuli. $n = 6$ mice EYFP group and $n = 6$ mice Mscl group. Data are shown as mean \pm SEM; Two-tailed unpaired t-test. **(D)** Comparison of distance of the EYFP and Mscl mice, with (0.3 MPa pressure) and without ultrasound stimulation. $n = 6$ mice EYFP group and $n = 6$ mice Mscl group. Data are shown as mean \pm SEM; Unpaired two-tailed t-test. **(E)** Summary of distance of EYFP and Mscl-expression mice with ultrasound stimulation of different ultrasonic intensities from 0.1 – 0.35 MPa pressure. Green bars indicate the timing of ultrasonic stimuli. $n = 6$ mice EYFP group and $n = 6$ mice Mscl group. Data are shown as mean \pm SEM; Two-tailed unpaired t-test.

4.2.4 Benchmark with optogenetics

Furthermore, to identify whether the outcome of this sonogenetics method was reliable. We used the effective and common method, optogenetic, to verify our concern. We transduced the opsin virus with the same hSyn-promoter (hSyn:ChR2-mCherry) into the dorsal striatum in the mouse brain, and followed by an optical fiber insertion. The viruses were allowed to express for four weeks before performing experiment (Fig.

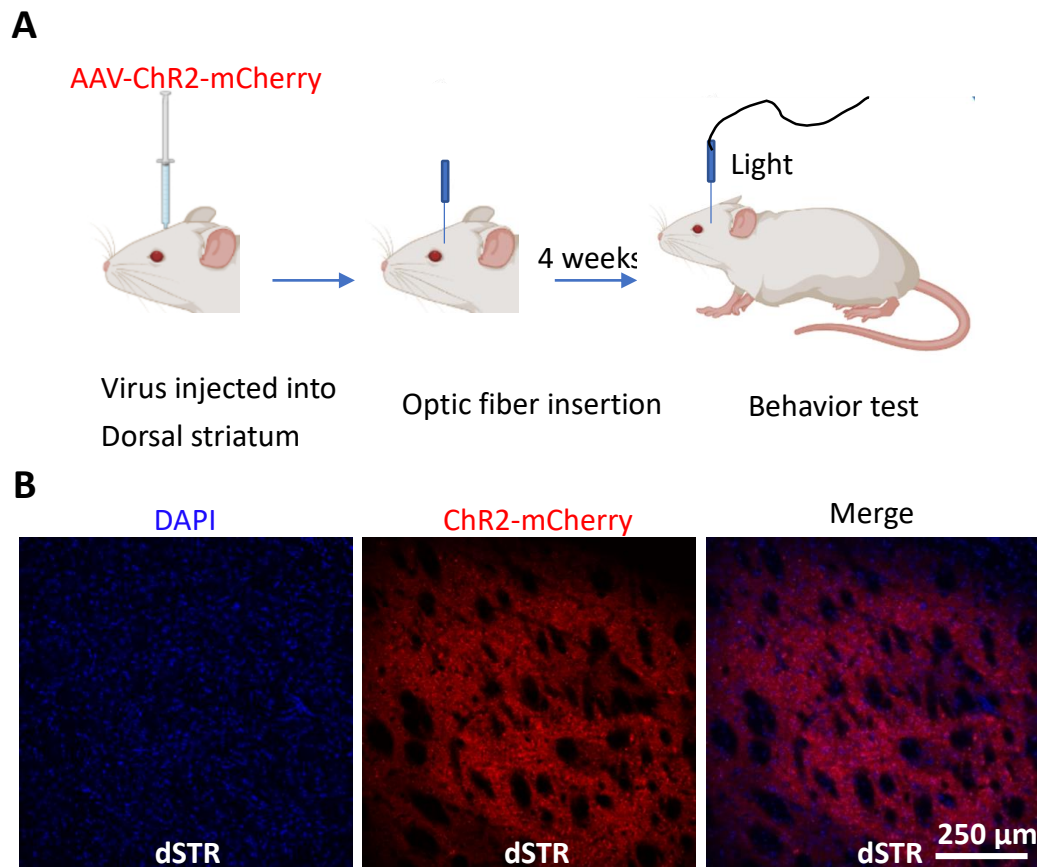


Figure 32 Light stimulation plan and preparation for locomotion test in awake and freely moving mice. (A) Schematic of optogenetic experimental steps. Briefly, mice were injected in their dorsal striatum of the right side of the brain with hSyn:ChR2-mCherry, followed with optical fiber inserting at the same region. Four weeks later, a light adaptor attached to the optical fiber and delivered appropriate light into the mouse brain. Mice were placed in a square box and their movement were recorded before, during and after light stimulation. **(B)** Confocal images indicating ChR2-mCherry in the dorsal striatum (dSTR).

32A). Before we conducted the light stimulation experiment, we used confocal images confirmed that strong ChR2-mCherry fluorescent signal located in the dorsal striatum of right side of mouse brain (Fig. 32B).

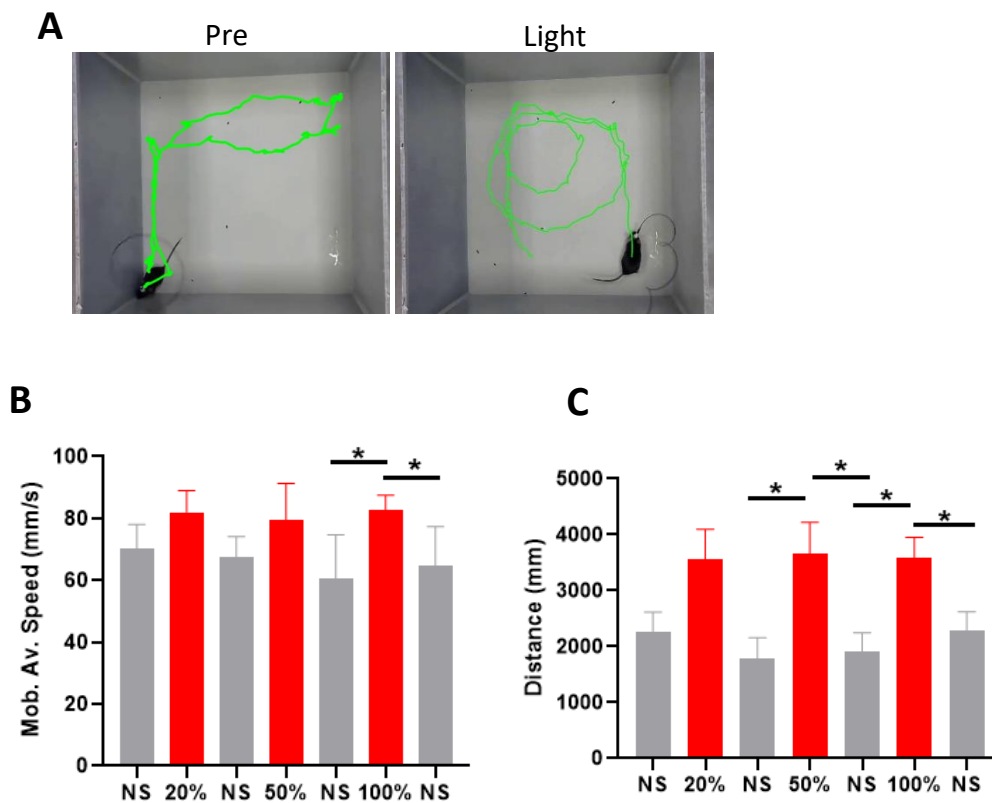


Figure 33 Optogenetic stimulation evoked significant increase in locomotor behavior in mice with ChR2 expression in the dorsal striatum. (A) Representative trajectories recorded from mice stimulated in the dorsal striatum pre-light, during light stimulation (50%, 10 ms, 15 Hz) periods, post-light (each trace 1 min long). **(B)** Summary of mobility average speed of hSyn:ChR2-mCherry mice, with (20% / 50% / 100% power, 10 ms, 15 Hz) and without light stimulation. $n = 3$ mice each group. Data are shown as mean \pm SEM; $*p < 0.05$, Unpaired two-tailed t -test. NS indicates light off. **(C)** Summary of distance of hSyn:ChR2-mCherry mice, with (20% / 50% / 100%, 10 ms, 15 Hz) and without light stimulation. $n = 3$ mice each group. Data are shown as mean \pm SEM; $*p < 0.05$, Unpaired two-tailed t -test

Four-week post-injection, mice were performed the same experimental procedures as in above ultrasonic ultrasound mice, except these mice were treated with light

stimulation instead of ultrasound stimulation. Mice with ChR2 expression in dorsal striatum obviously increased their locomotor activity during light treatment, and

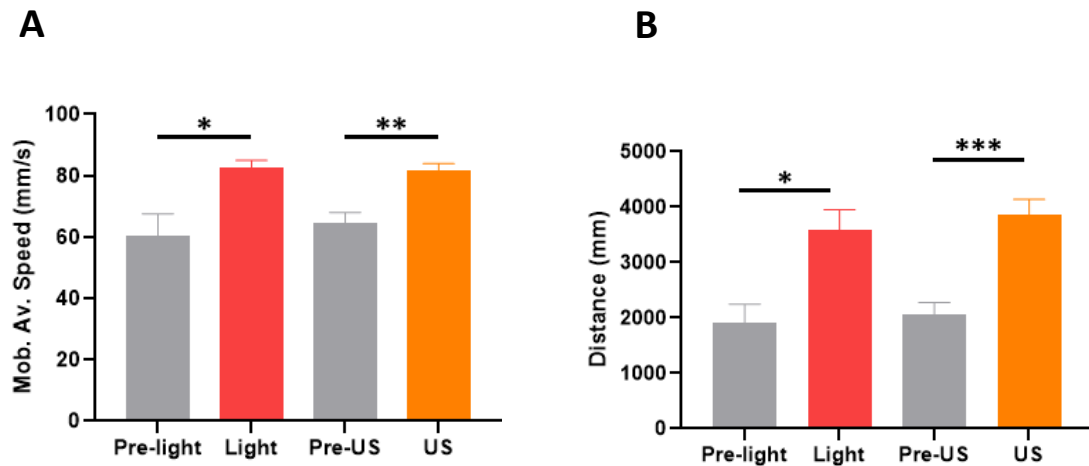


Figure 34 The increasing locomotor behavior evokes by optogenetic and sonogenetic is similar. **(A)** Comparison of mobility average speed of hSyn:ChR2-mCherry mice, with (100%, 10 ms, 15 Hz) light stimulation and of hSyn:MscL-EYFP mice with 0.3 MPa ultrasound stimulation. $n = 3$ mice in optogenetic experiment, $n = 6$ mice in the sonogenetics experiment. Data are shown as mean \pm SEM; * $p < 0.05$, ** <0.01 , Two-tailed unpaired t-test. **(B)** Summary of distance in hSyn:ChR2-mCherry mice, with (100%, 10 ms, 15 Hz) light stimulation and of hSyn:MscL-EYFP mice with 0.3 MPa ultrasound stimulation. $n = 3$ mice in optogenetic experiment, $n = 6$ mice in the sonogenetics experiment. Data are shown as mean \pm SEM; * $p < 0.05$, *** $P < 0.001$, Two-tailed unpaired t-test.

returning to their baselines post-light, (10 ms, 15 Hz, 100% power intensity of light treatment pre-light speed = 60.43 mm/s, speed during light speed = 82.52 mm/s; distance during light = 3585 mm, EYFP = 1902 mm; Fig. 33A-C). This data indicated that light successfully induced locomotive response in ChR2 expression mice.

Next, we made a comparison of locomotion induced by optogenetic method and sonogenetic method, identifying the efficiency of sonogenetics method. We observed that, both, optogenetics and sonogenetics method could enhance the motor activity in freely moving mice. The increasing of the mobility average speed and distance response to light or ultrasound was almost the same (10 ms, 15 Hz, 100% power intensity of light treatment, speed during light speed = 82.52 mm/s; distance during light = 3585 mm; speed during US: MscL speed = 81.69 mm/s, distance during US: MscL = 3871 mm) (Fig. 34A-B). Therefore, we suggested that our sonogenetics strategies successfully modulate freely moving animal's motor movement.

CHAPTER 5 Modulating mesolimbic circuit by MscL-mediated ultrasound stimulation

In addition to the various behavioral indicators, we tested whether US stimulation of a relatively - deep region of the mouse brain could stimulate the secretion of the neurotransmitter dopamine. It has been proposed that technological advances enabling circuit manipulation may open the door to probe neuronal activities that lead to behavior changes [159]. To establish the circuit manipulation, we targeted the mesolimbic circuit, which the dopaminergic projection from the VTA to NAc. VTA (about 4.5 mm deep below the skull surface), a midbrain region where dopaminergic circuits to several other influential regions originate, plays an important functions in various vital dopamine circuits (reward and aversion [160-162]) and is implicated in diverse conditions and diseases [5]. We reasoned that since US stimulation of the upon MscL channel induces a robust calcium influx into neurons, it should also be able to enable dopamine secretion by neurons. Beyond the simple secretion of dopamine in neurons projecting from the VTA, we next evaluated whether we could efficiently stimulate the VTA to induce downstream behavioral changes using sonnon-genetic method.

5.1 Materials and methods

5.1.1 Animal subjects

The animal subjects used in this part are the same as described section 2.2.1.

5.1.2 stereotactic injection

Adult C57BL/6 mice were anesthetized with ketamine and xylazine. Viral vectors were micro-injected into the targeted areas on the right side of the mouse brain by

standard stereotaxic procedures. AAV vectors were injected at the rate of 0.05 μ l per minute through a microinjection pump with a 45-gauge syringe. The syringe was paused in the injected area for 10 min before withdrawal.

a) For the fiber photometry experiments of dopamine release, a volume of 300 nl AAV-hSyn-EYFP or AAV-hSyn-Mscl-G22S-EYFP were micro-injected into the ventral tegmental area applying these coordinates: DV: -4.5 mm, AP: - 2.9 mm, ML: -0.5 mm. 1 μ l hSyn-DA2m then were injected into the nucleus accumbens on the same side using the following coordinates: AP: 1 mm, DV: -4.1 mm, ML: -1.1 mm. Optical fibers were inserted in the NAc region after AAV injection.

b) For reward-related experiments (targeted excitatory neurons in VTA), 300 nl either AAV-CamKII-EYFP or AAV-CamKII-Mscl G22S-EYFP was injected into the ventral tegmental area at DV -4.2 mm, and AP - 2.9 mm, ML -0.5 mm; and. After 3 weeks of viral vectors expression, ultrasound adaptors were installed above the injected VTA regions.

c) For the real time place preference experiments (Targeted dopaminergic neurons in VTA), a volume of 300 nl AAV-hSyn-EYFP or AAV-hSyn-Mscl-G22S-EYFP mixed with pAAV-TH-Cre-WPRE-hGHpA (1:1) were micro-injected into VTA on the right side of mouse brain using these coordinates: AP: - 2.9 mm, ML: -0.5 mm; DV: -4.5 mm. Three-week post-injection, an ultrasound adaptor was installed above the targeted region.

Mice were placed to their original housing areas for recovery.

5.1.3 Fiber photometry recording of ultrasonic induced dopamine release in

anesthesia mice

4 weeks later performed fiber photometry experiment recording. Appropriate ultrasound gel was applied to the head which was shaved to promote acoustic coupling. A 0.5 MHz ultrasound transducer with a water tank was placed on the VTA on the right side of the brain. The DA activity recording in the NAc was conducted by a 488 nm laser at 40 uW for DA2m. Before recording, the mice were allowed rest for 2 – 5 min. Before applying ultrasound, using fiber photometry recorded the spontaneous dopamine activity of mice for 1-2 min. Then, mice were treated with two trials (0.1 MPa and 0.3 MPa) ultrasound stimulation separately. Each trial consisted of 5-15 times stimulation, there would be 3 s interval between each stimulation. And mice were allowed to rest for 45 s – 60 s between different trials of stimulation. Calcium fluorescence was capture with a fiber photometry system. Data were analyzed using custom MATLAB scripts.

5.1.4 Real time place preference assay [84]

After three-week virus expression, mice were installed with ultrasound adaptor and placed the original cages for recover a week. Then, mice were placed to the procedure area and habituated for at least 30 min. Appropriate US gel was placed into the US adaptor for coupling the 0.9 MHz US transducer. After the installment of ultrasound transducer, put the mice into the non-stimulation side of arena(50 cm length × 30 cm width × 30 cm height). Mice were allowed to explore freely two-chambered arenas for 5-10 min. One randomly assigned one side as the US-stimulation side, the other side as non-stimulation side. Once the animal across to the US-stimulation side, the ultrasound wave was delivered until the animal across into the non-stimulation side. Before the test was completed, difference ultrasound power pressures were allocated

every day. The movements of the mice were monitored by a digital camera. The percentage of time spent in both sides (US-stimulated and non-stimulated) was measured. Any mouse with a high initial preference or avoidance for left or right side was discarded [163].

5.1.5 Immunohistochemical fluorescent staining

The process of staining as mentioned above. Coronal brain slices were collected from brain -2.6 mm to 3.3 mm for VTA region and + 0.7 mm to -1.3 mm for NAc region based on the coordinates. Slices were incubated in blocking buffer for 2 h at room temperature. Then, brain slices were incubated in primary antibody (Tyrosine hydroxylase [MAB318, Millipore, 1:500] solution diluted in the blocking buffer overnight. After slices were washed with PBS, bathed with goat anti-rabbit secondary antibodies which was diluted in PBS buffer for two hours at room temperature. Slices were washed, and placed brain slices on glass slide. Samples were captured with the confocal microscope.

5.1.6 Statistical analysis.

Data were shown as the mean \pm SEM. Statistical analyses were processed by the software of GraphPad Prism.

5.2 Results and discussion

5.2.1 Efficient sonogenetically-enabled dopamine release in the NAc by modulating the mesolimbic pathway

To measure the levels of dopamine in the brain upon sonication, we chose to use green, fluorescent GRAB_{DA} sensors. This novel genetically encoded fluorescent DA2m

sensors could be used to specific, real-time detecting of endogenous dopamine dynamic *in vitro* and *in vivo* [164]. Neurons in the ipsilateral VTA were induced by hSyn-promoted EYFP or MscL AAVs, while AAVs for the fluorescent dopamine sensor DA2m under a hSyn promoter were introduced into the NAc (Fig. 35A). An optical fiber was then inserted into NAc to monitor the fluorescence changes of sensors. Four-week post-injection, brain slices were used to assess the efficient of virus expression to determine whether further experiment could be carried out. We can observe robust expression of DA2m signal in the NAc (Fig. 35B), and strong EYFP or MscL signal successfully expressed in dopaminergic neurons in the VTA (Fig. 35C, D).

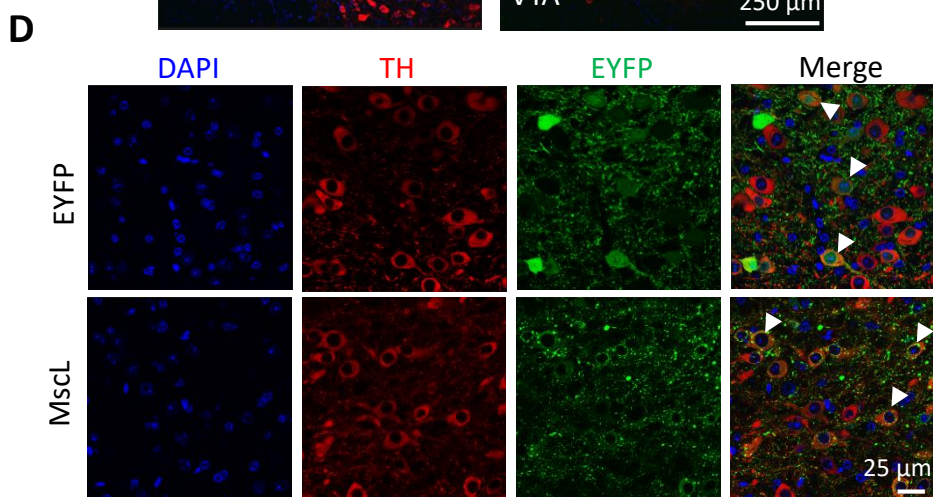
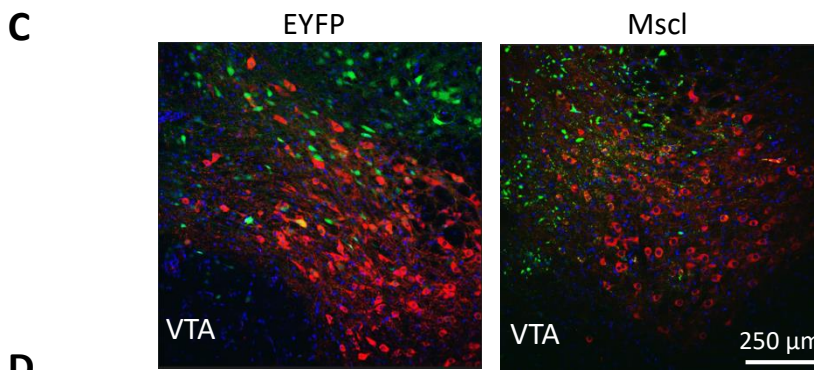
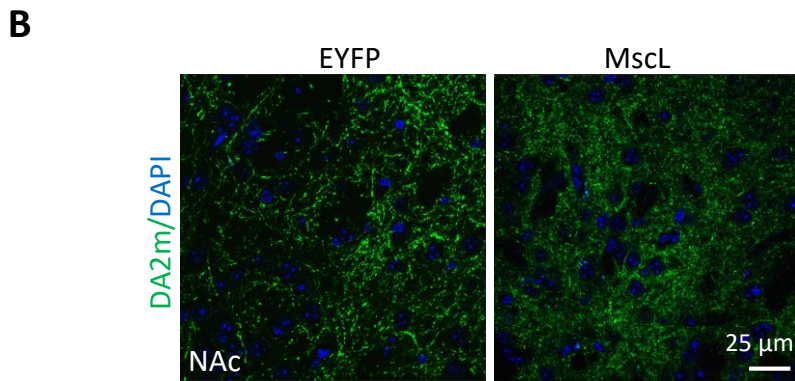
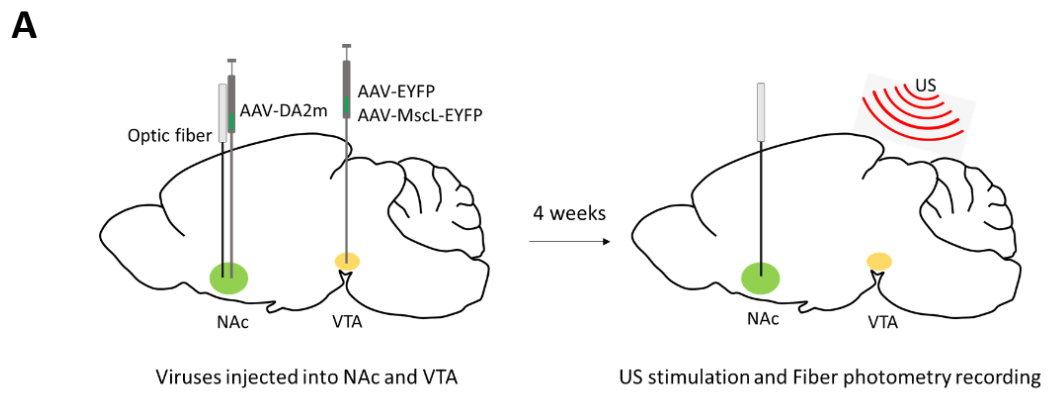
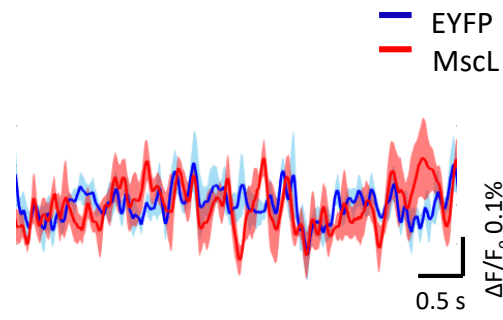
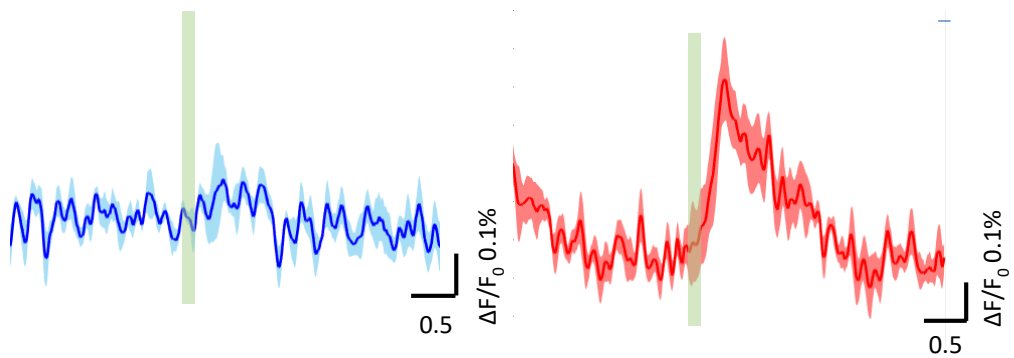
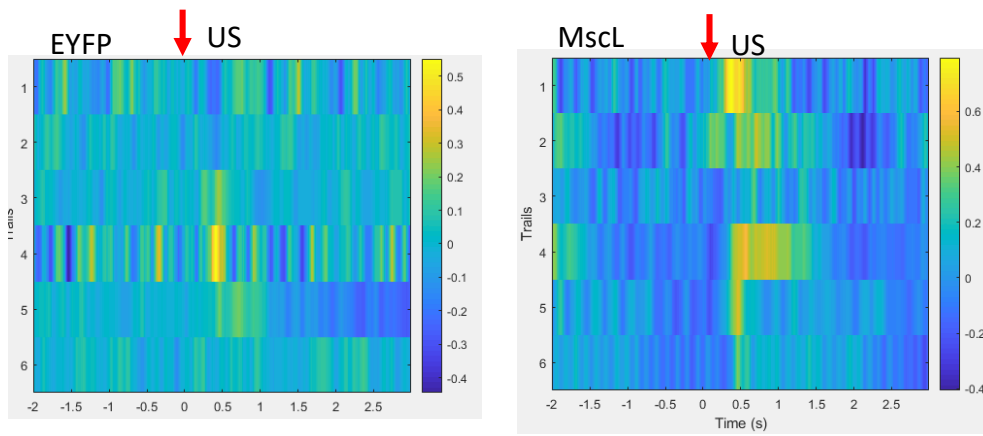
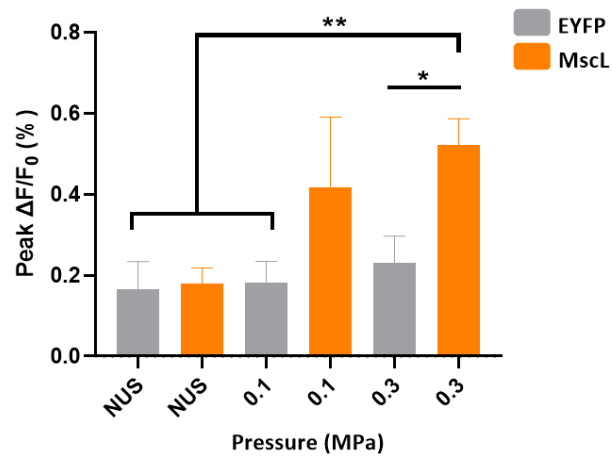


Figure 35 An experimental setup for dopamine signal recording in vivo. (A) Schematic showing the hSyn-DA2m, hSyn-EYFP and hSyn-MscL-EYFP virus delivery, fiber implantation and ultrasound stimulation in the mouse brain. Mice were injected AAV-hSyn-DA2m in the NAc of the right brain and hSyn-EYFP or hSyn-MscL-EYFP in the VTA at the same hemisphere. After virus injection, an optical fiber was inserted into NAc for detecting DA signals. 4-week later, mice were stimulated with ultrasound stimulation and detect DA signals simultaneously. **(B)** Confocal images of NAc region expressing DA2m (green) with DAPI (blue) in EYFP and MscL-expressing brain. **(C)** Confocal images of low magnification of depicting DAPI (blue), TH (red), and EYFP neurons (green) in the VTA. **(D)** Confocal images of high magnification of representing DAPI (blue), TH (red), EYFP (green) neurons in the VTA. White arrows indicated example EYFP+/TH+ neurons.

Next, we monitored the effect of MscL-mediated ultrasound stimulation of the mesolimbic pathway on the dynamic of dopamine. An ultrasound transducer was attached to the head above the injected VTA region and glue it with appropriate US gel. We collected the spontaneous DA dynamic before applying any ultrasound stimulation. The spontaneous DA signals were stable and consistent in both EYFP group and MscL group (Fig. 36A). Upon stimulation of the VTA with pulses of 0.3 MPa pressure of ultrasound, we found rapid synchronous increases in DA2m fluorescence in the NAc of the MscL + US condition but not with EYFP + US (Peak $\Delta F/F_0$, EYFP = 0.23%, MscL = 0.52%) (Fig. 36B). NUS and EYFP+US conditions at both the tested US intensities were found to show very little fluorescence change, and the MscL + US conditions were much larger in magnitude at both 0.1 MPa (Peak $\Delta F/F_0$, EYFP = 0.18%, MscL = 0.42%) and 0.3 MPa, although only the 0.3 MPa condition was statistically significant (Fig. 36). These results suggested that low pressure sonication could

efficacious activate VTA neurons with MscL-expression and induce an obvious DA increasing in nucleus accumbens *in vivo*.

We then tested whether the ultrasound stimulation can repeatedly evoke neural activity in the VTA neurons which expressed MscL in mice, leading to dopamine release in NAc. Five times of ultrasound pulses, each with 3 s interval, were delivered to the US transducer above the VTA region *in vivo*. We observed stable and synchronous increasing DA fluorescence in response to each US stimulation trial in MscL expressing mice, while EYFP mice did not (Fig. 36D). Thus, we suggested that stimulating the MscL-expressing VTA of mice could successfully and specifically induce DA secretion in neurons projected to the NAc *in vivo*.

A**B****C**

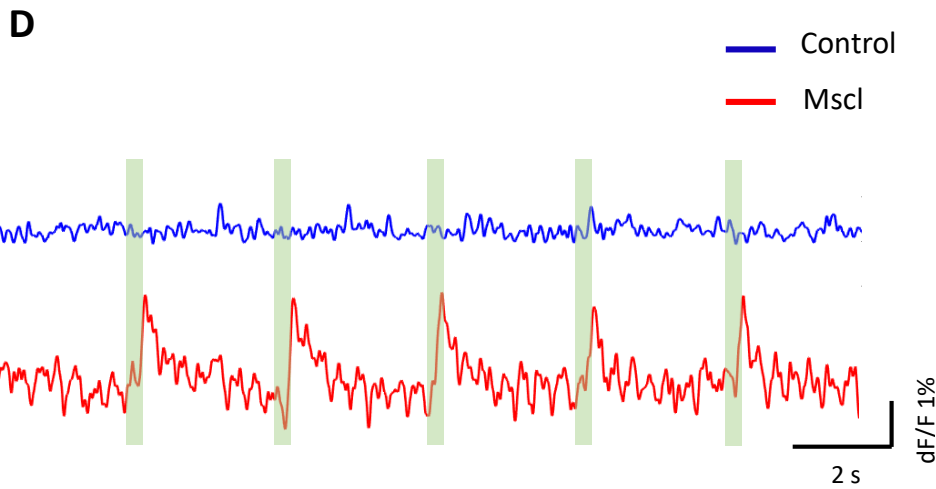


Figure 36 Sonogenetic stimulation of VTA neurons evokes DA release in NAc in vivo. (A) Averaged DA2m fluorescence signal without ultrasound stimulation in the NAc of the anesthetized EYFP- mice and MscL-expressing mice. $n = 6$ trials, 4 mice in EYFP group. $n = 6$ trials, 5 mice in the MscL group. **(B)** Average DA2m fluorescence signal response to ultrasound stimulation in the NAc of the anesthetized EYFP- mice and MscL-expressing mice. $n = 6$ trials, 4 mice in EYFP group. $n = 6$ trials, 5 mice in the MscL group. **(C)** Average peak DA2m activity responds to 0.3 MPa ultrasound stimulation in EYFP- mice and MscL-expressing mice. $n = 6$ trials, 4 mice in EYFP- group. $n = 6$ trials, 5 mice in the MscL-expressing group. * $P < 0.05$, ** $P < 0.01$, Unpaired two-tailed t -tests. Data are shown as mean \pm SEM. **(D)** DA2m fluorescence traces in the NAc of EYFP and MscL mice undergone repeated ultrasound stimulation (0.3 MPa). The blue and red examples represent the EYFP group and MscL group, respectively. Light green rectangular shows the timing of ultrasound stimulation.

5.2.2 Inducing appetite preference by MscL-mediated ultrasound stimulation in excitatory neurons of VTA

Data above showed that MscL-mediated ultrasound could modulate the mesolimbic circuit, resulting in DA release in NAc. We next examined whether these changes were sufficient to influence animal's behavior. VTA plays a vital role in reward and aversion [160, 161]. Dopaminergic neurons [79, 165] and Glutamatergic neurons [166] in VTA have been reported participating in the reward process. First, to test whether transcranial MscL-mediated ultrasound stimulation in excitatory neurons of VTA could particularly control appetitive conditioning, we performed real-time place preference test. The VTAs of mice were transduced with EYFP or MscL AAVs under a CaMKII promoter to induce their expression in excitatory neurons. After a 4-week span for virus expression in the brain, mice were examined with behavioral test (place preference test, Fig. 37A, B). Confocal images indicated that CamKII-EYFP and CamKII-MscL-EYFP successfully expressed in VTA region, and some of EYFP / MscL – EYFP signal expressed in dopaminergic neurons (TH antibody is a marker of dopaminergic neurons) (Fig. 37C).

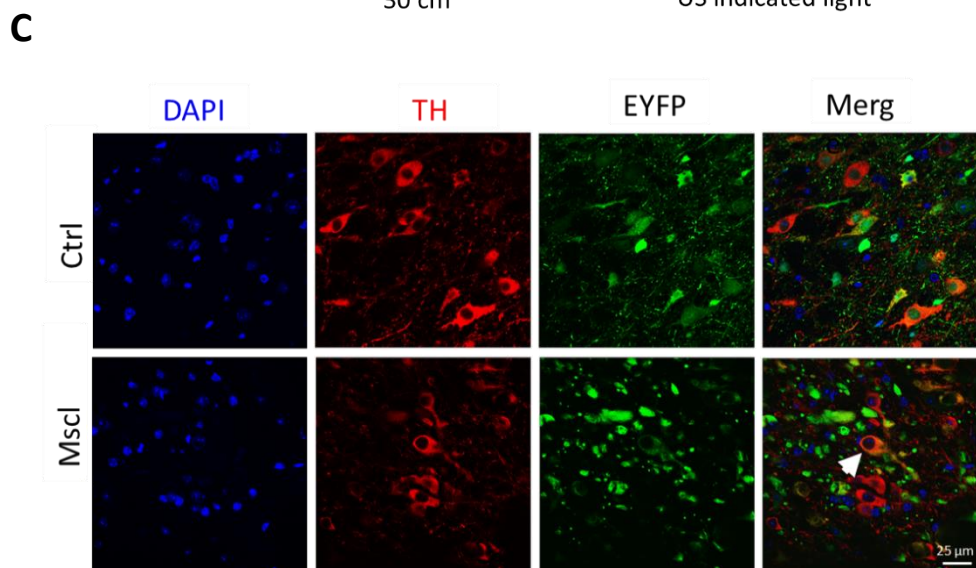
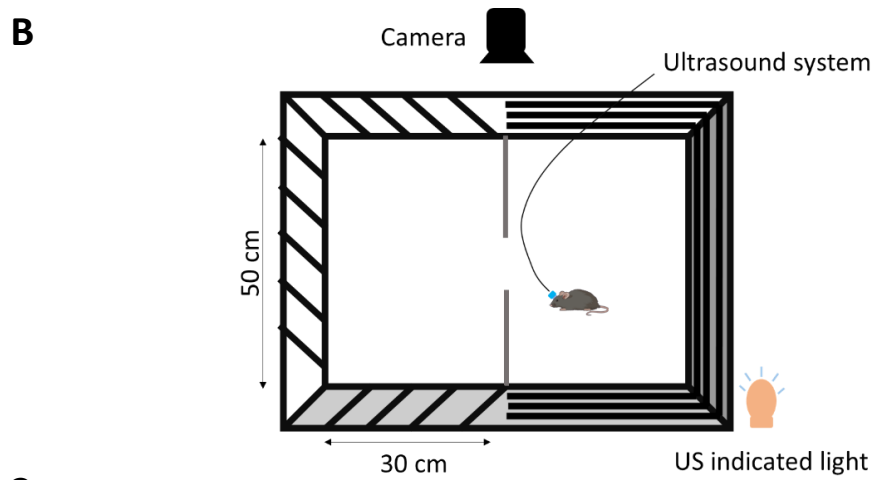
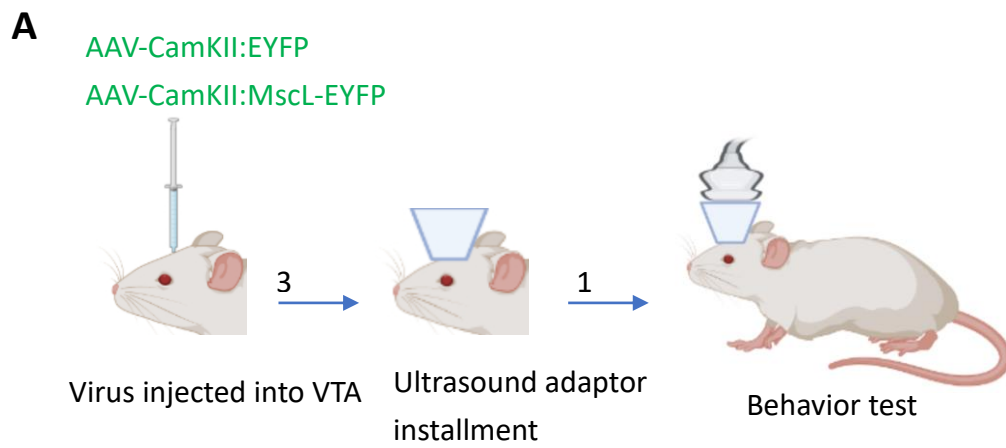


Figure 37 Ultrasound stimulation plan and setup for the place preference test in awake and freely moving mice. (A) Schematic of our experimental scheme. Briefly, mice were injected into their right ventral tegmental area with CamKII:EYFP or CamKII:MscL-EYFP. Three weeks later, an ultrasound adaptor was installed and one week after recovery that mice were stimulated with ultrasound. Mice were put in a rectangle arena and were recorded their trajectories with a camera. The behavior documented in the video was then analyzed and quantified. **(B)** An illustration of the real time place preference apparatus. Our RPP apparatus consists of a chamber divides into two equal side, one side with vertical stripes walls and the other side with horizontal stripes walls. Mouse movement in the two sides during each preference test detected by a digital camera. An US indicated light indicates the start and end of ultrasound. **(C)** Confocal images indicating expression of CamKII:EYFP (Top) or CamKII:MscL-EYFP (Below) in the VTA. DAPI (blue), TH (red), EYFP (green) neurons, and in the VTA. White arrows showed representative EYFP+/TH+ neurons.

Next, in real time place preference assay, the animal is placed in a rectangular open field with two distinct halves. One of these sides is paired with ultrasound stimulation. It can be classified as rewarding or aversive stimulation for mice, by depending on whether this stimulation is activating or suppressing. If the mice spend more time in the side where stimulation is activated, this activation is defined as rewarding. Instead, if the animal spends less time on the side where stimulation is on, this suppression is considered as aversion. In this studies, EYFP mice and MscL mice were placed in one side of chambers. After finishing videos recording, we calculated the time proportion in the stimulation side, average mobility speed, and distance.

As shown in our results, in the absent of ultrasound stimulation, no obvious difference in the spent time proportion in the stimulation side between EYFP mice and

MscL mice can be detected. However, MscL + US mice were found to spend significantly more time in the US stimulation side than pre-US stimulation, or compared to pre- and post-US EYFP mice (time in US stimulation side, EYFP + US = 35.20%, MscL + US = 60.36%; Fig. 38A, B). In addition, MscL + US mice also covered significantly higher distances during their recorded time inside the box, indicating that they had greater motivation to move around and explore in this condition (distance in US stimulation side, EYFP + US = 9122 mm, MscL + US = 17300 mm; Fig. 38C). However, the various groups of mice showed little difference in their average mobile speed, indicating that the MscL + US group's increased movement was not due to any changes in their ability to move compared to other groups (Fig. 38D). Hence, we found that US stimulation of mice VTAs expressing MscL could successfully and specifically affect the activity of excitatory neurons and induce appetitive conditioning behavior.

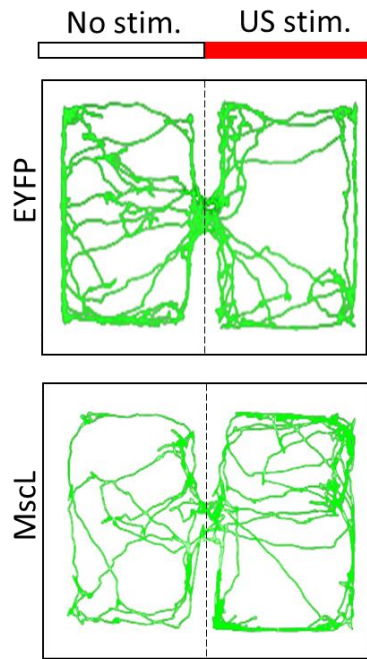
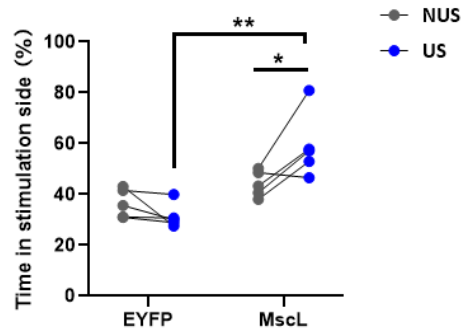
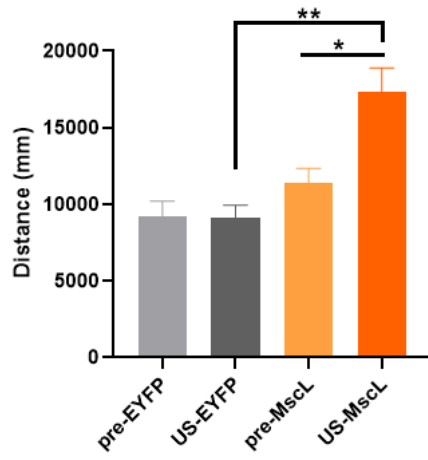
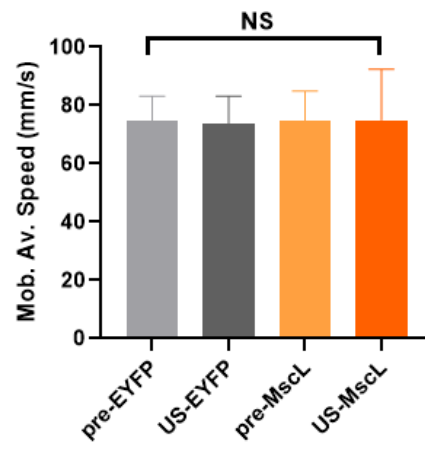
A**B****C****D**

Figure 38 Deep MscL-mediated ultrasound stimulation can induce appetitive conditioning.

(A) Examples path-trajectories of a mouse with CamKII:EYFP or CamKII:MscL-EYFP expression during the appetition test. Red rectangle showed the US-stimulation side. **(B)** Percentage of time spent on the US stimulation side at 0.05 MPa pressure ultrasound in EYFP (control, gray) and MscL mice (orange) ($n = 4$ mice in EYFP- mice; $n = 4$ mice in MscL-expressing mice, Repeated two rounds. * $P < 0.05$, two-tailed unpair t -test. Data are shown as mean \pm SEM. **(C)** Average distance during 0.05 MPa sonication epoch on the US stimulation side was noticeable higher than the non-stimulation side in MscL group, and showed significantly different than the EYFP-US. ($n = 4$ mice in EYFP mice; $n = 4$ mice in MscL-expressing mice, * $P < 0.05$, two-tailed unpair t -test. Data are shown as mean \pm SEM. **(D)** Average mobility velocity during sonication epoch on the stimulation side was not obvious changes than the non-stimulation side in EYFP and MscL group. * $P < 0.05$, ** $P < 0.01$, one-way ANOVA with post-hoc Tukey test. Data are shown as mean \pm SEM.

In addition, we examined the effects of higher intensities of ultrasound stimulation in transduced mice. Different intensities of ultrasound stimulation were stochastically distributed each daily trial until the end of examination (Fig. 39A). We observed that in EYFP mice, the proportion of time spent on the US stimulation side decreased as the ultrasound pressure increased. The mobility speed in these two groups did not show obvious difference (Fig. 39C). At the 0.25 MPa ultrasound stimulation, EYFP mice showed the aversion response that spent notably smaller time in the stimulation side compare the Non-US stimulation day, which consistent with the results of Niu et al. [167]. They showed that applying sonication on NAc led to a notable avoidance behavior. At 0.1-0.25 MPa, certain degree of avoidance response could be observed in

MscL group. However, in the MscL-mice, the time percentages spent on the stimulation side (0.1 MPa and 0.25 MPa) were notably higher than EYFP mice (Fig. 39B). We suggested that the outcome of MscL-mediated ultrasound stimulation on VTA was to rescue of aversive conditioning which caused by ultrasound itself.

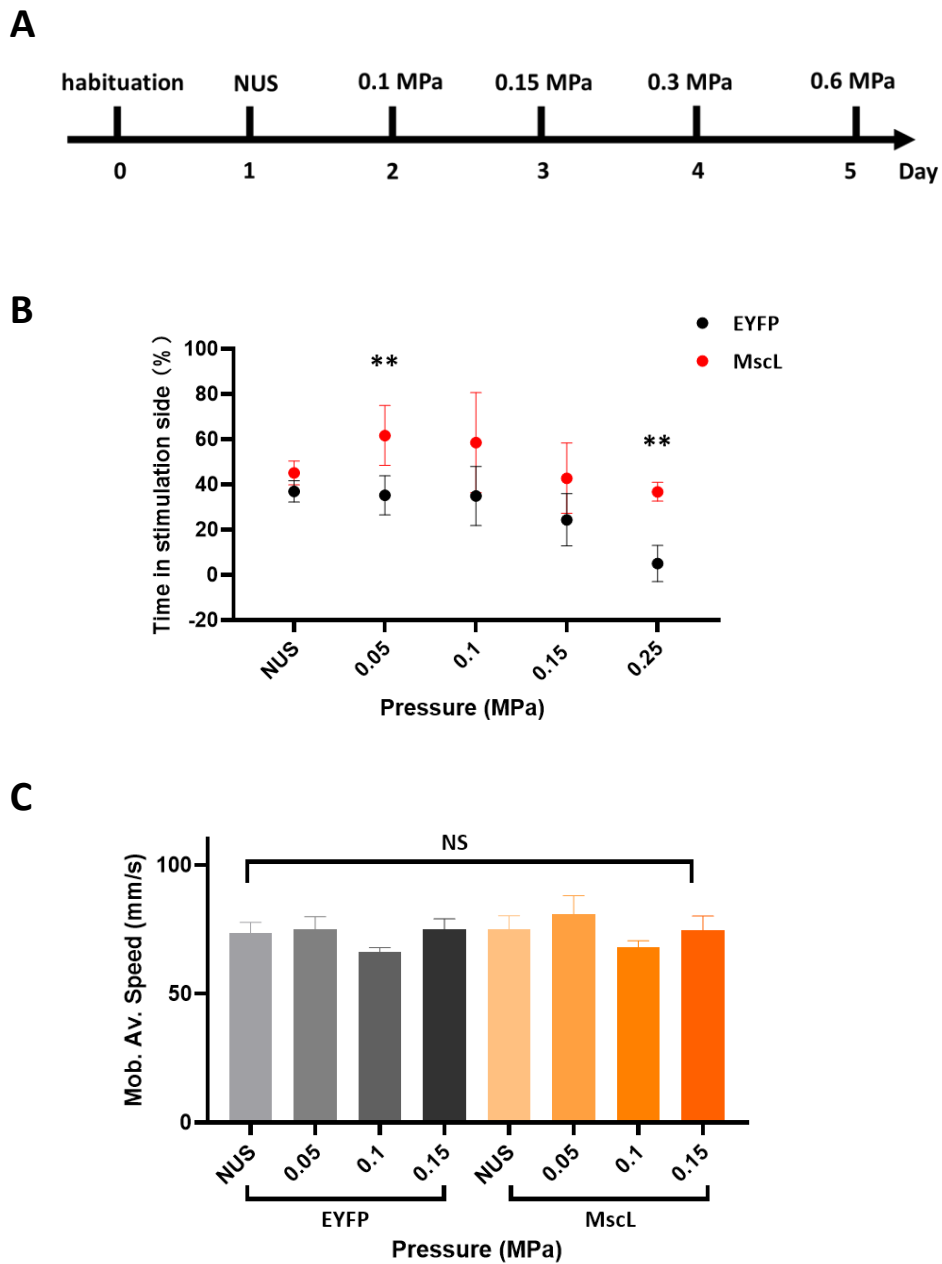


Figure 39 MscL-mediated ultrasound stimulation activates the excitatory neurons in VTA. (A)

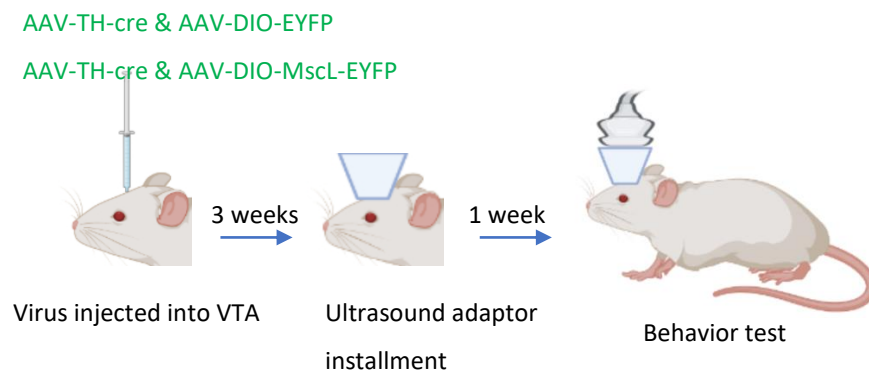
The workflow of appetite test with ultrasound stimulus. **(B)** Percentage of time spent on the US stimulation side at difference pressures of ultrasound stimulation in EYFP and MscL mice. $n = 4$ mice in EYFP- mice; $n = 4$ mice in MscL-expressing mice, Repeated two rounds. * $P < 0.05$, unpair two-tailed t -test. Data are shown as mean \pm SEM. **(C)** Average mobility velocity during different pressure sonication epoch on the stimulation side was not obviously different than the non-stimulation side in EYFP and MscL group. $n = 4$ mice in EYFP mice; $n = 4$ mice in MscL-expressing mice. * $P < 0.05$, ** $P < 0.01$, one-way ANOVA with post-hoc Tukey test. Data are shown as mean \pm SEM.

5.2.3 Inducing appetite preference by MscL-mediated ultrasound stimulation in dopaminergic neurons of VTA

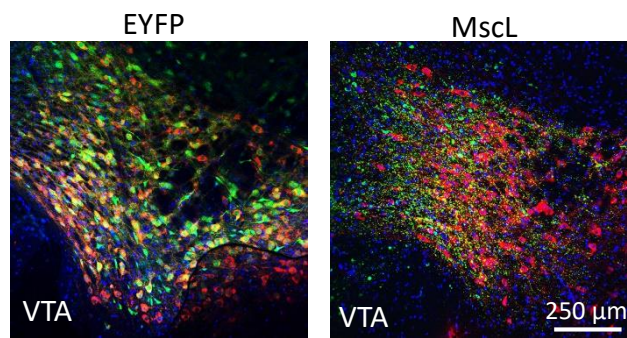
To test the circuit-level functionality in nervous system, above MscL-mediated ultrasound stimulation experiment have used general promoter (hSyn promoter) or excitatory neuron specific (CamKII-promoter) promoter. In this session, to test whether MscL could be targeted into the specific neuron type (dopaminergic neurons) of VTA in wildtype mouse, we used two viral vectors to carry it out: one vector carried Cre recombinase under the modulation of a tyrosine hydroxylase promoter (TH-promoter) [168, 169], the other viral vector was responsible for delivering a Cre-recombinase-dependent EYFP or MscL-EYFP fragment (Fig. 40A). AAV-TH-cre viral vectors were mixed with AAV- EF1 α ::DIO-EYFP or AAV-EF1 α ::DIO-MscL-EYFP together and injected into the VTA. Viruses were allowed to express for 4 -5 weeks. Brain slices were used to staining with TH antibody (a marker of dopaminergic neurons). The low

magnification of confocal images showed the EYFP / MscL -EYFP fluorescence was successfully transfected into VTA region (Fig. 40 B). Moreover, the high magnification pictures demonstrated highly specific EYFP or MscL expression in dopaminergic neurons (Fig. 40C).

A



B



C

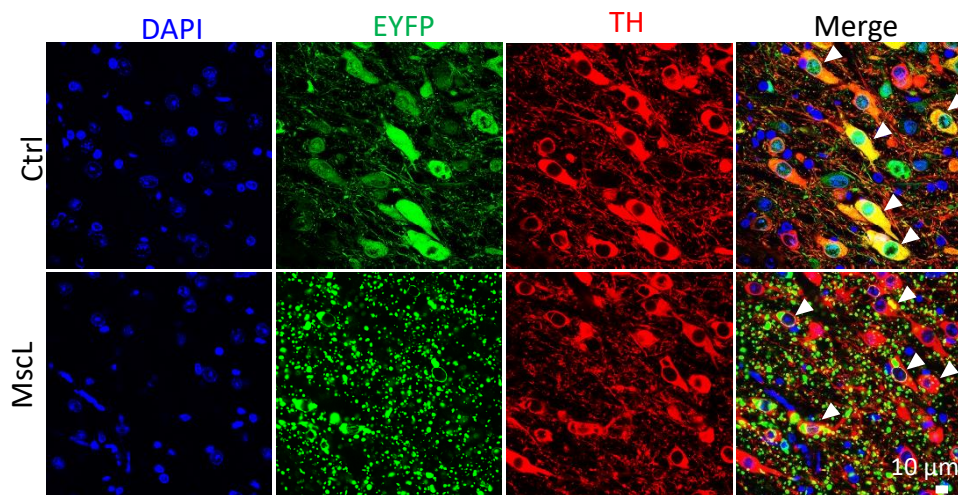


Figure 40 Ultrasound stimulation plan and setup for the real time place preference assay in TH-cre mice. (A) Schematic of our experimental scheme. Briefly, mice were injected into their right ventral tegmental area were co-injected with AAV-TH-cre mix with AAV- EF1 α ::DIO-EYFP or AAV-EF1 α ::DIO-MscL-EYFP. Three weeks later, an ultrasound adaptor was installed, and one week after recovery that mice were stimulated with ultrasound. Mice were put in a rectangle chamber and were monitored their trajectories. The behavior documented in the video was then analyzed and quantified. **(B)** Low magnification of confocal images indicating expression of TH:EYFP or TH:MscL-EYFP in the VTA. DAPI (blue), EYFP neurons (green), and TH (red) in the VTA. **(C)** High magnification of images showing TH:EYFP (Top) or TH:MscL-EYFP (Below) in the VTA. White arrows indicate example EYFP+/TH+ neurons.

After confirming the virus expression was successful, we also tested whether MscL mediated ultrasound stimulation could specifically modulate appetitive conditioning. It has been reported that appropriate ultrasonic stimuli could induce aversion in wild-type mice [167]. Our study also indicated that EYFP mice showed a little aversion response while mice were received 0.1 MPa ultrasound stimulation. A larger aversion response can be observed while the mice were stimulated with 0.3 MPa sonication in EYFP mice (Fig. 41B). In contrast, MscL-expressing mice spent a higher proportion of time in the 0.1 MPa stimulation-paired chamber compared to the non-stimulation chamber. In addition, MscL mice showed spent obviously more time on the stimulation side with 0.1 MPa and 0.15 MPa pressure compared to EYFP group (Fig.41A, B). In summary, we found that US stimulation of mouse of MscL-expressing dopaminergic neurons in the VTA could successfully and specifically induce appetitive

conditioning behavior, while mice without MscL showed obvious aversive responses.

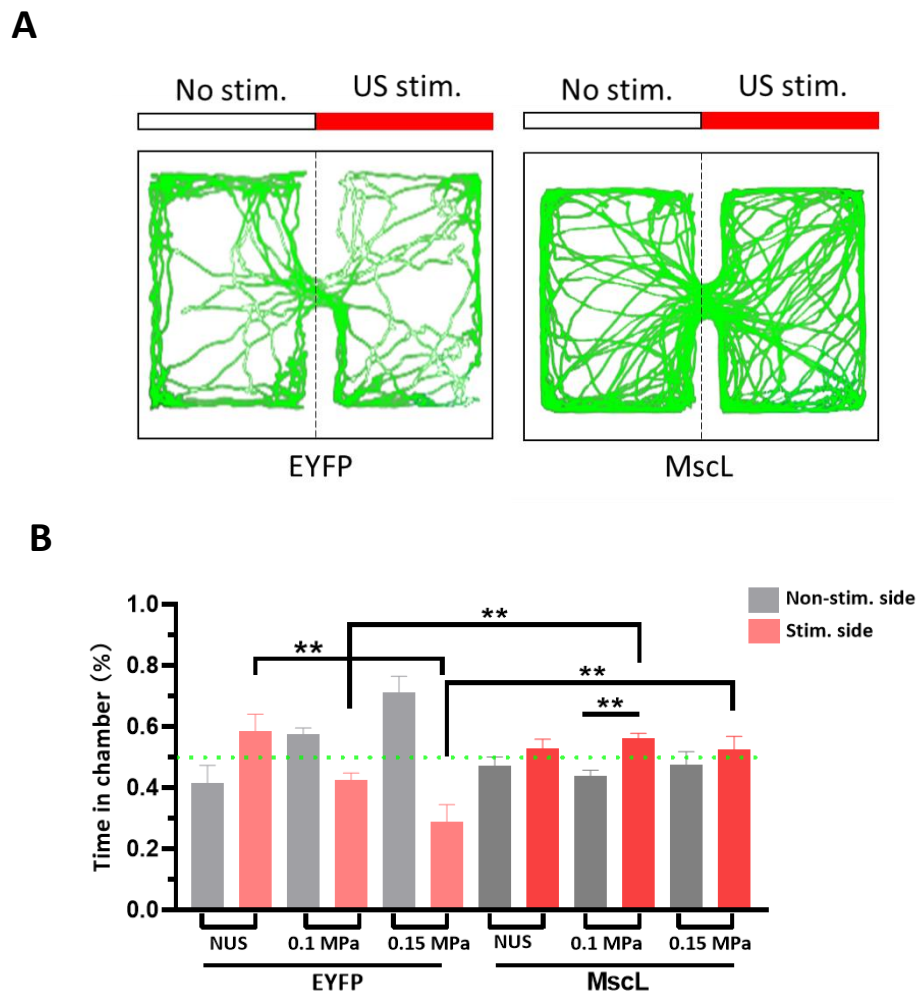


Figure 41 Selective targeted dopaminergic neurons in VTA by MscL-mediated ultrasound stimulation enable change mice's appetitive conditioning. (A) Examples path-tracing of a mouse with TH-cre-EYFP or TH-cre-MscL-EYFP expression during the appetition test (0.1 MPa ultrasound stimulation). A Red bar indicates the stimulation side. A White bar indicates the non-stimulation side. **(B)** Percentage of time spent on the stimulation side at NUS, 0.1 MPa, 0.15 MPa pressure of ultrasound in EYFP and MscL mice. $n = 5$ mice in EYFP mice; $n = 5$ mice in MscL-expressing mice. ** $P < 0.01$, unpair two-tailed t -test. Data are mean \pm SEM.

Thus, the MscL channels' expression could successfully mediate ultrasound stimuli to enable neuronal activation and repressing the aversive response.

CHAPTER 6 Conclusions and future work

In summary, based on the results described above, we elicited neuronal activity *in vivo* and, more importantly, demonstrated four significant behavioral outcomes using the MscL-mediated ultrasound stimulation of four well-defined neuronal circuits.

First, in anesthetized mice, we found that the effect of MscL-mediated ultrasound stimulation of the motor cortex could evoke strong muscular contractions. Second, in awake and head-restrained mice, low-intensity sonication activated MscL-expressing excitatory neurons in the barrel cortex *in vivo*, inducing high-level changes of the whisker movement angle by activating the whisker-to-barrel cortex pathway. Third, in freely-moving mice, we targeted dorsal striatum neurons that expressed MscL and enhanced motor function using low-intensity ultrasound stimulation. Fourth, using this method, we successfully evoked endogenous DA release in the NAc by modulating the mesolimbic pathway in mice. Moreover, we specifically targeted dopaminergic neurons in the VTA and affected appetitive conditioning through MscL-mediated ultrasound stimulation. In conclusion, our sonogenetics approach could modulate the neuronal activity of specific cell types and selectively alter related behaviors in animals in a non-invasive manner with high spatial precision.

Our sonogenetic method has high spatial precision. The deepest target region we selected was the VTA, which is located approximately 4.5 mm below the skull. To control the diameter of the omnidirectional ultrasonic wave delivered into the brain, we use a plastic tube/ultrasound adaptor. Both the diameter of the surface contact between the mouse brain and of the plastic tube/ultrasound adaptor were around 5 mm. We observed that the 5-mm omnidirectional ultrasonic wave generated by the ultrasound system could selectively activate a 1.5-mm diameter region of MscL-expression but not

the surrounding areas. A key merit of sonogenetics over traditional ultrasound stimulation is that sonogenetics selectively emits omnidirectional acoustic waves and activates only MscL-expressing regions, affirming the high spatial precision of our technique. Next, we plan to investigate whether a smaller target area can be activated using the same ultrasound modality.

Several researchers have debated whether the motor response caused by ultrasound stimulation arises from direct activation of the target regions or from indirect sensory effects (auditory effects) [126, 127]. To address this concern, all of the experiments of this project were conducted on an EYFP (control group) and MscL group. Both groups were subjected to the same procedures and ultrasound stimulation, with the only difference being the type of viral vectors (EYFP or MscL-EYFP) that was injected. If the auditory circuit is indeed involved in mediating the response, we might expect to detect similar Ca^{2+} fluorescence responses or behavioral responses in both the EYFP and MscL mice. However, as shown by our data, there was a notable difference between the responses of the EYFP and MscL groups to low-intensity ultrasound, verifying that the responses in the MscL mice were not mediated by indirect acoustic effects. We also designed a simple sham treatment for the awake whisker movement experiment and observed that the mice did not produce whisker movements without ultrasound gel to guide the sound wave. In addition, although we detected neuronal activation of the auditory cortex in both the wild-type + ultrasound and deaf + ultrasound groups, the c-Fos expression level was not obviously different between the two groups. Collectively, these data showed that MscL-mediated ultrasound stimulation generates direct neuronal stimulation *in vivo* with sharp spatiotemporal resolution and the auditory circuit does not play major role on the process of sonogenetics.

A meaningful understanding of brain function and disease treatment requires the development of non-invasive neuromodulation technology for the causal modulate of

specific neuron types without the requirement for fiber implantation. Ultrasound is a promising neuromodulation modality that can potentially modulate brain activities in a non-invasive manner. By combining the properties of different MS ion channels, ultrasound can selectively and non-invasively manipulate neuronal activity in both surface and deep brain regions. This project showed that MscL-mediated ultrasound stimulation can affect the primary motor cortex, somatosensory cortex, dorsal striatum, and VTA and alter related behaviors in mice by modulating specific neural circuits. Sonogenetics might therefore facilitate our understanding of fundamental and pathological brain neural circuits, which might contribute to make pathway abnormalities the basis of diagnostics and the normalization of pathway functions as a goal of future interventions. Although a variety of studies have proposed the potential mechanisms by which ultrasound stimulation exerts its influences on the brain, the main principle of ultrasound stimulation has not yet been elucidated. Further experiments are required to outline these mechanisms before sonogenetics can be more extensively adopted by neuroscientists and translated to clinical practice.

6.1 Optimization of ultrasound parameters

In this study, we combined ultrasound stimulation with advanced fiber photometry and used genetically encoded Ca^{2+} indicators to detect the real-time Ca^{2+} dynamics induced by MscL-mediated ultrasound stimulation *in vivo*. Low-intensity ultrasound stimulation successfully modulated the MscL-expressing neurons in the barrel cortex and dorsal striatum in anesthetized mice, resulting in a robust and rapid increase in Ca^{2+} spikes; the EYFP mice showed no or little response to ultrasound stimulation. As the intensity of ultrasound increased, so did the Ca^{2+} peak amplitudes of the neurons, which was consistent with previous *in vitro* reports [112]. In addition, the response latencies of the MscL group were markedly shorter than those of the EYFP group. The latencies

of both groups were 200–300 ms, which corresponded with the findings reported by Shapiro et al. [112]. Interestingly, in the whisker-barrel cortex experiment, the EFYP group showed some response to ultrasound stimulation both in terms of Ca^{2+} dynamics and whisker movement. We found that the EYFP group also responded to relatively high-intensity ultrasound stimulation, indicating the presence of some endogenous MS ion channels (such as Piezo1 [170], TRPV1[171], TRPP1/2[172]) in the brain, which is consistent with our previous *in vitro* data. Hence, low-intensity ultrasound or a short pulse width/stimulation duration could limit the ultrasound influences to the targeted cells and regions.

The physical effects of ultrasound depend on several factors, such as central frequency, pulse width, pulse interval, stimulation duration, and stimulation interval. Ultrasound parameters above a certain range might generate heat, which has been demonstrated to decrease the firing rates of neurons and, in turn, change an animal's behavior [173]. Ultrasound-induced heat generation can be controlled by the appropriate choice of US parameters. Previous studies have indicated that low acoustic intensity, low frequency, and short duration do not produce any heat effects [87, 96, 110]. Based on current results, we carefully consider the ultrasound parameters to prevent heat generation. In our protocol, the pulse width was set at 400 - 500 μs , the stimulation duration was set at 300 ms, and the interval was either 3 s or 10 s. It has been shown that diverse neuronal types respond differently to different PRFs of ultrasound stimulation [174]. To more thoroughly understand the effects of ultrasound stimulation, further parameter-dependent studies are required. In addition, there are several factors that could minimize ultrasound wave delivery. More efficient expression of MS ion channels is necessary to further characterize the effects of ultrasound stimulation. It has been shown that channelrhodopsin-2 (ChR2) is expressed well within

approximately 2 weeks of injection, whereas inhibitory opsins such as halorhodopsin (eNpHR3.0) need 6–8 weeks for sufficient expression and photocurrent development [175]. To further optimize the toolkit, we plan to perform detailed experiments that will allow us to determine the optimal virus injection volume and expression time.

6.2 Potential applications of MscL-mediated ultrasound stimulation in neurological disorders

For detecting the dopamine dynamic changes in real time, we used a genetically encoded fluorescent DA sensor that is faster and more sensitive than conventional DA-detection methods [164]. Using this sensor, we detected the real-time effects of MscL-mediated ultrasound stimulation on DA dynamics *in vivo*. Our sonogenetic technique induced DA release in the mesolimbic pathway and affected the animal's behavior without the need for surgical interventions. DA is an important neurotransmitter that is correlated to a wide range of complicated processes, such as reward signals [176], learning [177], and motor control [178]. Impaired dopamine transmission in the human brain can cause neuro-psychiatric disorders, such as PD [179, 180], schizophrenia [181], depression [182].

Levodopa (L-DOPA) has been widely utilized to treat patients with PD and alleviate their motor and cognitive symptoms by increasing the DA level. However, a principle shortcoming of this drug is the lack of selectivity and the occurrence of side effects, such as dyskinesia (levodopa-induced dyskinesia [LID]) [183], that can arise due to overdose or long-term use [184]. Although the drug can help correct DA levels in seriously depleted brain regions, it might also have unwanted effects on other brain regions. By regulating the level of DA in target physiological regions, one can not only treat diseases but also prevent adverse effects. In addition to regulating DA levels,

sonogenetics may have a regulatory effect on other neurotransmitters, such as glutamate and GABA, by manipulating related neuron types, such as glutamatergic and GABAergic neurons, respectively. Therefore, we propose sonogenetics as a potential novel alternative method to the therapy of neurological and psychiatric diseases [185].

6.3 Optimizing the MS ion channel and exploring its mechanisms

The development of remote neuromodulation and neurostimulation methods is of considerable interest for the therapy of many neurological diseases. Ultrasound is a candidate with immense potential, as it can elicit neural activity non-invasively and at large depths of penetration. To enhance the sensitivity of neurons to ultrasound and control the safety limits, a variety of studies have investigated the combination of ultrasound stimulation with nanobubbles [186] or microbubbles [187-189]. Genetically encoded MS ion channels such as Piezo1 [139], TRPC1 [112], Prestin [134], MscL [136, 140] have also been studied in this context. In this project, we used MscL as our ultrasound mediator. It is a non-selective ion channel that opens to a width of 3 nm upon activation [190, 191]. During our experiments, we did not detect any serious adverse effects of MscL expression, as tested by immune responses, cell death, physiological neuronal properties, and spontaneous activity. However, more detail studies are required to test the possible potential of such a clinical treatment. This is particularly important because the MscL gene was isolated from *Escherichia coli* and has a large pore-size ($> 30 \text{ \AA}$) [192], making it an exogenous substance in other species. We previously observed a little increase in the c-Fos expression level in target areas such as the DMS, which expressed MscL, indicating some background influences of this channel [136]. It is crucial to confirm whether the expression of MscL in cells causes significant adverse short-term and long-term effects. Thus far, most studies on MS ion channels have investigated the activation of neurons. Efforts should be made to develop

inhibitory MS ion channels (K^+ , Cl^-) that can enhance responses to ultrasound and suppress neuronal activity, similar to the halorhodopsin (NpHR) channel used in optogenetics. To truly understand brain function using sonogenetics, it is vital to achieve functional activation and inhibition in central and peripheral nervous systems.

In addition, mechanisms by which ultrasound stimulation elicits neuronal activity remain unclear. It is important to identify the kinetics and dynamics of this process. We used fiber photometry to demonstrate the effects of MscL-mediated sonication on Ca^{2+} dynamics, but the dynamics of other ions such as sodium and chloride still need to be examined. The best way to determine this would be to use electrophysiological recordings. However, a major challenge of using electrophysiological methods in combination with ultrasound is that the vibration generated by ultrasound could vibrate the recording electrode and cause the cell to rupture. A new electrophysiological method compatible with the ultrasound system would help elucidate the functions of MscL and better understand the biophysical and cellular mechanisms of ultrasound neuromodulation. Additionally, as the MscL protein is extracted from *Escherichia coli* [192], further studies should focus on characterizing the interactions of the MscL protein with neuronal tissue, which could inform long-term applications of the technique. In parallel, this MS ion channel should be functionally refined to control the pore size, thereby restricting ion influx and establishing a selective ion channel. Developing new channel candidates derived from mammalian proteins might also help alleviate any long-term unpredictable side effects.

6.4 Combining existing technologies to eliminate the need for surgical disruption

Overall, we selectively modulated neuronal activity and altered behaviors in a non-invasive manner using MscL-mediated low-intensity ultrasound stimulation. In this

technique, there is no requirement for the insertion of fibers or electrodes into the brain tissue, as the ultrasound wave can pass through the brain efficiently. However, we did have to transduce the AAV through stereoscopic positioning injection, which was a minimal surgical intervention. In future studies, we can engineer the MS ion channel into the AAV-PHP.eB viral vector, which can reportedly cross the BBB[193, 194]. This would allow AAV-PHP.eB-MscL to be transfected into mice via retro-orbital injection. By utilizing the Cre-Lox system, we can then specifically and selectively overexpress the MS ion channel in the target neurons of desired regions. Moreover, AAV-PHP.eB not only can transfect the central nervous system, it also can selectively target specific organs or the peripheral nervous system of Cre transgenic mice. These regions cannot be easily transfected by conventional AAV vectors or traditional virus injection methods. AAV-PHP.eB therefore provides an opportunity for peripheral sonogenetic modulation and treatment. By harnessing the advantages of such advanced techniques, in future we will explore the development of a non-invasive and selective neuromodulatory approach with high spatiotemporal precision that is suitable for use in humans.

References

- [1] Benabid, A.L., Deep brain stimulation for Parkinson's disease. *Current opinion in neurobiology*, 2003. 13(6): p. 696-706.
- [2] Benabid, A.L., et al., Long-term suppression of tremor by chronic stimulation of the ventral intermediate thalamic nucleus. *The Lancet*, 1991. 337(8738): p. 403-406.
- [3] Gildenberg, P.L., Treatment of spasmodic torticollis with dorsal column stimulation, in *Advances in Stereotactic and Functional Neurosurgery 2*. 1977, Springer. p. 65-66.
- [4] Theodore, W.H. and R.S. Fisher, Brain stimulation for epilepsy. *The Lancet Neurology*, 2004. 3(2): p. 111-118.
- [5] Perlmutter, J.S. and J.W. Mink, Deep brain stimulation. *Annu. Rev. Neurosci.*, 2006. 29: p. 229-257.
- [6] Lozano, A.M., et al., Deep brain stimulation: current challenges and future directions. *Nature Reviews Neurology*, 2019. 15(3): p. 148-160.
- [7] Sparing, R. and F.M. Mottaghy, Noninvasive brain stimulation with transcranial magnetic or direct current stimulation (TMS/tDCS)—from insights into human memory to therapy of its dysfunction. *Methods*, 2008. 44(4): p. 329-337.
- [8] Herculano-Houzel, S., The remarkable, yet not extraordinary, human brain as a scaled-up primate brain and its associated cost. *Proceedings of the National Academy of Sciences*, 2012. 109(Supplement 1): p. 10661-10668.
- [9] Jorgenson, L.A., et al., The BRAIN Initiative: developing technology to catalyse neuroscience discovery. *Philosophical Transactions of the Royal Society B: Biological Sciences*, 2015. 370(1668): p. 20140164.
- [10] Cheng-yu, T.L., et al., Burst spiking of a single cortical neuron modifies global

- brain state. *Science*, 2009. 324(5927): p. 643-646.
- [11] Lee, S.-H. and Y. Dan, Neuromodulation of brain states. *Neuron*, 2012. 76(1): p. 209-222.
- [12] Marder, E., Neuromodulation of neuronal circuits: back to the future. *Neuron*, 2012. 76(1): p. 1-11.
- [13] Lindenbach, D. and C. Bishop, Critical involvement of the motor cortex in the pathophysiology and treatment of Parkinson's disease. *Neuroscience & Biobehavioral Reviews*, 2013. 37(10): p. 2737-2750.
- [14] Lotharius, J. and P. Brundin, Pathogenesis of Parkinson's disease: dopamine, vesicles and α -synuclein. *Nature reviews neuroscience*, 2002. 3(12): p. 932-942.
- [15] Galvan, A., et al., Alterations in neuronal activity in basal ganglia-thalamocortical circuits in the parkinsonian state. *Frontiers in neuroanatomy*, 2015. 9: p. 5.
- [16] Kühn, A.A., et al., High-frequency stimulation of the subthalamic nucleus suppresses oscillatory β activity in patients with Parkinson's disease in parallel with improvement in motor performance. *Journal of Neuroscience*, 2008. 28(24): p. 6165-6173.
- [17] Valverde, S., et al., Deep brain stimulation-guided optogenetic rescue of parkinsonian symptoms. *Nature communications*, 2020. 11(1): p. 1-17.
- [18] Poux, P., et al., Subthalamic nucleus stimulation reduces abnormal motor cortical overactivity in Parkinson disease. *Archives of neurology*, 2004. 61(8): p. 1307-1313.
- [19] Polanía, R., et al., Studying and modifying brain function with non-invasive brain stimulation. *Nature neuroscience*, 2018. 21(2): p. 174-187.
- [20] Bernstein, J.G. and E.S. Boyden, Optogenetic tools for analyzing the neural circuits of behavior. *Trends in cognitive sciences*, 2011. 15(12): p. 592-600.

- [21] Johansen, J.P., et al., Controlling the elements: an optogenetic approach to understanding the neural circuits of fear. *Biological psychiatry*, 2012. 71(12): p. 1053-1060.
- [22] Ramirez, S., et al., Identification and optogenetic manipulation of memory engrams in the hippocampus. *Frontiers in behavioral neuroscience*, 2014. 7: p. 226.
- [23] Felix-Ortiz, A.C. and K.M. Tye, Amygdala inputs to the ventral hippocampus bidirectionally modulate social behavior. *Journal of Neuroscience*, 2014. 34(2): p. 586-595.
- [24] Jego, S., et al., Optogenetic identification of a rapid eye movement sleep modulatory circuit in the hypothalamus. *Nature neuroscience*, 2013. 16(11): p. 1637-1643.
- [25] Dyson, F.J., Is science mostly driven by ideas or by tools? *Science*, 2012. 338(6113): p. 1426-1427.
- [26] Breit, S., et al., Deep brain stimulation. *Cell and tissue research*, 2004. 318(1): p. 275-288.
- [27] Volkmann, J., Deep brain stimulation for the treatment of Parkinson's disease. *Journal of clinical neurophysiology*, 2004. 21(1): p. 6-17.
- [28] Cole, E.J., et al., Stanford accelerated intelligent neuromodulation therapy for treatment-resistant depression. *American Journal of Psychiatry*, 2020. 177(8): p. 716-726.
- [29] Groiss, S., et al., Deep brain stimulation in Parkinson's disease. *Therapeutic advances in neurological disorders*, 2009. 2(6): p. 379-391.
- [30] Levy, R.M., et al., Treatment of chronic pain by deep brain stimulation: long term follow-up and review of the literature. *Neurosurgery*, 1987. 21(6): p. 885-893.

- [31] Flora, E.D., et al., Deep brain stimulation for essential tremor: a systematic review. *Movement disorders*, 2010. 25(11): p. 1550-1559.
- [32] Gabriëls, L., et al., Deep brain stimulation for treatment-refractory obsessive-compulsive disorder: psychopathological and neuropsychological outcome in three cases. *Acta Psychiatrica Scandinavica*, 2003. 107(4): p. 275-282.
- [33] Kringelbach, M.L., et al., Translational principles of deep brain stimulation. *Nature Reviews Neuroscience*, 2007. 8(8): p. 623-635.
- [34] Jankovic, J., Complications and limitations of drug therapy for Parkinson's disease. *Neurology*, 2000. 55(12 Suppl 6): p. S2-6.
- [35] Gradinaru, V., et al., Optical deconstruction of parkinsonian neural circuitry. *science*, 2009. 324(5925): p. 354-359.
- [36] Dostrovsky, J., et al., Microstimulation-induced inhibition of neuronal firing in human globus pallidus. *Journal of neurophysiology*, 2000. 84(1): p. 570-574.
- [37] Filali, M., et al., Stimulation-induced inhibition of neuronal firing in human subthalamic nucleus. *Experimental brain research*, 2004. 156(3): p. 274-281.
- [38] Ciechanski, P. and A. Kirton, Transcranial direct-current stimulation (tDCS): principles and emerging applications in children, in *Pediatric Brain Stimulation*. 2016, Elsevier. p. 85-115.
- [39] Lattari, E., et al., Can transcranial direct current stimulation improve the resistance strength and decrease the rating perceived scale in recreational weight-training experience? *The Journal of Strength & Conditioning Research*, 2016. 30(12): p. 3381-3387.
- [40] Nitsche, M.A., et al., Modulation of cortical excitability by transcranial direct current stimulation. *Der Nervenarzt*, 2002. 73(4): p. 332-335.
- [41] Batsikadze, G., et al., Effects of cerebellar transcranial direct current stimulation on cerebellar-brain inhibition in humans: A systematic evaluation. *Brain*

- stimulation*, 2019. 12(5): p. 1177-1186.
- [42] Antal, A., et al., Anodal transcranial direct current stimulation of the motor cortex ameliorates chronic pain and reduces short intracortical inhibition. *Journal of pain and symptom management*, 2010. 39(5): p. 890-903.
- [43] Reinhart, R.M., et al., Using transcranial direct-current stimulation (tDCS) to understand cognitive processing. *Attention, Perception, & Psychophysics*, 2017. 79(1): p. 3-23.
- [44] Nieratschker, V., et al., The COMT Val/Met polymorphism modulates effects of tDCS on response inhibition. *Brain stimulation*, 2015. 8(2): p. 283-288.
- [45] Fonteneau, C., et al., Frontal transcranial direct current stimulation induces dopamine release in the ventral striatum in human. *Cerebral Cortex*, 2018. 28(7): p. 2636-2646.
- [46] Stagg, C.J., et al., The role of GABA in human motor learning. *Current Biology*, 2011. 21(6): p. 480-484.
- [47] Bystad, M., et al., Transcranial direct current stimulation as a memory enhancer in patients with Alzheimer's disease: a randomized, placebo-controlled trial. *Alzheimer's research & therapy*, 2016. 8(1): p. 1-7.
- [48] Hansen, N., Action mechanisms of transcranial direct current stimulation in Alzheimer's disease and memory loss. *Frontiers in psychiatry*, 2012. 3: p. 48.
- [49] Brunelin, J., et al., Examining transcranial direct-current stimulation (tDCS) as a treatment for hallucinations in schizophrenia. *American Journal of Psychiatry*, 2012. 169(7): p. 719-724.
- [50] Mattai, A., et al., Tolerability of transcranial direct current stimulation in childhood-onset schizophrenia. *Brain stimulation*, 2011. 4(4): p. 275-280.
- [51] Fregni, F., et al., Treatment of major depression with transcranial direct current stimulation. 2006.

- [52] Rahman, A., et al., Cellular effects of acute direct current stimulation: somatic and synaptic terminal effects. *The Journal of physiology*, 2013. 591(10): p. 2563-2578.
- [53] Ambrus, G.G., et al., Cutaneous perception thresholds of electrical stimulation methods: comparison of tDCS and tRNS. *Clinical Neurophysiology*, 2010. 121(11): p. 1908-1914.
- [54] Poreisz, C., et al., Safety aspects of transcranial direct current stimulation concerning healthy subjects and patients. *Brain research bulletin*, 2007. 72(4-6): p. 208-214.
- [55] Shin, Y.-I., et al., Reprint of: transcranial direct current stimulation (tDCS)–Application in neuropsychology. *Neuropsychologia*, 2015. 74: p. 74-95.
- [56] Fitzgerald, P.B. and Z.J. Daskalakis, Repetitive transcranial magnetic stimulation treatment for depressive disorders: a practical guide. 2013: Springer Science & Business Media.
- [57] Huerta, P.T. and B.T. Volpe, Transcranial magnetic stimulation, synaptic plasticity and network oscillations. *Journal of neuroengineering and rehabilitation*, 2009. 6(1): p. 1-10.
- [58] Larson, J., et al., Patterned stimulation at the theta frequency is optimal for the induction of hippocampal long-term potentiation. *Brain research*, 1986. 368(2): p. 347-350.
- [59] Dudek, S.M. and M.F. Bear, Homosynaptic long-term depression in area CA1 of hippocampus and effects of N-methyl-D-aspartate receptor blockade, in *How We Learn; How We Remember: Toward An Understanding Of Brain And Neural Systems: Selected Papers of Leon N Cooper*. 1995, World Scientific. p. 200-204.
- [60] Du, X., et al., Individualized brain inhibition and excitation profile in response to paired-pulse TMS. *Journal of motor behavior*, 2014. 46(1): p. 39-48.

- [61] Fox, P.T., et al., Intensity modulation of TMS-induced cortical excitation: Primary motor cortex. *Human brain mapping*, 2006. 27(6): p. 478-487.
- [62] Daskalakis, Z.J., et al., Long-interval cortical inhibition from the dorsolateral prefrontal cortex: a TMS–EEG study. *Neuropsychopharmacology*, 2008. 33(12): p. 2860-2869.
- [63] Rodriguez-Martin, J.L., et al., Transcranial magnetic stimulation for treating depression. *Cochrane Database of Systematic Reviews*, 2002(2).
- [64] Herrmann, L.L. and K.P. Ebmeier, Factors modifying the efficacy of transcranial magnetic stimulation in the treatment of depression: a review. *Journal of Clinical Psychiatry*, 2006. 67(12): p. 1870-1876.
- [65] Pridmore, S., et al., Transcranial magnetic stimulation and chronic pain: current status. *Australasian Psychiatry*, 2005. 13(3): p. 258-265.
- [66] Wagner, T., et al., Transcranial magnetic stimulation and stroke: a computer-based human model study. *Neuroimage*, 2006. 30(3): p. 857-870.
- [67] Berman, R.M., et al., A randomized clinical trial of repetitive transcranial magnetic stimulation in the treatment of major depression. *Biological psychiatry*, 2000. 47(4): p. 332-337.
- [68] Li, R., et al., Enhancing the effects of transcranial magnetic stimulation with intravenously injected magnetic nanoparticles. *Biomaterials science*, 2019. 7(6): p. 2297-2307.
- [69] Lu, Q.-B., et al., Magnetic brain stimulation using iron oxide nanoparticle-mediated selective treatment of the left prelimbic cortex as a novel strategy to rapidly improve depressive-like symptoms in mice. *Zoological research*, 2020. 41(4): p. 381.
- [70] Lee, J.-u., et al., Non-contact long-range magnetic stimulation of mechanosensitive ion channels in freely moving animals. *Nature materials*,

2021: p. 1-8.

- [71] Wassermann, E.M. and S.H. Lisanby, Therapeutic application of repetitive transcranial magnetic stimulation: a review. *Clinical Neurophysiology*, 2001. 112(8): p. 1367-1377.
- [72] Wagner, T., et al., Noninvasive human brain stimulation. *Annu. Rev. Biomed. Eng.*, 2007. 9: p. 527-565.
- [73] Keller, A., et al., Minimal stimulus parameters and the effects of hyperpolarization on the induction of long-term potentiation in the cat motor cortex. *Experimental brain research*, 1991. 87(2): p. 295-302.
- [74] Deisseroth, K.J.N.m., Optogenetics. 2011. 8(1): p. 26.
- [75] Fenno, L., et al., The development and application of optogenetics. 2011. 34.
- [76] Yizhar, O., et al., Optogenetics in neural systems. 2011. 71(1): p. 9-34.
- [77] Tung, J.K., et al., Optogenetic approaches for controlling seizure activity. *Brain stimulation*, 2016. 9(6): p. 801-810.
- [78] Kos, A., et al., Recent developments in optical neuromodulation technologies. *Molecular neurobiology*, 2013. 47(1): p. 172-185.
- [79] Adamantidis, A.R., et al., Optogenetic interrogation of dopaminergic modulation of the multiple phases of reward-seeking behavior. *Journal of Neuroscience*, 2011. 31(30): p. 10829-10835.
- [80] Allsop, S.A., et al., Optogenetic insights on the relationship between anxiety-related behaviors and social deficits. *Frontiers in behavioral neuroscience*, 2014. 8: p. 241.
- [81] Tye, K.M. and K. Deisseroth, Optogenetic investigation of neural circuits underlying brain disease in animal models. *Nature Reviews Neuroscience*, 2012. 13(4): p. 251-266.
- [82] Chen, S., et al., Near-infrared deep brain stimulation via upconversion

- nanoparticle-mediated optogenetics. *Science*, 2018. 359(6376): p. 679-684.
- [83] Miyazaki, T., et al., Large timescale interrogation of neuronal function by fiberless optogenetics using lanthanide micro-particles. *Cell reports*, 2019. 26(4): p. 1033-1043. e5.
- [84] Chen, R., et al., Deep brain optogenetics without intracranial surgery. *Nature biotechnology*, 2021. 39(2): p. 161-164.
- [85] Miyashita, T., et al., Long-term channelrhodopsin-2 (ChR2) expression can induce abnormal axonal morphology and targeting in cerebral cortex. *Frontiers in neural circuits*, 2013. 7: p. 8.
- [86] Tyler, W.J., Noninvasive neuromodulation with ultrasound? A continuum mechanics hypothesis. *The Neuroscientist*, 2011. 17(1): p. 25-36.
- [87] Blackmore, J., et al., Ultrasound neuromodulation: a review of results, mechanisms and safety. *Ultrasound in medicine & biology*, 2019. 45(7): p. 1509-1536.
- [88] Clement, G., Perspectives in clinical uses of high-intensity focused ultrasound. *Ultrasonics*, 2004. 42(10): p. 1087-1093.
- [89] Rezaayat, E. and I.G. Toostani, A review on brain stimulation using low intensity focused ultrasound. *Basic and clinical neuroscience*, 2016. 7(3): p. 187.
- [90] Plaksin, M., et al., Cell-type-selective effects of intramembrane cavitation as a unifying theoretical framework for ultrasonic neuromodulation. *Eneuro*, 2016. 3(3).
- [91] Wang, S., et al., Ultrasonic Neuromodulation and Sonogenetics: A New Era for Neural Modulation. *Frontiers in Physiology*, 2020. 11.
- [92] Carovac, A., et al., Application of ultrasound in medicine. *Acta Informatica Medica*, 2011. 19(3): p. 168.
- [93] Meng, Y., et al., Applications of focused ultrasound in the brain: From

- thermoablation to drug delivery. *Nature Reviews Neurology*, 2020: p. 1-16.
- [94] Chang, W.H.S., et al., Study of thermal effects of ultrasound stimulation on fracture healing. *Bioelectromagnetics: Journal of the Bioelectromagnetics Society, The Society for Physical Regulation in Biology and Medicine, The European Bioelectromagnetics Association*, 2002. 23(4): p. 256-263.
- [95] Gong, C. and D.P. Hart, Ultrasound induced cavitation and sonochemical yields. *The Journal of the Acoustical Society of America*, 1998. 104(5): p. 2675-2682.
- [96] Dalecki, D., Mechanical bioeffects of ultrasound. *Annu. Rev. Biomed. Eng.*, 2004. 6: p. 229-248.
- [97] Rossmann, C. and D. Haemmerich, Review of temperature dependence of thermal properties, dielectric properties, and perfusion of biological tissues at hyperthermic and ablation temperatures. *Critical Reviews™ in Biomedical Engineering*, 2014. 42(6).
- [98] Jagannathan, J., et al., High-intensity focused ultrasound surgery of the brain: part 1—a historical perspective with modern applications. *Neurosurgery*, 2009. 64(2): p. 201-211.
- [99] Weintraub, D. and W.J. Elias, The emerging role of transcranial magnetic resonance imaging-guided focused ultrasound in functional neurosurgery. *Movement Disorders*, 2017. 32(1): p. 20-27.
- [100] Jung, H., et al., Bilateral thermal capsulotomy with MR-guided focused ultrasound for patients with treatment-refractory obsessive-compulsive disorder: a proof-of-concept study. *Molecular psychiatry*, 2015. 20(10): p. 1205-1211.
- [101] Davidson, B., et al., Magnetic resonance-guided focused ultrasound capsulotomy for refractory obsessive compulsive disorder and major depressive disorder: clinical and imaging results from two phase I trials. *Molecular psychiatry*, 2020. 25(9): p. 1946-1957.

- [102] Jeanmonod, D., et al., Transcranial magnetic resonance imaging-guided focused ultrasound: noninvasive central lateral thalamotomy for chronic neuropathic pain. *Neurosurgical focus*, 2012. 32(1): p. E1.
- [103] Badran, B.W., et al., Sonication of the anterior thalamus with MRI-Guided transcranial focused ultrasound (tFUS) alters pain thresholds in healthy adults: A double-blind, sham-controlled study. *Brain Stimulation*, 2020. 13(6): p. 1805-1812.
- [104] Hauptmann, M., et al., Enhancement of cavitation activity and particle removal with pulsed high frequency ultrasound and supersaturation. *Ultrasonics sonochemistry*, 2013. 20(1): p. 69-76.
- [105] Paliwal, S. and S. Mitragotri, Ultrasound-induced cavitation: applications in drug and gene delivery. *Expert opinion on drug delivery*, 2006. 3(6): p. 713-726.
- [106] Izadifar, Z., et al., Ultrasound cavitation/microbubble detection and medical applications. *Journal of Medical and Biological Engineering*, 2019. 39(3): p. 259-276.
- [107] Palmeri, M.L. and K.R. Nightingale, Acoustic radiation force-based elasticity imaging methods. *Interface focus*, 2011. 1(4): p. 553-564.
- [108] Lipsman, N., et al., Blood-brain barrier opening in Alzheimer's disease using MR-guided focused ultrasound. *Nature communications*, 2018. 9(1): p. 1-8.
- [109] Kubanek, J., et al., Ultrasound modulates ion channel currents. *Scientific reports*, 2016. 6(1): p. 1-14.
- [110] Tyler, W.J., et al., Remote excitation of neuronal circuits using low-intensity, low-frequency ultrasound. *PloS one*, 2008. 3(10): p. e3511.
- [111] Kubanek, J., et al., Ultrasound elicits behavioral responses through mechanical effects on neurons and ion channels in a simple nervous system. *Journal of Neuroscience*, 2018. 38(12): p. 3081-3091.

- [112] Yoo, S., et al., Focused ultrasound excites neurons via mechanosensitive calcium accumulation and ion channel amplification. *bioRxiv*, 2020.
- [113] Kubanek, J., Neuromodulation with transcranial focused ultrasound. *Neurosurgical focus*, 2018. 44(2): p. E14.
- [114] Gibson, B.C., et al., Increased excitability induced in the primary motor cortex by transcranial ultrasound stimulation. *Frontiers in neurology*, 2018. 9: p. 1007.
- [115] Legon, W., et al., A retrospective qualitative report of symptoms and safety from transcranial focused ultrasound for neuromodulation in humans. *Scientific reports*, 2020. 10(1): p. 1-10.
- [116] Pang, N., et al., Transcranial ultrasound stimulation of hypothalamus in aging mice. *IEEE transactions on ultrasonics, ferroelectrics, and frequency control*, 2020. 68(1): p. 29-37.
- [117] Gaur, P., et al., Histologic safety of transcranial focused ultrasound neuromodulation and magnetic resonance acoustic radiation force imaging in rhesus macaques and sheep. *Brain stimulation*, 2020. 13(3): p. 804-814.
- [118] Hameroff, S., et al., Transcranial ultrasound (TUS) effects on mental states: a pilot study. *Brain stimulation*, 2013. 6(3): p. 409-415.
- [119] Legon, W., et al., Transcranial focused ultrasound modulates the activity of primary somatosensory cortex in humans. *Nature neuroscience*, 2014. 17(2): p. 322-329.
- [120] Lee, W., et al., Transcranial focused ultrasound stimulation of human primary visual cortex. *Scientific reports*, 2016. 6(1): p. 1-12.
- [121] Lee, W., et al., Transcranial focused ultrasound stimulation of motor cortical areas in freely-moving awake rats. *BMC neuroscience*, 2018. 19(1): p. 1-14.
- [122] Yuan, Y., et al., Cortical hemodynamic responses induced by low-intensity transcranial ultrasound stimulation of mouse cortex. *NeuroImage*, 2020. 211: p.

116597.

- [123] Min, B.K., et al., Focused ultrasound modulates the level of cortical neurotransmitters: potential as a new functional brain mapping technique. *International Journal of Imaging Systems and Technology*, 2011. 21(2): p. 232-240.
- [124] Deffieux, T., et al., Low-intensity focused ultrasound modulates monkey visuomotor behavior. *Current Biology*, 2013. 23(23): p. 2430-2433.
- [125] Yoo, S.-S., et al., Focused ultrasound modulates region-specific brain activity. *Neuroimage*, 2011. 56(3): p. 1267-1275.
- [126] Sato, T., et al., Ultrasonic neuromodulation causes widespread cortical activation via an indirect auditory mechanism. *Neuron*, 2018. 98(5): p. 1031-1041. e5.
- [127] Guo, H., et al., Ultrasound produces extensive brain activation via a cochlear pathway. *Neuron*, 2018. 98(5): p. 1020-1030. e4.
- [128] Mohammadjavadi, M., et al., Elimination of peripheral auditory pathway activation does not affect motor responses from ultrasound neuromodulation. *Brain stimulation*, 2019. 12(4): p. 901-910.
- [129] Jiang, Y., et al., Optoacoustic brain stimulation at submillimeter spatial precision. *Nature communications*, 2020. 11(1): p. 1-9.
- [130] Folloni, D., et al., Manipulation of subcortical and deep cortical activity in the primate brain using transcranial focused ultrasound stimulation. *Neuron*, 2019. 101(6): p. 1109-1116. e5.
- [131] Ibsen, S., et al., Sonogenetics is a non-invasive approach to activating neurons in *Caenorhabditis elegans*. *Nature communications*, 2015. 6(1): p. 1-12.
- [132] Zhou, W., et al., Ultrasound neuro-modulation chip: activation of sensory neurons in *Caenorhabditis elegans* by surface acoustic waves. *Lab on a Chip*,

2017. 17(10): p. 1725-1731.

- [133] Duque, M., et al., Targeted millisecond-scale activation of cells using non-invasive Sonogenetics. *bioRxiv*, 2020.
- [134] Huang, Y.-S., et al., Sonogenetic modulation of cellular activities using an engineered auditory-sensing protein. *Nano letters*, 2019. 20(2): p. 1089-1100.
- [135] Yang, Y., et al., Sonogenetics for noninvasive and cellular-level neuromodulation in rodent brain. *bioRxiv*, 2020.
- [136] Qiu, Z., et al., Targeted neurostimulation in mouse brains with non-invasive ultrasound. *Cell reports*, 2020. 32(7): p. 108033.
- [137] Xian, Q., et al., Protocol for the sonogenetic stimulation of mouse brain by non-invasive ultrasound. *STAR protocols*, 2021. 2(2): p. 100393.
- [138] Qiu, Z., et al., The mechanosensitive ion channel Piezo1 significantly mediates in vitro ultrasonic stimulation of neurons. *IScience*, 2019. 21: p. 448-457.
- [139] Prieto, M.L., et al., Activation of Piezo1 but not NaV1.2 channels by ultrasound at 43 MHz. *Ultrasound in medicine & biology*, 2018. 44(6): p. 1217-1232.
- [140] Ye, J., et al., Ultrasonic control of neural activity through activation of the mechanosensitive channel MscL. *Nano letters*, 2018. 18(7): p. 4148-4155.
- [141] Maingret, F., et al., Mechano-or acid stimulation, two interactive modes of activation of the TREK-1 potassium channel. *Journal of Biological Chemistry*, 1999. 274(38): p. 26691-26696.
- [142] Aryal, P., et al., Bilayer-mediated structural transitions control mechanosensitivity of the TREK-2 K2P channel. *Structure*, 2017. 25(5): p. 708-718. e2.
- [143] Sorum, B., et al., Ultrasound activates mechanosensitive TRAAK K⁺ channels through the lipid membrane. *Proceedings of the National Academy of Sciences*, 2021. 118(6).

- [144] Kim, H., et al., Noninvasive transcranial stimulation of rat abducens nerve by focused ultrasound. *Ultrasound in medicine & biology*, 2012. 38(9): p. 1568-1575.
- [145] Lee, W., et al., Image-guided focused ultrasound-mediated regional brain stimulation in sheep. *Ultrasound in medicine & biology*, 2016. 42(2): p. 459-470.
- [146] Bystritsky, A., et al., A review of low-intensity focused ultrasound pulsation. *Brain stimulation*, 2011. 4(3): p. 125-136.
- [147] O'Brien Jr, W.D., Ultrasound–biophysics mechanisms. *Progress in biophysics and molecular biology*, 2007. 93(1-3): p. 212-255.
- [148] King, R.L., et al., Effective parameters for ultrasound-induced in vivo neurostimulation. *Ultrasound in medicine & biology*, 2013. 39(2): p. 312-331.
- [149] Crochet, S. and C.C. Petersen, Correlating whisker behavior with membrane potential in barrel cortex of awake mice. *Nature neuroscience*, 2006. 9(5): p. 608-610.
- [150] Brecht, M., Barrel cortex and whisker-mediated behaviors. *Current opinion in neurobiology*, 2007. 17(4): p. 408-416.
- [151] Petersen, C.C., The functional organization of the barrel cortex. *Neuron*, 2007. 56(2): p. 339-355.
- [152] Sreenivasan, V., et al., Parallel pathways from motor and somatosensory cortex for controlling whisker movements in mice. *European Journal of Neuroscience*, 2015. 41(3): p. 354-367.
- [153] Clack, N.G., et al., Automated tracking of whiskers in videos of head fixed rodents. *PLoS Comput Biol*, 2012. 8(7): p. e1002591.
- [154] O'Connor, D.H., et al., Neural activity in barrel cortex underlying vibrissa-based object localization in mice. *Neuron*, 2010. 67(6): p. 1048-1061.

- [155] Guo, Q., et al., Multi-channel fiber photometry for population neuronal activity recording. *Biomedical optics express*, 2015. 6(10): p. 3919-3931.
- [156] Cui, G., et al., Concurrent activation of striatal direct and indirect pathways during action initiation. *Nature*, 2013. 494(7436): p. 238-242.
- [157] Barbera, G., et al., Spatially compact neural clusters in the dorsal striatum encode locomotion relevant information. *Neuron*, 2016. 92(1): p. 202-213.
- [158] Meng, C., et al., Spectrally resolved fiber photometry for multi-component analysis of brain circuits. *Neuron*, 2018. 98(4): p. 707-717. e4.
- [159] Mott, M.C., et al., The NIH BRAIN Initiative: Advancing neurotechnologies, integrating disciplines. *PLoS biology*, 2018. 16(11): p. e3000066.
- [160] Tzschentke, T.M. and W.J. Schmidt, Functional relationship among medial prefrontal cortex, nucleus accumbens, and ventral tegmental area in locomotion and reward. *Critical Reviews™ in Neurobiology*, 2000. 14(2).
- [161] Lammel, S., et al., Input-specific control of reward and aversion in the ventral tegmental area. *Nature*, 2012. 491(7423): p. 212-217.
- [162] Morales, M. and E.B. Margolis, Ventral tegmental area: cellular heterogeneity, connectivity and behaviour. *Nature Reviews Neuroscience*, 2017. 18(2): p. 73-85.
- [163] Zhang, F., et al., Optogenetics in freely moving mammals: dopamine and reward. *Cold Spring Harbor Protocols*, 2015. 2015(8): p. pdb. top086330.
- [164] Sun, F., et al., A genetically encoded fluorescent sensor enables rapid and specific detection of dopamine in flies, fish, and mice. *Cell*, 2018. 174(2): p. 481-496. e19.
- [165] Cohen, J.Y., et al., Neuron-type-specific signals for reward and punishment in the ventral tegmental area. *nature*, 2012. 482(7383): p. 85-88.
- [166] Wang, H.-L., et al., Rewarding effects of optical stimulation of ventral

- tegmental area glutamatergic neurons. *Journal of Neuroscience*, 2015. 35(48): p. 15948-15954.
- [167] Niu, L., et al., Noninvasive ultrasound deep brain stimulation of nucleus accumbens induces behavioral avoidance. *Science China Life Sciences*, 2020: p. 1-9.
- [168] Stauffer, W.R., et al., Dopamine neuron-specific optogenetic stimulation in rhesus macaques. *Cell*, 2016. 166(6): p. 1564-1571. e6.
- [169] Gompf, H.S., et al., Targeted genetic manipulations of neuronal subtypes using promoter-specific combinatorial AAVs in wild-type animals. *Frontiers in behavioral neuroscience*, 2015. 9: p. 152.
- [170] Syeda, R., et al., Piezo1 channels are inherently mechanosensitive. *Cell reports*, 2016. 17(7): p. 1739-1746.
- [171] Cao, E., et al., TRPV1 channels are intrinsically heat sensitive and negatively regulated by phosphoinositide lipids. *Neuron*, 2013. 77(4): p. 667-679.
- [172] Sharif-Naeini, R., et al., Polycystin-1 and-2 dosage regulates pressure sensing. *Cell*, 2009. 139(3): p. 587-596.
- [173] Owen, S.F., et al., Thermal constraints on in vivo optogenetic manipulations. *Nature neuroscience*, 2019. 22(7): p. 1061-1065.
- [174] Yu, K., et al., Intrinsic functional neuron-type selectivity of transcranial focused ultrasound neuromodulation. *Nature communications*, 2021. 12(1): p. 1-17.
- [175] Gradinaru, V., et al., Molecular and cellular approaches for diversifying and extending optogenetics. *Cell*, 2010. 141(1): p. 154-165.
- [176] Wise, R.A. and P.-P. Rompre, Brain dopamine and reward. *Annual review of psychology*, 1989. 40(1): p. 191-225.
- [177] Wise, R.A., Dopamine, learning and motivation. *Nature reviews neuroscience*, 2004. 5(6): p. 483-494.

- [178] Crocker, A.D., The regulation of motor control: an evaluation of the role of dopamine receptors in the substantia nigra. *Reviews in the neurosciences*, 1997. 8(1): p. 55-76.
- [179] Oertel, W. and J.B. Schulz, Current and experimental treatments of Parkinson disease: a guide for neuroscientists. *Journal of neurochemistry*, 2016. 139: p. 325-337.
- [180] Evans, A.H. and A.J. Lees, Dopamine dysregulation syndrome in Parkinson's disease. *Current opinion in neurology*, 2004. 17(4): p. 393-398.
- [181] Abi-Dargham, A., et al., Increased striatal dopamine transmission in schizophrenia: confirmation in a second cohort. *American Journal of Psychiatry*, 1998. 155(6): p. 761-767.
- [182] Dunlop, B.W. and C.B. Nemeroff, The role of dopamine in the pathophysiology of depression. *Archives of general psychiatry*, 2007. 64(3): p. 327-337.
- [183] Huot, P., et al., The pharmacology of L-DOPA-induced dyskinesia in Parkinson's disease. *Pharmacological reviews*, 2013. 65(1): p. 171-222.
- [184] Cools, R., Dopaminergic modulation of cognitive function-implications for L-DOPA treatment in Parkinson's disease. *Neuroscience & Biobehavioral Reviews*, 2006. 30(1): p. 1-23.
- [185] Xu, T., et al., Ultrasonic stimulation of the brain to enhance the release of dopamine—A potential novel treatment for Parkinson's disease. *Ultrasonics sonochemistry*, 2020. 63: p. 104955.
- [186] Pellow, C., et al., Simultaneous intravital optical and acoustic monitoring of ultrasound-triggered nanobubble generation and extravasation. *Nano letters*, 2020. 20(6): p. 4512-4519.
- [187] Tran, T.A., et al., Characterization of cell membrane response to ultrasound activated microbubbles. *IEEE transactions on ultrasonics, ferroelectrics, and*

- frequency control*, 2008. 55(1): p. 43-49.
- [188] Scarcelli, T., et al., Stimulation of hippocampal neurogenesis by transcranial focused ultrasound and microbubbles in adult mice. *Brain stimulation*, 2014. 7(2): p. 304-307.
- [189] Hou, X., et al., Enhanced ultrasound neuromodulation in vitro using nanobubble actuators. *bioRxiv*, 2020.
- [190] Haswell, E.S., et al., Mechanosensitive channels: what can they do and how do they do it? *Structure*, 2011. 19(10): p. 1356-1369.
- [191] Corry, B., et al., Conformational changes involved in MscL channel gating measured using FRET spectroscopy. *Biophysical journal*, 2005. 89(6): p. L49-L51.
- [192] Chang, G., et al., Structure of the MscL homolog from *Mycobacterium tuberculosis*: a gated mechanosensitive ion channel. *Science*, 1998. 282(5397): p. 2220-2226.
- [193] Dayton, R.D., et al., More expansive gene transfer to the rat CNS: AAV PHP. EB vector dose–response and comparison to AAV PHP. B. *Gene therapy*, 2018. 25(5): p. 392-400.
- [194] Chan, K.Y., et al., Engineered AAVs for efficient noninvasive gene delivery to the central and peripheral nervous systems. *Nature neuroscience*, 2017. 20(8): p. 1172-1179.